1990

Spectral hole burning and fluorescence studies of a synthetic chlorophyll dimer, a bacterial antenna system and a bacterial reaction center

Stephen Guy Johnson
Iowa State University

Order Number 9100443

Spectral hole burning and fluorescence studies of a synthetic chlorophyll dimer, a bacterial antenna system and a bacterial reaction center

Johnson, Stephen Guy, Ph.D.

Iowa State University, 1990

U·M·I
300 N. Zeeb Rd.
Ann Arbor, MI 48106

Spectral hole burning and fluorescence studies of a synthetic chlorophyll dimer, a bacterial antenna system and a bacterial reaction center

by

Stephen Guy Johnson

A Dissertation Submitted to the
Graduate Faculty in Partial Fulfillment of the
Requirements for the Degree of
DOCTOR OF PHILOSOPHY

Department: Chemistry
Major: Physical Chemistry

Approved:

Signature was redacted for privacy.

In Charge of Major Work

Signature was redacted for privacy.

For the Major Department

Signature was redacted for privacy.

For the Graduate College

Iowa State University
Ames, Iowa

1990

TABLE OF CONTENTS

		Page
EXPLANATION OF DISSERTATION FORMAT		v
GENERAL INTRODUCTION		1
SECTION I.	A SPECTROSCOPIC STUDY OF A SYNTHETIC MODEL OF THE SPECIAL PAIR	13
INTRODUCTION		14
EXPERIMENTAL METHODS		24
PAPER I.	TEMPERATURE AND SOLVENT-POLARITY DEPENDENCE OF THE ABSORPTION AND FLUORESCENCE SPECTRA OF A FIXED-DISTANCE SYMMETRIC CHLOROPHYLL DIMER	28
ABSTRACT		30
INTRODUCTION		31
EXPERIMENTAL		35
RESULTS		36
DISCUSSION		49
CONCLUDING REMARKS		58
ACKNOWLEDGEMENT		60
REFERENCES		61

ADDITIONAL RESULTS AND DISCUSSION 64
REFERENCES 74

SECTION II PERSISTENT SPECTRAL HOLE BURNING OF A STRONGLY EXCITON COUPLED ANTENNA COMPLEX 79

INTRODUCTION 80
EXPERIMENTAL METHODS 90

PAPER I. SPECTRAL HOLE BURNING OF A STRONGLY EXCITON COUPLED BACTERIOCHLOROPHYLL a ANTENNA COMPLEX 92

ABSTRACT 94
ACKNOWLEDGEMENTS 104
REFERENCES 105

ADDITIONAL RESULTS AND DISCUSSION 107
REFERENCES 111

SECTION III. TRANSIENT PHOTOCHEMICAL HOLE BURNING STUDIES OF REACTION CENTERS FROM *RHODOBACTER SPHAEROIDES* 113

INTRODUCTION 114

EXPERIMENTAL METHODS 126

ADDITIONAL RESULTS 130

PAPER I. PRIMARY DONOR STATE MODE STRUCTURE AND ENERGY TRANSFER IN BACTERIAL REACTION CENTERS 150

ABSTRACT 152

INTRODUCTION 153

EXPERIMENTAL 156

RESULTS 157

DISCUSSION 173

CONCLUSION 177

ACKNOWLEDGMENTS 178

REFERENCES 179

ADDITIONAL CONCLUSIONS 182

REFERENCES 184

GENERAL CONCLUSIONS 188

LITERATURE CITED 190

ACKNOWLEDGEMENTS 193

EXPLANATION OF DISSERTATION FORMAT

This dissertation contains the candidate's original work on spectral hole burning and fluorescence of a synthetic chlorophyll dimer, a bacterial antenna system and a bacterial reaction center. Chapter I contains one published paper describing a spectroscopic study of a synthetic special pair model. Chapter II contains one published paper which reports hole burning experiments performed on a strongly exciton coupled antenna system from the green sulfur bacteria *Prosthecochloris aestuarii*. Chapter III consists of one published paper describing photochemical hole burning experiments performed on the reaction center from the purple bacteria *Rhodobacter sphaeroides*. Each chapter contains an introduction, experimental methods, one paper and additional results. The references for the introduction, experimental methods and additional results are located at the end of that chapter. The references for each paper are found at the end of that paper.

GENERAL INTRODUCTION

"Life is woven out of air by light"

-I. Moleschott

Photosynthesis is the process by which living organisms convert solar energy to chemical energy. Photosynthesis is performed by both green plants, as most people know, and many species of bacteria. The chemical equation describing the event of photosynthesis is similar in each instance and can be written generally,

$$2H_2D + CO_2 \Rightarrow (CH_2O) + H_2O + 2D \qquad (1)$$

Where H_2D is understood to be a hydrogen donor such as, water, hydrogen sulfide or lactate depending on whether one is discussing photosynthesis in green plants or bacteria.

This equation is deceptively simple looking, yet it involves an enormous number of physical and chemical processes which are not all understood at present. These processes can be divided up in terms of time scale. This has been accomplished by Kamen [1]. He assigned three arbitrary "time eras" as follows: (1) Era of Radiation Physics (10^{-15} to 10^{-6} s), (2) Era of Photochemistry (10^{-10} to 10^{-3} s), and (3) Era of Biochemistry (10^{-4} to 10^{-2} s). There are longer lived reactions occurring involving enzymatic reactions which are not considered in this scheme. The Era of Radiation Physics is concerned with excitation of chlorophyll (bacteriochlorophyll) molecules and the transferring and/or sharing of that energy among other chlorophyll molecules. This would include the processes of intersystem crossing, excitation energy transfer, fluorescence and trapping of energy [2]. The second era, Photochemistry, would include primary oxidation-reduction reactions or charge separation processes. The last era, Biochemistry, involves reactions such as: the reduction of $NADP^+$, oxygen evolution, carbon fixation and cyclic photophosphorylation (ATP production). These are, of course, general categories and involve some temporal

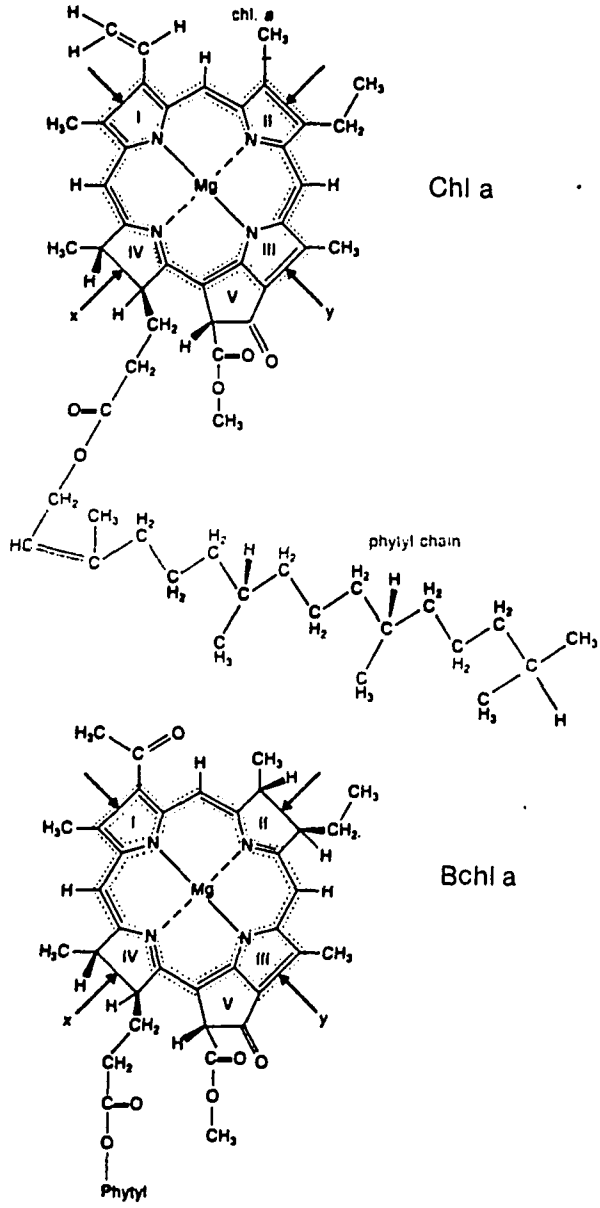

Figure 1. Chlorophyll *a* and Bacteriochlorophyll *a* structure. Axes X and Y represent the principal electronic transitions. Dotted lines represent delocalized electrons

overlap; other authors have discussed photosynthesis in different ways [2-8]. The bulk of this dissertation will be concerned with the time era of Radiation Physics.

~$5.2x10^{21}$ kJ/year reaches the earth's surface from the sun of which ~50% is of wavelengths that are useful for photosynthesis [3]. The wavelength range of this light is 300-1150 nm. The longer wavelength light (>1150 nm) is absorbed by atmospheric water vapor and carbon dioxide while the shorter wavelength light (<300 nm) is is absorbed by ozone and other molecules (N_2) [4]. Of the 50% of the total energy incident upon the earth only .1% ($3x10^{18}$kJ/Year) is converted to organic matter by photosynthesis, while the remaining portion is re-radiated as heat [3]. The percentage of the photosynthetic activity that occurs on the land and in the sea is split evenly.

The basic structure responsible for converting the photons from the sun into photochemical energy, in both green plants and bacteria, has the generic name of the photosynthetic unit (PSU). Its size varies depending on the species [9] and its consists of a number of antenna molecules, usually chlorophylls (but not always), and a reaction center. The antenna molecules, as the name implies, absorb photons and transfer this energy to the reaction center which initiates the formation of a charge separated state. This charge separated state enables the electron to be mobile and it "migrates" along the electron transfer chain to initiate the primary oxidation-reduction reactions.

The composition of the antenna for the PSU varies depending on the species and can include: Bchl *a*, Bchl *b*, Bchl *c*, Bchl *g*, BPheo *a*, BPheo *b*, Chl *a*, Chl *b*, Chl *c*, Pheo *a*, Pheo *b*, Phycocyanin, Phycoerythrin, Allophycocyanin, carotenoid α and β and Xanthophylls [3] (see Fig. 1 for the structure of chlorophyll). Any single species will usually have several of the above mentioned types of antenna molecules. This allows for the more efficient usage of the sun's energy, since these molecules have a variety of energies for their $S_1 \leftarrow S_0$ transitions ranging from ~450 to 900 nm(in their monomeric forms) [3], thus the solar spectrum is covered fairly completely. The number of antenna molecules to reaction center in a PSU varies from as few as 50 to as many as 1000 [2,3] (see Fig. 2), but this is a topic still under debate. The crux of the debate centers around the definition of PSU [2,3].

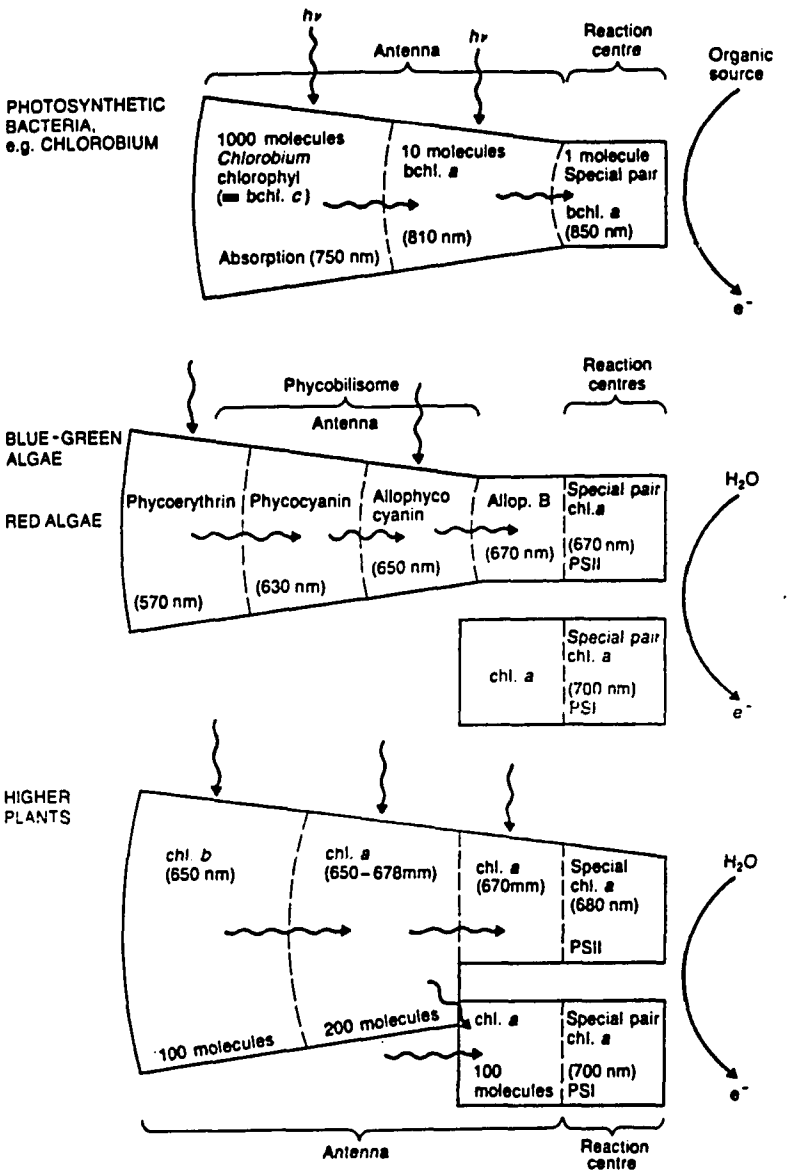

Figure 2. Different representations of the PSUs of the major classes of photosynthetic organisms. The numbers of various pigments should be viewed as approximate

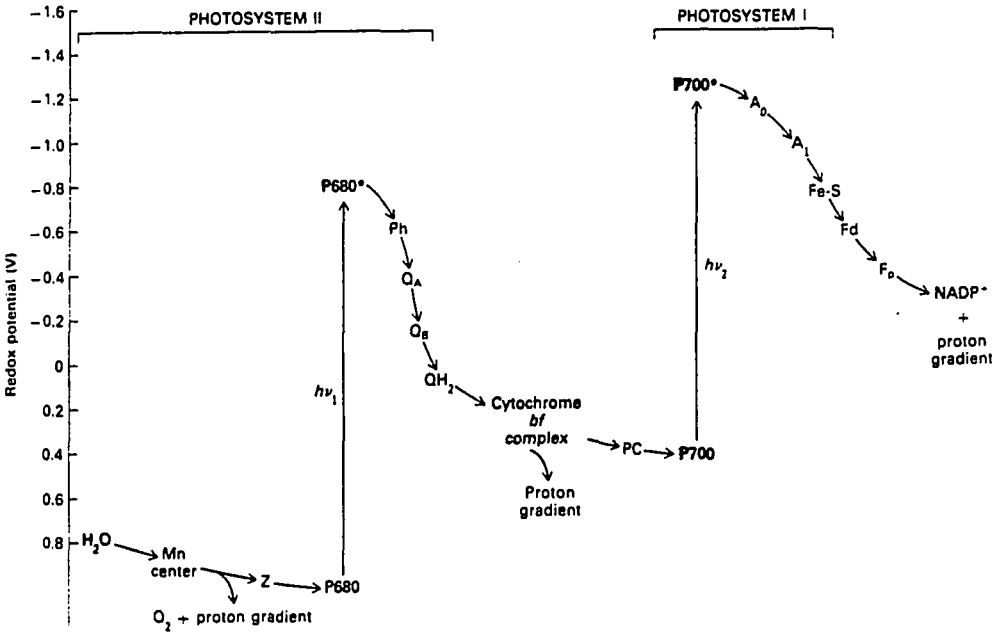

Figure 3. The Z-scheme for noncyclic electron transfer in green plants

The structure of the reaction center (RC) for several species of photosynthetic bacteria have been obtained via single crystal x-ray diffraction [10-13], but other than these two species of bacteria the RC is a relatively unknown entity (in terms of its structure). For green plants two RC, or more precisely, two primary electron donors (PED) are known to exist, photosystem I (PSI) and photosystem II (PS II) [2,3,9]. These two PED are connected via an electron transport chain (see Fig. 3).

The PED in any PSU absorbs at a lower energy than any other entity in the PSU (antenna or accessory molecules). This facilitates the excitation energy transfer from the antenna to the PED by making this a "downhill" energy process. In most cases the PED is simply denoted by P(NUM), where NUM is the approximate absorption maximum for the PED. This somewhat misleading in that this designation does not specify what temperature or solvent the information pertains to. For example P870 is the PED for *Rhodobacter sphaeroides*, a purple photosynthetic bacteria, and it absorbs ~870 nm at room temperature in glycerol/water (2:1). However, it absorbs at ~860 nm in PVOH films at room temperature and at ~ 890 nm in glycerol/water at 4.2 K [14]. Thus, the designations of P700, P865 and P960 for the PEDs in PS I, *Chloroflexus aurianticus* and *Rhodopseudomonas viridis*, respectively, should be viewed cautiously in terms of providing absorption maxima, but these numbers do give a general idea of the absorption maxima.

Figure 4 is the absorption spectrum for the RC from the photosynthetic bacteria *Rb. sphaeroides*, T=4.2 K. This spectra displays only the Q_y ($S_1 \leftarrow S_0$) spectral region. As was mentioned earlier the lowest energy absorbing feature is the PED (~890 nm) and the other two bands represent accessory pigments from the RC (not antenna). The chlorophyll contained in the RC of this species is Bchl *a*, and BPheo *a* is also present. The two lowest energy features, ~890 nm and ~800 nm, are both due to Bchl *a* but a huge red shift (shift to lower energy), ~1300 cm^{-1}, separates the two. From structural information available [12,13] on this RC excitonic interactions are thought to play a significant role in this red shift. Additional information can be unlocked from the absorption spectrum concerning homogeneous widths, intermolecular and intramolecular vibrational frequencies, low

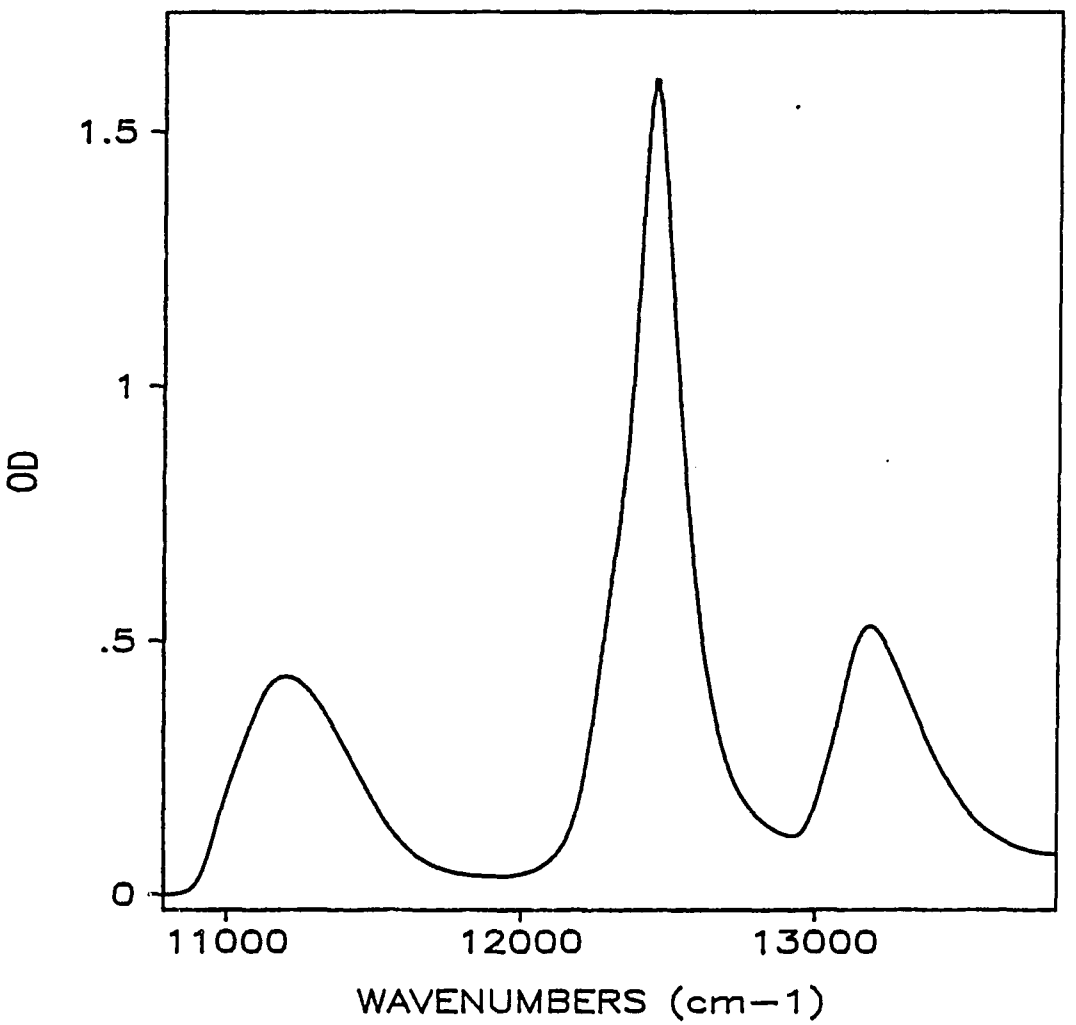

Figure 4. Absorption spectra for RC of *Rb. sphaeroides* in glycerol/NGP, T=4.2 K. Resolution is 4 cm^{-1}

frequency lattice vibrations (phonons), electronic excitation transport times and the extent of correlation between coupled molecular states using site selective spectroscopies.

Site selective spectroscopies include spectral hole burning and fluorescence line narrowing. Both of these techniques use a laser to obtain single site information from an inhomogeneously broadened absorption spectrum. Both of these techniques utilize dilute samples (~10^{-5} M) in amorphorus hosts. Fluorescence line narrowing spectroscopy was initiated by Szabo [15] and Personov et al. [16] who worked on inorganic (ruby) and organic doped solids, respectively. Fluorescence line narrowing (FLN) has been the subject of several excellent review articles [17,18]. A narrow line laser is used to selectively excite a subset of the molecules in the inhomogeneously broadened profile, a site, for the $S_1 \leftarrow S_0$ absorption band (see Fig. 5) at 4.2 K. For this origin band excitation the FLN spectrum consists in part of a series of relatively narrow (few cm^{-1}) fluorescence lines. These lines are displaced from the excitation frequency by an amount of energy equal to a vibrational mode of S_0, for origin excitation. Their intensity relative to their phonon side band is governed by the strength of the linear electron-phonon coupling (Huang-Rhys factor, S). The widths of the zero-phonon vibronic lines are determined by the uncertainty broadening due to vibrational relaxation from the final vibrational state and incomplete site correlation between the zero-point of S_1 and the vibrational manifold of S_0. This technique has been applied to a variety of systems including DNA adducts [19,20], photosynthetic pigments in glasses [21-24], proteins [25,26] and etiolated leaves [27,28]. By using excitation in the spectral region of the S_1 vibrational manifold the vibrational frequencies of the S_1 state can also be obtained. Excitation into higher electronic levels yields broad featureless spectra due to loss of correlation between electronic levels [18].

Spectral hole burning provides information similar to FLN but is more powerful in that it can give more detailed information concerning excited state dynamics, among other useful quantities [29]. In hole burning a narrow line laser irradiates in the inhomogeneously broadened $S_1 \leftarrow S_0$ profile and provides energy to the molecules absorbing there. These molecules can undergo hole burning in one of two ways. They

may experience a change in their chemical make-up, photochemistry, as has been observed for color centers [30], free base porphyrin [31], RC of photosynthetic bacteria [14,32,33] and H_2-phthalocyanine [34,35]. This type of hole burning is termed photochemical hole burning (PHB). A second type of hole burning is called nonphotochemical hole burning (NPHB) or photophysical hole burning. It involves a change in the microenvironment around the solute molecule so that it absorbs either slightly higher or sligthly lower in energy. In PHB the product (antihole) typically absorbs much further away from the original site [36,37]. Whatever the mechanism the result is a dip or "hole" in the absorption spectrum whose width, providing the experiment has been done properly, can be related to the excited state lifetime by the following expression,

$$1/\tau_2 = 1/(2\tau_1) + 1/\tau_2^* \qquad (2)$$

Where τ_2 is the total dephasing time ($\tau_2=(\pi\Delta\nu_h)^{-1}$), τ_1 is the homogeneous lifetime and τ_2^* is the pure dephasing time. The experiment must be performed with a laser whose width is less than the homogeneous width, with a sufficiently low burn intensity and such that only a shallow zero-phonon hole (ZPH) ($\leq$5% ΔOD) is created in order to obtain accurate dynamical information. The measured hole width is $1/\tau_2$ (in cm^{-1}) and can be directly related to the excited state lifetime, τ_1, in the cases where the hole burning is much faster than the pure dephasing. It is τ_1 which is of interest for photosynthetic pigments. Hole burning has also been accomplished in the fluorescence excitation profile by using two lasers in the process [21].

Spectral hole burning as applied to photosynthetic systems can provide several important pieces of information. First, hole burning can provide detailed information concerning vibrational modes (frequencies, Franck-Condon factors) for the $S_0 \Rightarrow S_1$ absorption band. This can indicate which modes may play a role in electronic excitation transport (EET) and by comparing with information available on the same pigment in an "unnatural" host (such as a glass) the extent of interaction (coupling) with the protein can be investigated. The role of the protein in energy and electron transfer is still a much

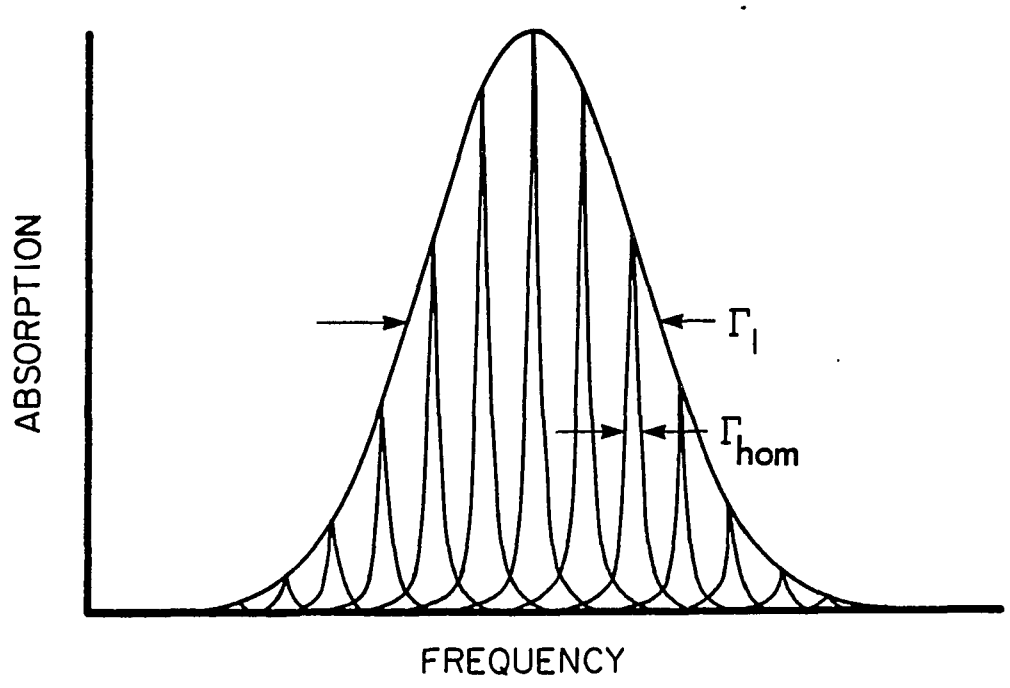

Figure 5. Schematic of an inhomogeneously broadened absorption profile of width Γ_I with a single site of width Γ_{homo} highlighted

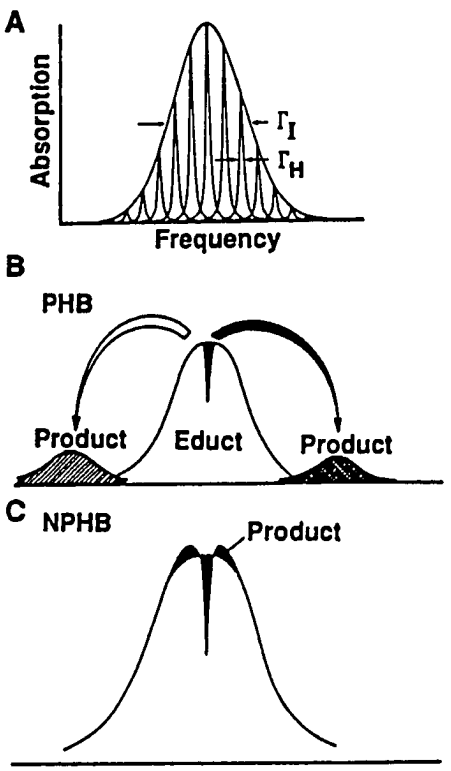

Figure 6. Schematic for hole burning A. Inhomogeneous line broadening; B. Photochemical hole burning (see text for details); C. Photophysical hole burning (see text for details)

debated subject, but it is generally acknowledged that the protein plays an important role. Hole burning can also be used to determine the extent of linear electron-phonon coupling for the optical transition to protein phonons. Phonons for chlorophyll-protein systems being of fairly low frequency, ≤ 35 cm^{-1} [38-41]. The strength of the coupling to the protein phonon is an important point for considering the mechanism of EET [38]. Lastly, the degree of inhomogeneous broadening can be determined via hole burning as well. The process of hole burning is shown in Fig. 6 for both mechanisms (photochemical and photophysical). A large variety of systems have been shown to undergo hole burning [26,29-43].

Holes can be persistent or transient in nature. Persistent holes can last indefinitely at 4.2 K [37]. The length of time which the transient hole can be observed depends on its bottleneck state. This bottleneck can be the triplet state in photophysical hole burning or, in photochemical hole burning, the cation or anion of the molecule under study. For free base porphyrin the photoproduct is a tautomer [31]. For photosynthetic systems both types of holes have proved to be of importance [29].

Pure dephasing and spectral diffusion can play significant roles in the measured holewidth under certain circumstances [36,37,43-45]. These processes, as well as, spontaneous hole filling and laser induced hole filling can interfere with the ability to determine T_1 cleanly. The mechanisms for these processes have been studied for organic laser dyes in polymers [42,46,47]. When the experiment is performed the time frame between burning and probing must be controlled so that spontaneous hole filling is minimized. Hayes and Small [48] have proposed that two level systems (TLS) can be used to model photophysical hole burning with a phonon assisted tunneling process connecting the glassy states TLS. TLS being utilized previously to describe other physical phenomena in glasses [49,50].

The application of the spectral techniques of fluorescence line narrowing and hole burning to photosynthetic pigments, both synthetically prepared and naturally occurring, is the object of this study. A primary electron donor synthetic model, an antenna-protein complex and a reaction center-protein complex are the specific subjects of this study.

SECTION I.

A SPECTROSCOPIC STUDY OF A SYNTHETIC MODEL OF THE SPECIAL PAIR

INTRODUCTION

Interest in the primary charge separation process and the excited electronic state structure of photosynthetic reaction centers (RC) has, for many years, stimulated discussions as to whether the primary electron donor (PED) is of a monomer or a dimer. There has been support for both monomer [1-3] and dimer [4-6] of various chlorophylls molecules for the PED in green plants. The PED in photosynthetic bacteria had been described as primarily dimeric in nature [2,7] before the recent x-ray structural determinations for *Rhodopseudomonas viridis* [8-10] and *Rhodobacter sphaeroides* [11-13]. Even with the structure determinations for the two species of photosynthetic bacteria, the structure of P^* (the excited electronic state of the PED) has not been elucidated fully. The role of the protein environment of the RC for both green plants and photosynthetic bacteria is not yet clear. Is the protein merely a "glue" to hold the pigments together or does it mediate the energy and electron transfer in the RC? Because of the complexity of the RC in both plants and bacteria, and also since the structure of the bacterial RC was not known until 1984 [8], the approach of constructing, synthetically, molecular systems that mimic the optical, electronic, magnetic and redox properties of real photosynthetic systems evolved and has flourished even after the structure determinations of the bacterial RC [8-13]. The sheer variety and number of model systems [14-43] that have been constructed is most impressive.

Model systems, which are comprised either entirely or partly of chlorophyll molecules [14-32], as well as, other types of porphyrins [33-43] have been the subject of several recent review articles [44-47]. The goal of the majority of these models was to provide an entity that mimicked the capabilities of the primary electron donor [14-32,34-37,39-42]. However modelling of the antenna molecules, which serve to funnel the energy to the PED state, received attention as well [14]. Even when considering the models just for the PED the number is vast [14-32,34-37,39-42]. It is the object of this section to discuss the study undertaken on one of these synthetic models, but it is important to understand why this molecule was constructed in the specific manner that it was. To best

understand this, several of the earlier molecules and systems that were built to mimic the behavior of the PED in green plants and photosynthetic bacteria will be described and discussed. By analyzing the abilities and limitations of the earlier models the logic behind the synthesis of the molecule studied in this work can be seen.

The most important early experimental result concerning the PED for both green plants and photosynthetic bacteria was the red shift exhibited in the absorption spectra. For example, Chl *a* absorbs ~670 nm while the PED for PSI absorbs ~700 nm [15]. Photosynthetic bacteria have an even more pronounced red shift for the PED [19]. Mimicking this redshift, as well as, modelling other experimentally observed properties was the goal of the many groups synthesizing model systems.

Shipman et al. [17] proposed in 1976 a model for P700, the PED in photosystem I for green plants, which consisted of two Chl *a* molecules held together via hydrogen bonding and ligand-Mg interactions (see Fig. 1). A number of molecules were suggested to be capable of providing the "glue" holding the Chl *a* molecules together but only ethanol data was presented [17]. This system gave an absorption maximum for the $S_1 \leftarrow S_0$ (Q_y) transition at 700 nm which is where P700, the PED for green plants, was thought to absorb. The ESR signal from a sample of this molecular assembly was gaussian in shape and was 7.5 G wide. The absorption maximum and ESR signal match those from the P700 in *Chlorella vulgaris* [6,48]. This system was thought to possess C_2 symmetry, although this was experimentally unconfirmed, with the two Chl *a* macrocycles being parallel with ring 3 and 5 overlapping and their π systems being 3.6 Å apart (in the ring 3 and 5 area). The center-to-center distance was estimated to be 8.9 Å. The -OH functional group served to both coordinate to one of the Mg ions, via one of the lone pairs of electrons on the oxygen, and hydrogen bond to the C-9 keto group on the other Chl *a*. Similarly, a second ethanol molecule aided in the formation in the exact same manner reversing the roles of the two Chl *a* molecules. This model relied on "solvent assembly" for its construction. A solution of ethanol (.14 M) cooled past the glass formation temperature resulted in a gradual change in both absorption and the IR spectra from that of monomer Chl *a* to that of the dimer described above. This self-assembled or solvent-assembled system was first observed by

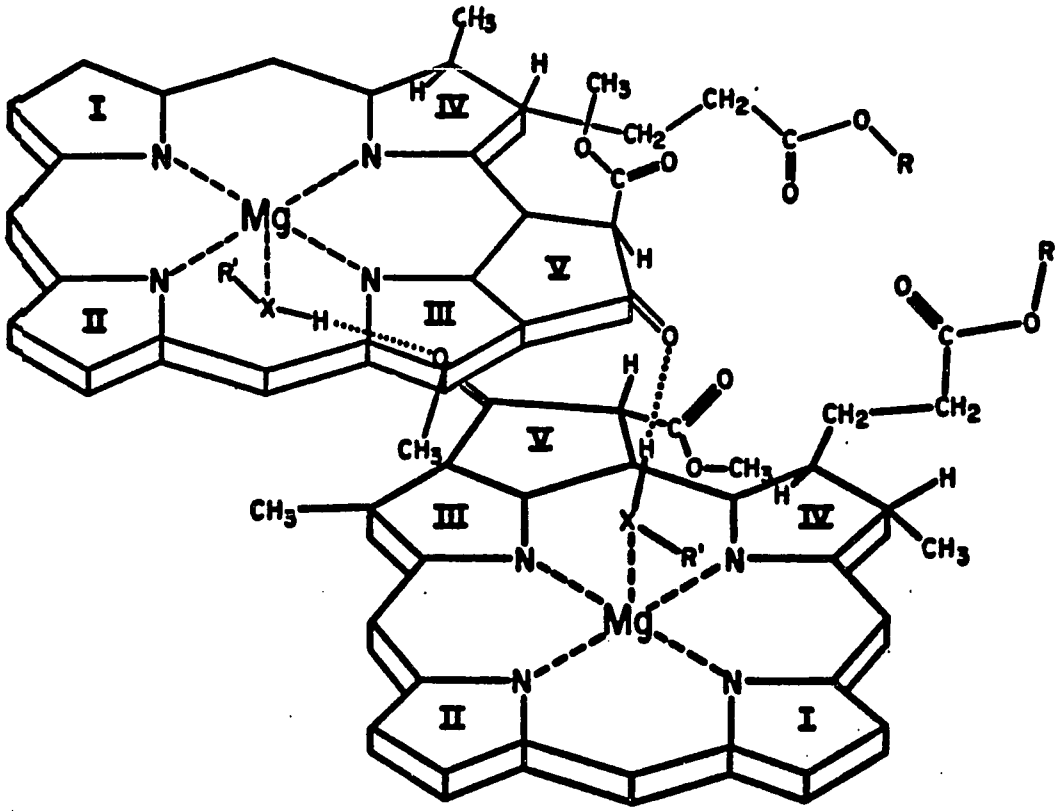

Figure 1. Model for primary electron donor in green plants (P700) by Shipman et al. [17]

Brody and Brody [49], but extensive investigative work concerning its properties was not undertaken until Shipman et al. did so [17].

This model was attractive for several reasons. Importantly it did absorb in the proper position (700 nm) of the spectrum and its ESR mimicked that of a real green plant system's PED [6,48]. The type of interactions necessary to form it were possible in the protein environment of the leaf it was reasoned, since amino acid residues could provide the -OH, -NH, and -SH functional groups necessary. Furthermore, the species fluoresced at 720 nm which was similar to that observed for PS I in green plants [17]. It was thought that the proposed geometry of this molecule (C_2), as well as, the closeness of the two chlorophylls composing it would stabilize an unpaired electron. This was considered a factor in support of the model since delocalization of the unpaired electron been observed for $P700^+$ in green plants [6,48].

There were several drawbacks of this assembly. The lack of a well defined structure, although a structure had been proposed it was not experimentally confirmed [17]. Also the solvent conditions for assembly, although reasonable in terms of the protein providing the functional groups necessary to facilitate the two molecules, were in fact unrealistic. The nonaqueous environment called for would be difficult to find in a living cell, especially, in view of Chl *a*'s nature as a hydrophilic molecule [50]. Despite its deficiencies this early model was successful in showing that excitonic interactions between closely situated chlorophyll molecules could be responsible for the observed red shifted absorption spectra.

A second model (see Fig. 2) which was constructed by Boxer and Closs [15] shortly after the system discussed above is similar to it but improves on some of its shortcomings. It consists of two molecules of methyl pyropheophorbide *a* transesterfied with ethylene glycol to yield the glycol monoester. The magnesium was then inserted back into the pheophytin ring. The molecule exhibited monomer-like absorption and fluorescence characteristics when in a solution of benzene and pyridine. When in a solution of wet benzene (containing water) the absorption maximum shifted from 666 to 696 nm and the fluorescence maximum shifted to 717 nm. The pyridine served as a strong ligand for the

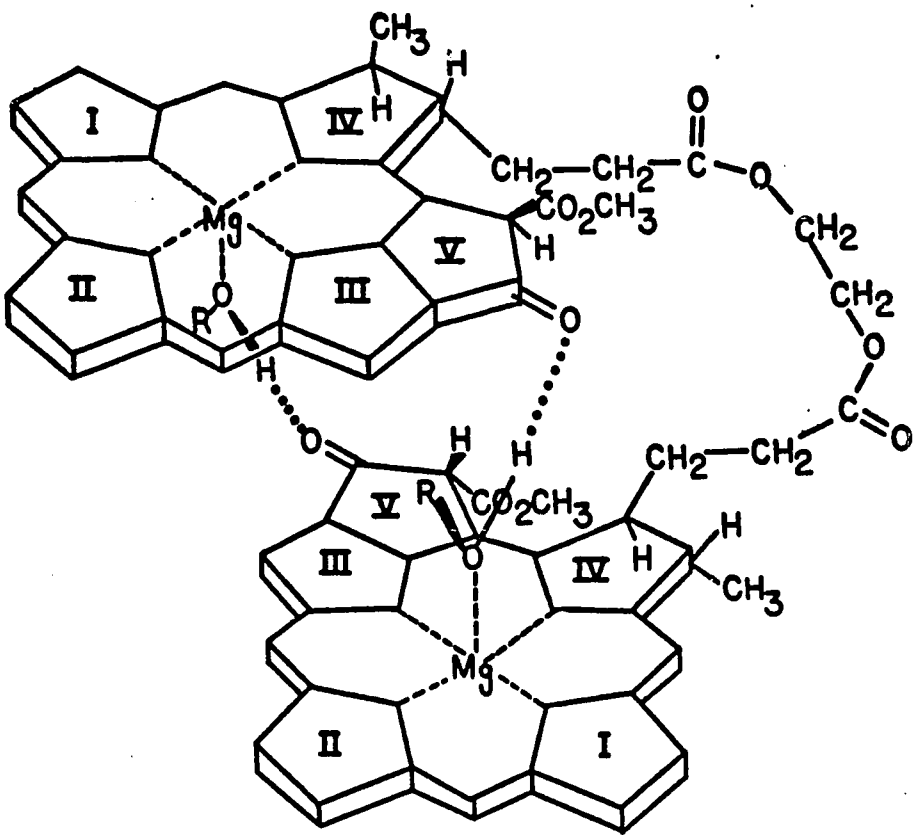

Figure 2. Structure for covalently linked dimer of Chl *a* by Wasielewski et al. [16]. This is very much the same as the model prepared by Boxer and Closs [15]

magnesium in the first case. A structure in which the two Chl *a* macrocycles fold back onto one another in such a way that a pair of water molecules can bind them together was proposed by Boxer and Closs [15]. The water molecules coordinated to the Mg ion and hydrogen bonded to the C-9 keto group in a fashion similar to that described for the ethanol-Chl *a* model of Shipman et al. [17]. C_2 symmetry was again proposed and collaborated by available NMR data showing one set of resonances (at least on an NMR time scale). A connecting chain consisting of 10 atoms was estimated to be long enough to allow the folding to occur.

A second spectroscopic study of an almost identical molecule (pyrochlorophyll *a* were replaced by chlorophyll *a*) (see Fig. 2) was undertaken at approximately the same time by Wasielewski et al. [16]. This study confirmed the experimental observations of Boxer and Closs [15]. The study of Wasielewski et al. [16] went further in that other, nucleophilic, hydrogen bonding molecules, in addition to water, were demonstrated to promote the folding. Primary alcohols (methanol, ethanol) and primary alkanethiols were stated as being effective in this role [16].

One of the shortcomings of the first model discussed, that of forming in a nonaquaeous environment, was overcome in this second system. The structure of the molecule seems better established (with the NMR data), but the dependence of the system on solvent assembly still made it less than a perfect model for the PED for green plants. The red shifted absorption maximum was obtained for this system as well.

The last model system which will be discussed consists of a trio of zinc or magnesium containing pyrochlorophyllide *a* molecules covalently linked in a trio(hydroxymethyl) ethane triester (see Fig. 3). This was constructed and reported on by Yuen et al. [14]. It was meant to serve as a crude model for an antenna and the PED of green plants [14]. In nucleophillic (nonhydrogen bonding) solvents this molecule assumes an open configuration with each chlorophyllic molecule projecting away from the central "hub" (ethane triester backbone) and not interacting with one another. Upon the addition of a small amount (.1 M) of hydrogen bonding nucleophile in a nonnucleophillic solution the

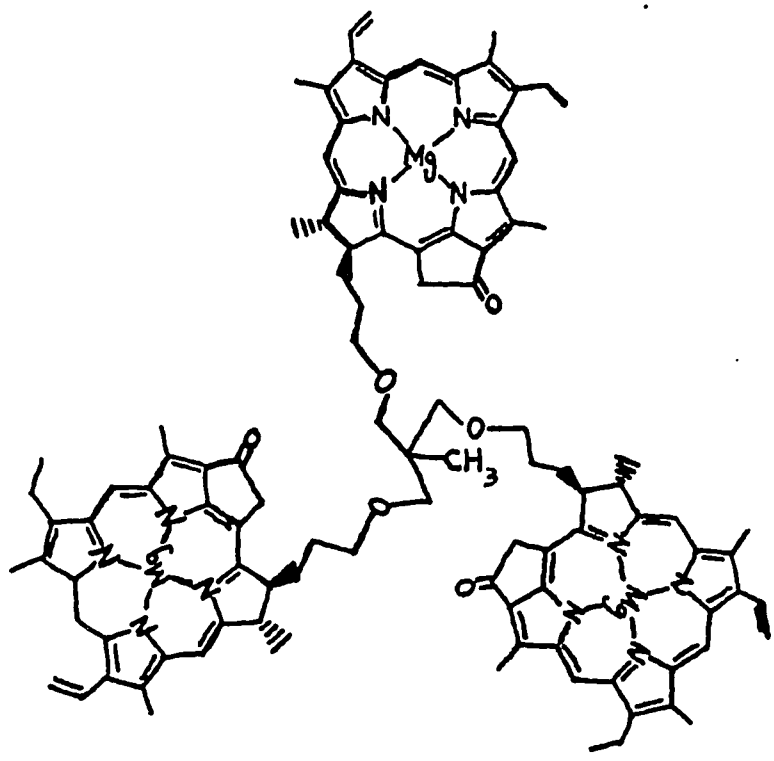

Figure 3. Antenna/PED model of Yuen et al. [14]

molecule would form a closed configuration which involves the crosslinking of two of the chlorophyll molecules. The third molecule would remain free in this type of solution.

The absorption and fluorescence properties of this unusual molecular assembly were similar to that for the PED of PSI and its antenna. The absorption maximum for the folded pair of molecules was 685 nm, and the entire assembly (when it was 100% converted to the folded config.) fluoresced at 712 nm. The fluorescence peak represented very complete energy transfer to the PED model from the antenna molecule. If the energy transfer were not very efficient then fluorescence from the antenna chlorophyll would be observed, which did not occur [14].

This molecular assembly was a clever model for the antenna-PED in PS I and its property of efficient energy transfer between "antenna" and "PED" is intriguing, however the dependence upon solvent assembly persists.

The need for an effective model system which did not depend upon the solvent for construction was clear. Even after the elucidation of the structure of the bacterial RC the need for models of the PED, a special pair(SP) in the case of the bacterial RC, was not diminished. The study of models of the SP , which could now be much more accurately built, could still give valuable information concerning singlet excitation, charge delocalization and formation of charge transfer states. Even with the exact composition and structure of the bacterial RC known the precise role of the solvent (protein) in the process of charge separation was not totally clear.

The need to have a SP model that was solvent independent in regard to its geometry was clear. In addition, the recent experiments on the RC of *Rps. viridis* and *Rb. Sphaeroides* using photochemical hole burning [51-55] and Stark effect spectroscopy [56,57] suggested that excitation of the SP results in an excited state with some charge transfer(CT) character. Since the SP in the RC is made of identical chromophores in C_2 symmetry the formation of a CT state is strictly speaking forbidden. The protein, however, may provide the asymmetry necessary to promote the formation of a CT state. With the preceding information in mind Johnson et al. [58] constructed the SP model system featured in this study and investigated the solvent polarity dependence of the excited state

absorption and emission properties. Their goals when constructing this "facsimile" for the SP were " (1) the distance between the two chromophores of the dimer should be fixed; (2) the structure of the dimer, and therefore the monomer-monomer distance, must be solvent independent; (3) the molecule should have C_2 symmetry similar to that of the SP; (4) the orientation of the transition dipoles of each chromophore should be as much like that in the SP as possible; (5) the two chromophores must be held close to one another; (6) the two chromophores must be electronically coupled; and (7) the two macrocycles should be in an edge-to-edge conformation rather than face-to-face" [58]. To that end they constructed a covalently bonded dimer of methyl pyrochlorophyllide *a*. It is unfortunate that their model proved not to have a rigid structure as was intended, however the system did exhibit extremely interesting excited state dynamics and was a rewarding molecule to study regardless.

Strictly speaking, a model for the SP should be constructed of Bchl *a* or *b*, but these are more chemically unstable [19] then methyl pyrochlorophyllide *a* and so the latter was used. The methyl pyrochlorophyllide *a* is very similar to Bchl *a* or *b*, differing only in the absence of the non-polar phytyl chain and a couple of other minor changes in the substituient groups on the macrocycle. The synthesis of SP models which use Bchl *a* or *b* has received less attention [19,22] than with Chl *a* or Chl *a* derivatives [14-18,20,21,23-31]. The basic properties of the molecules in regard to forming a C-T state should not be affected by these minor changes in molecular structure since the π-electron systems remain essentially unchanged.

The experimental data obtained by Johnson et al. [58] using picosecond spectroscopy is reviewed thoroughly in paper I contained in this section, and consequently will not be reviewed here. It was obvious that their results were very intriguing and the dynamical models which they considered to explain their results were likewise interesting, but they experienced some difficulties in fitting all their results to any one of their dynamical models. With these facts in mind, we undertook experiments involving T-dependent absorption, fluorescence excitation, and frequency domain fluorescence studies

of this synthetic dimer in order to further explore the nature of the absorbing and emitting species and their electronic states and how they depend on the polarity of the solvent.

EXPERIMENTAL METHODS

Samples

Solid samples of the covalently linked dimer of methyl pyrochlorophyllide *a* were generously provided to us by Dr. M. R. Wasielewski of Argonne National Laboratory. The solvents used for these experiments were purified by standard methods. Three solvents of widely differing polarity were used; 2-methyl tetrahydrofuran (MTHF), toluene and dimethylformamide (DMF). The MTHF was treated with lithium aluminum hydride, then distilled, and stored over molecular sieves. The toluene was distilled once, then stored over a drying agent (sodium/benzophenone), then vacuum distilled, and stored over molecular sieves in a nitrogen atmosphere. The DMF was treated with neutral alumina, then distilled, and stored over molecular sieves. Each solvent was freshly prepared before an experiment. To each solution ~1% pyridine (by volume, certifed ACS grade) was added to preclude aggregation of the dimers. It was of great importance to make each solution in a glove box in an inert, dry atmosphere and then seal the tube under several cm of $N_{2(g)}$. It was also very important to properly purify and dry each solvent because any water or renegade nucleophile that could engage in hydrogen bonding would lead to formation of aggregates of dimers. The utmost care was taken during all steps in sample preparations to eliminate any conditions that would promote aggregate formation.

The dimer concentrations were typically $1x10^{-5}$ M based on an $\varepsilon(Q_y)$ of 50,000 [58]. As previously mentioned the solutions were sealed in glass tubes (3 mm i.d.) under 4-5 cm of $N_{2(g)}$. The sealed tubes prevented water condensation from entering the tube when cycling in and out of the cryostat.

Cryogenic Equipment

As mentioned in the previous subsection the samples were in sealed glass tubes which were placed in an aluminum sample holder of local design which provided optical

access to the sample. The cooling rate of the samples varied upon the experiment being performed, however, the results at low temperature and intermediate temperatures were not cooling rate dependent. A model 8DT Janis liquid-helium cryostat (convection cooling) was used for the temperature dependent studies between 4.2 and 300 K. Temperature measurements were made with a Lakeshore Cryotronics DTC-500K calibrated silicon diode. Care was taken so that adequate equilibration time was given between temperatures where spectra were obtained.

Experimental Appartus

Figure 1 shows the configuration of the appartus used to obtain fluorescence line narrowed spectra and fluorescence excitation spectra. The laser system consists of an excimer laser (XeCl gas) (Lambda Physik EMG102) which is used to pump a dye laser (Lambda Physik FL2002). The dye laser provided tunable radiation in the 620-720 nm region using SR640 and OX720 laser dyes (Exciton). The laser linewidth was .2 cm^{-1} and its pulse width was 10 ns. In some cases a CW HeNe laser (Melles Groit), linewidth .03 cm^{-1}, was used as an excitation source.

The output of the dye laser was steered to impinge on the sample in the cryostat via two quartz turning prisms. The shape of the laser beam was also changed by the lenses placed before the cryostat so that the entire sample volume was excited. The fluorescence was collected at 90^{o} with respect to the excitation to reduce interference due to laser scatter. The two lenses placed between the cryostat and the monochromator served to collect and collimate the fluorescence into the monochromator. These lenses were chosen so that they would collect as much of the fluorescence as possible and introduce that into the monochromator while matching the F number of the monochromator. This last step provided the most resolution with the highest level of S/N (signal to noise) from the monochromator.

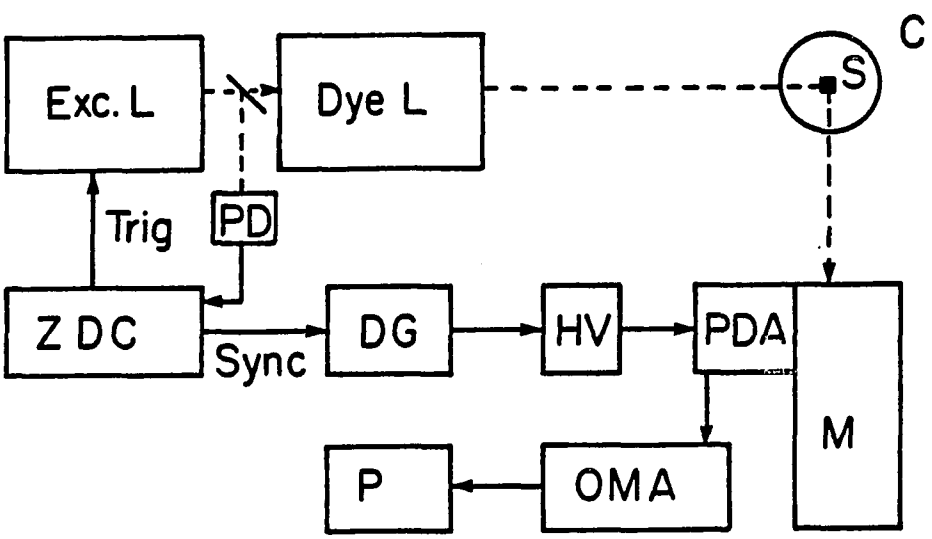

Figure 1. Block diagram of the fluorescence experimental set-up showing excimer laser (Exc. L), dye laser (Dye L.), cryostat (C), sample (S), photodiode (PD), photodiode array (PDA), optical multichannel analyzer (OMA), monochromator (M), and plotter (P). A photomultiplier tube was also used in place of the OMA as a detector. See text for details.

A 1 meter monochromator was used to disperse the fluorescence. Two monochromators were used during the course of the experiments, 1 m Mcpherson 2061 (R=160,000) or a 1 m Jarrel-Ash (R=60,000).

For CW excitation, a PMT and picoammeter were used for signal processing, while for pulsed excitation, either a Tracor Northern TN-6134 intensified diode array and TN-6500 OMA or PMT plus EG&G Model 162 boxcar averager (with two model 164 processer modules) was employed. The PMT used (RCA C31034 or EMI 9558-B) was cooled. For spectra obtained with the pulsed laser, normalization (via a photodiode) was performed to minimize the effect of pulse intensity jitter.

The spectra were either plotted out in real time on a chart recorder (Houston Instruments) or stored on computer diskette for latter retrival. For the fluorescence line narrowed spectra the laser remained at one wavelength and the monochromator was scanned to obtain a spectra. In the case of the fluorescence excitation spectra the monochromator remained at one wavelength and the dye laser was scanned (via a Lambda Physik FL512 scan controller) to obtain a spectra. The laser intensity was adjusted using neutral density filters and cut-off filters (Schott Glass Co.) were used in front of the monochromator to discriminate against laser scatter.

PAPER I. TEMPERATURE AND SOLVENT-POLARITY DEPENDENCE OF THE ABSORPTION AND FLUORESCENCE SPECTRA OF A FIXED-DISTANCE SYMMETRIC CHLOROPHYLL DIMER

Temperature and Solvent Polarity Dependence of the Absorption and Fluorescence Spectra of a Fixed-Distance Symmetric Chlorophyll Dimer

S. G. Johnson and G. J. Small
D. G. Johnson, W. A. Svec and M. R. Wasielewski

Journal of Physical Chemistry 1989, 93, 5437.

ABSTRACT

Temperature dependent absorption and fluorescence spectra and line narrowed fluorescence and excitation spectra are reported for a dimer consisting of two methyl pyrochlorophyllide *a* molecules which share a vinyl group at the 2-position of each macrocycle. The data (obtained for three solvents of widely differing polarity) show that the dimer exists in two conformations (A and B) and that excited state relaxation from A to B onsets near the glass transition temperature (T_g). Molecular modeling suggests that the two conformations are related by "bicycling" of the two single bonds joined to the vinyl group linkage. At sufficiently low temperature the solvent dynamics are rate limiting for the conformational relaxation. For a solvent of sufficiently high polarity (DMF), the excited state of B is shown to access a new radiationless decay channel for $T \geq T_g$. A charge transfer state is suggested to be important for this decay. The model presented is shown to provide a qualitative explanation for the frequency domain and recently obtained picosecond and fluorescence quantum yield room temperature data (D. G. Johnson, W. A. Svec and M. R. Wasielewski, Israel J. Chem., in press).

INTRODUCTION

Interest in the primary charge separation process and the excited electronic state structure of photosynthetic reaction centers (RC) has, for many years, stimulated studies of model dimeric and oligomeric chlorophyllic systems. In the case of bacterial RC the importance of a special bacteriochlorophyll (BChl) pair for the initial phase of charge separation was established prior to the structure determinations [1-3] for *Rps. viridis* and *Rb. sphaeroides*. The diversity of model systems constructed by covalent linkage, nucleophilic linkage, and self-aggregation is impressive and their study has provided valuable insights on singlet and triplet excitation and charge delocalization [4-6]. In what follows we mention only a few of the model systems studied.

Fong proposed [7] a dimer of Chl *a* • H_2O as a model for the primary electron donor (PED) of photosystem I (P700) whose assembly is dependent on solvent conditions. Shipman et al. [8] presented a similar model for P700 involving dimers formed by nucleophilic linkage of Chl *a* monomers. Nucleophiles employed were ROH, RSH or RNH_2, where R is an alkyl chain. A model for the PED state of Rb. sphaeroides, P870, suggested by Wasielewski et al. [9] is a pair of bacteriochlorophyllide *a* molecules covalently bound by an ethylene glycol diester bridge. A similar model for P700 was also constructed by Wasielewski et al. [10] in which two Chl *a* were linked by the same bridge. Boxer and Closs [11] presented a P700 model which is the ethylene glycol diester of methyl pyrochlorophyllide *a*. Pellin and Wasielewski [12] have synthesized a P700-electron acceptor model system consisting of an ethylene glycol diester of pyrochlorophyll *a* and two molecules of pyropheophorbide *a* ethylene glycol monoester. The pyropheophorbide *a* molecules acted as electron acceptors for the dimer. Yuen et al. [13] have constructed a model for a P700-antenna system using a tris (pyrochlorophyllide *a*) ethane triester. Two of the molecules folded upon one another when the solvent conditions were sufficient with the third molecule acting as an antenna. Wasielewski [5] proposed a model for P700 consisting of a bis(chlorophyll *a*) cyclophane. Bucks et al. [14] have investigated several dimers of chlorophyllic species (pyropheophorbide *a*, pyropheophytin

a) and trimers as models for primary electron donors and primary electron donor-antenna systems. Agostiano et al. [15] have proposed a model for P680 involving a dimer of Chl $a \bullet 2H_2O$.

Speculation concerning the geometry of the special pair in the RC of *Rps. viridis* and *Rb. sphaeroides* ended with the structure determination of the former by Deisenhofer et al. [1] and of the latter by Chang et al. [3] and Allen et al. [2]. The two BChl molecules have an edge-to-edge conformation with π-π overlap of the two macrocycles restricted to ring I and an angle between the two planes of about 15°. The Q_y-transition dipoles of the monomer are out-of-phase (anti-parallel) and from the geometry it is clear that the lowest energy mini-exciton state (denoted as P_-) is allowed and is anti-symmetric with respect to the C_2-symmetry axis. From the structures the importance of protein-pigment interactions for the special pair geometry is apparent.

With the above structural features in mind, Johnson et al. [16] synthesized the fixed-distance symmetric bis-pyrochlorophyllide *a* dimer shown in Fig. 1. The molecule has approximate C_2 symmetry and the double bond serves to hold the two macrocycles at a constant edge-to-edge distance of approximately 3.9 A. The Mg...Mg distance is about 12 A. The ^{1}H-NMR data (nuclear Overhauser effect) indicates the structure show. in Fig. 1 has a dihedral angle between the olefinic linkage and the macrocycles of 49-53°. The possibility that this structure is an average for two (or more) rapidly interconverting (at room T) conformers could not be excluded. The room T absorption and fluorescence spectra of the dimer reported [16] are interesting in that the lowest energy Q_y-absorption and fluorescence maxima depend only weakly on solvent polarity while the fluorescence lifetime and fluorescence quantum yield exhibit a two order of magnitude decrease as the solvent dielectric constant is increased from 2.4 (toluene) to 36.7 (DMF). The absorption and fluorescence maxima occur at ~690 and 720 nm at room T. Attempts to observe new emission which accompanies the diminuation of the 720 nm fluorescence intensity were unsuccessful. Johnson et al. [16] also demonstrated, based on stimulated emission studies (610 nm pumping), that the 720 nm emission exhibits a rise time which decreases from 18 psec for toluene to $\leq$1.5 psec for DMF. No prompt stimulated emission signal was

observed. In the absence of firm evidence to the contrary, Johnson et al. [16] assumed that the dimer exists in only one ground state conformation for consideration of dynamical models for interpretation of the time domain and fluorescence quantum yield data. Each model presented certain difficulties as will be briefly discussed later.

With this in mind we recently performed T-dependent absorption, fluorescence excitation and frequency domain fluorescence studies of the pyrochlorophyllide *a* dimer in order to further explore the nature of the absorbing and emitting species and their electronic states and how they depend on solvent polarity. These studies included fluorescence line narrowing measurements. The new data establish that the dimer exists in two conformations for both the ground and excited electronic states. The T-dependences of the absorption and fluorescence spectra establish that interconversion from the higher energy absorbing conformer to the lower energy conformer onsets in the excited state near the glass transition temperature (T_g) for all solvents utilized. The T-dependence of the 720 nm fluorescence intensity in different solvents provides an obvious connection with the time domain data of Johnson et al. [16]. This fluorescence is assigned to the lower energy absorbing conformer. A particular intra-dimer coordinate for conformer interconversion is suggested on the basis of molecular modeling. A two-conformer excited state model embellished with a charge-transfer (CT) state is shown to provide a consistent, albeit qualitative, interpretation of the time and frequency domain data. The CT state provides for decay of the 720 nm emitting state only in solvents of sufficiently high polarity and for $T \geq T_g$. The possibility that the CT state is a TICT (twisted intramolecular charge-transfer) state is considered.

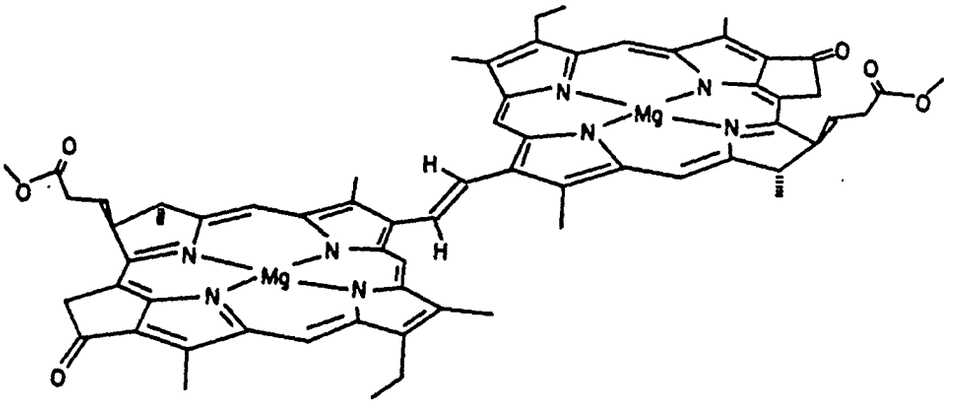

Figure 1. The methyl pyrochlorophyllide *a* dimer

EXPERIMENTAL

The covalently linked dimer of methyl pyrochlorophyllide *a* was prepared and purified using the procedure of Johnson et al. [16]. The solvents used for the experiments were purified by standard methods. The 2-methyl tetrahydrofuran (MTHF) was treated with lithium aluminum hydride and then distilled and stored over molecular sieve (3A or 4A). The toluene was distilled once and stored over sodium/benzophenone (a drying agent) and then vacuum distilled and stored over molecular sieve under nitrogen. The dimethyl formamide (DMF) was treated with neutral alumina then distilled and stored over molecular sieve. Each solvent was freshly prepared before being used. To each solution ~1% pyridine (by volume) was added (certified ACS grade) to preclude aggregation of the dimer. Dimer concentrations used were ~1 x 10^{-5} M based on an ε = 50,000 for the Q_y absorption band. The samples were sealed in glass tubes of ~3 mm I.D. under 4-5 cm of $N_{2(g)}$ to prevent contamination due to water. Absorption spectra were obtained with a Bruker IFS 120 HR Fourier-transform infrared (visible) spectrometer. The resolution was 4 cm^{-1} and each absorption spectrum presented is the average of 50 scans.

Fluorescence spectra were obtained using conventional set-ups in which either an excimer-pumped dye laser or CW He-Ne laser was used as an excitation source. The former, Lambda Physik FL2002 dye laser pumped by a Lambda Physik EMG102 excimer, was also utilized for fluorescence excitation measurements. Fluorescence was dispersed by either 1 m McPherson 2061 (R = 160,000) or 1 m Jarrel-Ash (R = 60,000) monochromator. For CW excitation, a PMT and picoammeter were used for signal processing while for pulsed excitation, either a Tracor Northern TN-6134 intensified diode array and TN-6500 OMA or PMT plus EG & G model 162 boxcar averager (with two model 164 processor modules) were employed. The PMT (RCA 31034C or EMI 9558-B) was cooled. Spectra obtained with the pulsed laser were normalized for pulse intensity jitter.

A model 8DT Janis liquid helium cryostat (convection cooling) was used for T-dependent studies between 4.2 and 300 K. Temperature measurements were made using a Lakeshore Cryotronics DTC-500 K calibrated silicon diode.

RESULTS

The dimer absorption exhibits a marked dependence on the temperature (T). At room T the absorption appears as a single band near 690 nm while at low T it appears as a doublet with components near 685 and 705 nm. The band positions exhibit a slight dependence on solvent, Table I. Temperature dependent spectra are shown in Fig. 2 for toluene. The spectra obtained for T < 160 K are essentially identical to the 160 K spectrum in Fig. 2. The spectra in Fig. 2 are off-set for inspection but their integrated intensities can be directly compared. In so doing it is found that the integrated absorption intensity is independent of T. The absorption band for the methyl pyrochlorophyllide *a* monomer is independent of solvent polarity and located at 660 nm [16]. Thus the dimer bands are significantly red shifted (≥25 nm) relative to that of the monomer. In what follows the two dimer components observed in absorption at low T will be referred to as the 685 and 705 nm bands.

The T-dependence of the dimer fluorescence excited at 632.8 nm (He-Ne laser) has also been determined for three solvents (toluene, MTHF, DMF). The excitation provides a vibrational excess energy for the 685 and 705 nm absorption components of ~1200 and ~1600 cm^{-1}. The excitation energy is too low to provide significant population of the dimer Q_x states at ~585 nm [16]. Spectra for MTHF and DMF are shown in Figs. 3 and 4, respectively. The intensity distributions of the spectra within a given figure can be directly compared. The T-dependence of the dimer fluorescence in toluene is similar to that in MTHF. For all three solvents two fluorescence bands at ~685 and ~720 nm are readily observed for $T \leq T_f$ (freezing point of the solvent). Only the 720 nm fluorescence band is observed for $T > T_f$. Thermal cycling experiments showed that the T-dependence exhibited in Figs. 3 and 4 is reversible.

The narrow line structure seen superimposed on the 685 nm fluorescence band in the lowest T spectra of Figs. 3 and 4 is a consequence of fluorescence line narrowing (FLN) [17]. It is firmly established that narrow line laser excitation into a vibronically congested region of the lowest excited singlet state (S_1) can produce vibrationally relaxed

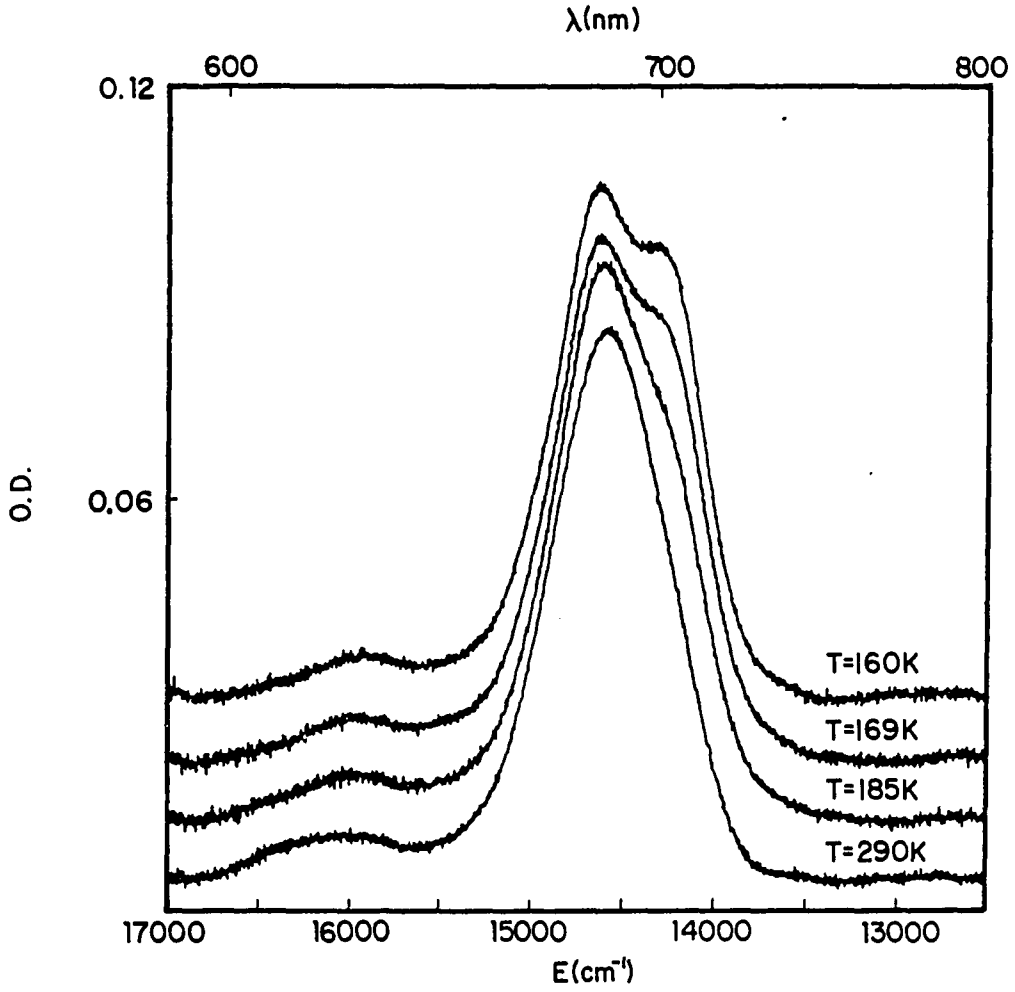

Figure 2. Temperature dependence of the dimer absorption in toluene. Spectra are off-set for clarity but integrated intensities may be directly compared. Spectra for T < 160 K do not exhibit further change

Table I. Absorption and Fluorescence Maxima

Solvent (ε)	T_g, T_m (K)[a]	Abs. Max. (nm)[b]	Fl. Max (nm)[c]	Fl. FWHM (cm^{-1})[d]
toluene (2.4)	117, 178	685, 705	690, 722	400, 650 (3.5:1)
MTHF (7.0)	95, 136	684, 702	690, 720	440, 550 (2.5:1)
DMF (36.7)	129, 212	680, 695	685, 725	360, 560 (5:1)

[a] T_g and T_m are the glass and melting transition temperatures.

[b] Absorption maxima in the low T limit. At room T the single absorption maximum in toluene, MTHF and DMF occurs at 686, 684, and 683 nm, respectively.

[c] Fluorescence maxima in the low T limit.

[d] Full-width-half-maximum for the 685, 720 fluorescence bands. The ratio in brackets is the 720:685 integrated fluorescence intensity ratio obtained with λ_{ex} = 632.8 nm at low T.

and line narrowed fluorescence bands in the region of the $S_0 \Rightarrow S_1$ absorption origin (685 nm region for the case at hand). The displacements of the line narrowed bands from the excitation frequency provide the excited state vibrational frequencies. Vibronically excited FLN spectroscopy has been applied to a variety of biomolecules including photosynthetic pigments [18-20] and DNA-carcinogen adducts [21]. Figure 5 shows the FLN spectrum obtained with λ_{ex} = 632.8 nm. Several of the bands are labeled with their associated excited state vibrational frequency (in cm^{-1}). As expected, the most intense features in Fig. 5 are located in the vicinity of 1200 cm^{-1} since this is the excess vibrational energy produced in the 685 nm state with λ_{ex} = 632.8 nm, vide supra. FLN spectra (not shown) obtained with several other λ_{ex}-values have been obtained and provide, together with Fig. 5, a rather complete picture of the fundamental vibrations for the 685 nm state. These frequencies are in good agreement with those obtained from line narrowed fluorescence excitation spectra. An example of such a spectrum is shown in Fig. 6 for fluorescence detection at 685.0 nm with a 2 cm^{-1} band pass, cf. Section II. Several of the zero-phonon excitation bands are labeled with a cm^{-1} value corresponding to the excited state vibrational frequency. Table II (first column) lists the frequencies and relative intensities of the modes belonging to the 685 nm dimer state provided by the FLN and line narrowed fluorescence excitation spectra. Also presented in Table II are excited state vibrational frequencies for Chl *a* in diethyl ether glass @ 5 K (third column) [18] and ground state vibrational frequencies for oligomers of pyrochlorophyll *a* @ 35 K (second column) [22]. Reasonable agreement exists between the vibrational frequencies and relative intensities for the dimer with those from these references. The FLN and line narrowed excitation spectra establish that the 685 nm fluorescence originates from the 685 nm absorbing dimer state. The small Stokes shift observed for the 685 nm state is consistent with small Franck-Condon factors for both the intramolecular and phonon modes. In addition, these spectra establish that the width of the 685 nm absorption band at low T is dominated by site inhomogeneous line broadening. This has also been confirmed by the nonphotochemical hole burned spectra for the 685 nm band (spectra not shown).

In contrast with the 685 nm emission, FLN for the 720 nm emission was not observed even with λ_{ex}-values significantly higher than 632.8 nm. The fluorescence observed appeared as it does with λ_{ex} = 632.8 nm, cf. Figs. 3 and 4. In order to determine whether the 720 nm fluorescence is connected with the 705 nm absorption band, fluorescence excitation spectra were obtained as a function of temperature for a detection wavelength of 730 nm (band pass = 30 cm^{-1}). Figure 7 shows the dependence of the fluorescence excitation band maximum on temperature for toluene. Also shown in this figure is the dependence of the 720 nm fluorescence band position on temperature. For both sets of data a significant band shift occurs near 180 K, which is close to the freezing point of toluene (T_f = 178 K [23]). From Fig. 7 it can be seen that the low and high T values for the fluorescence excitation band maximum are ~706 and 694 nm. This ~12 nm shift is the same as that observed for the 720 nm fluorescence band within experimental uncertainty. This together with the similarity between the two solid curves in Fig. 7 indicate that the 720 nm fluorescence originates from the 705 nm absorbing dimer state. Thus, this state is characterized by a Stokes shift of ~15 nm (~300 cm^{-1}), far larger than the Stokes shift for the 685 nm dimer state. These two dimer states are further contrasted by the facts that the maximum of the 685 nm band is only weakly dependent on the temperature and does not undergo an abrupt change at T~T_f.

Table II. Vibrational modes for the 685 nm dimer state

Excited State frequency (cm^{-1})[a]	Ground State frequency (cm^{-1})[b]	Excited State frequency (cm^{-1})[c]
298-W	307	
313-VW	317	
345-VS		348-S
364-M	358	
376-M		
384-M	390	390-W-Br
563-W		
570-S	572	570-W
595-M	603	600-VW
617-VW		
688-W		688-VW
711-W	703	
728-VW	733	
755-S	753	748-S
773-W		765-VW
804-M	803	
842-M	851	
868-M		
888-M		890-VW
903-S		910-VW
918-VS	918	925-W
931-S		
953-VW		

[a]Excited state vibrational frequencies this work. Relative intensities: S = Strong, M = Medium, V = Very, Br = Broad, sh= shoulder.

[b]From resonance Raman of pyrochlorophyll *a* oligomers. See ref. [24].

[c]Excited state vibrational frequencies of Chl *a* monomers. See ref. [20].

Table II. Continued

Excited State frequency (cm^{-1})[a]	Ground State frequency (cm^{-1})[b]	Excited State frequency (cm^{-1})[c]
990-VS	985	984-VS
1002-M		1005-VW
1011-W		
1025-M		1030-VW
1056-S	1046	
1083-M		1075-W-Br
1098-W		
1121-M	1115	1110-W
1148-S	1147	1135-W
1169-M	1162	1168-W
1181-S	1188	
1195-W		1195-VW
1244-S		1243-sh
1249-S		1250-VS
1270-S	1266	1275-VW
1288-S	1290	
1317-S	1312	1325-VW
1383-M	1380	1372-W
1402-M	1392	1395-VW
1565-W	1560	

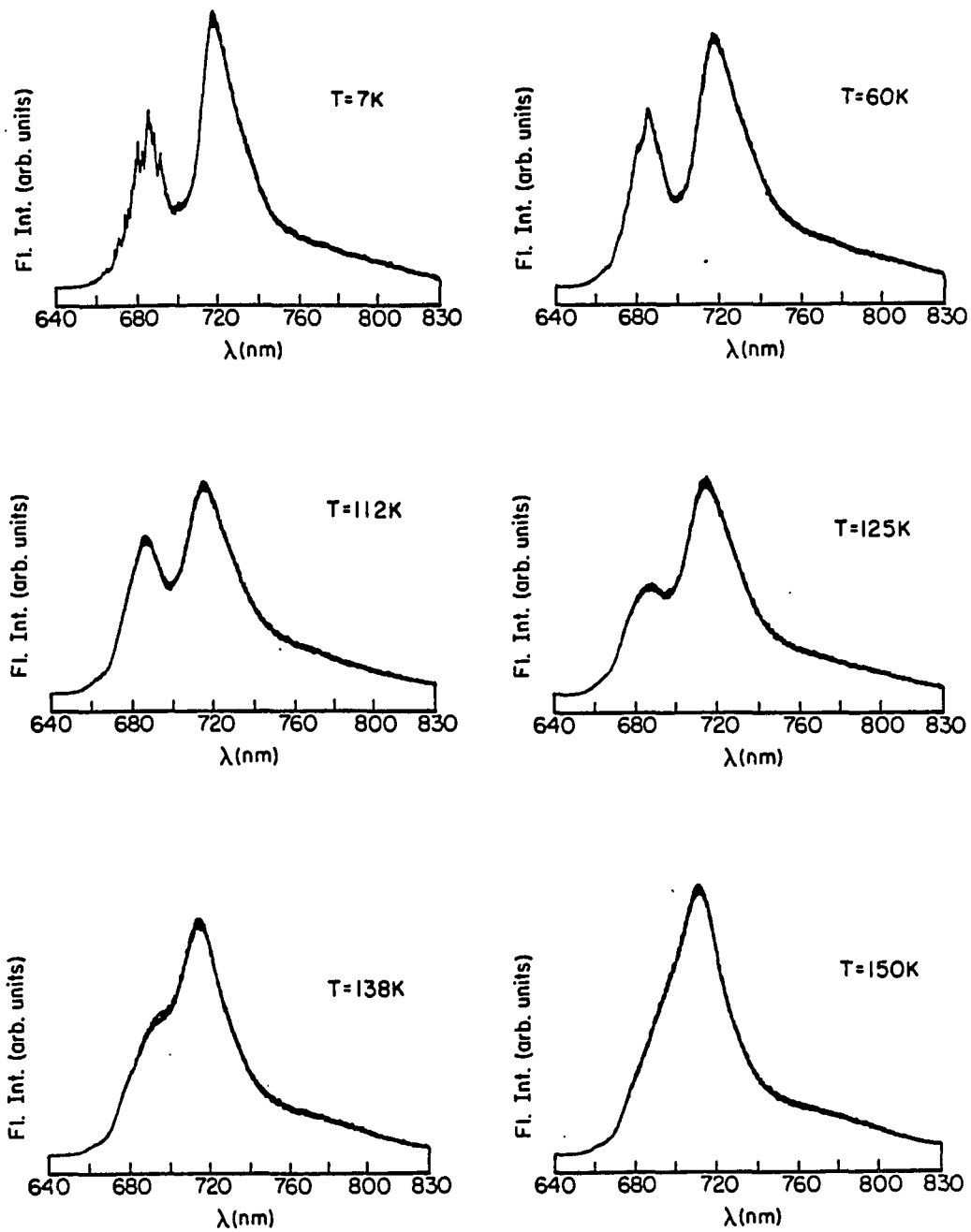

Figure 3. Temperature dependence of the dimer fluorescence in MTHF. λ_{ex} = 632.8 nm, 10 cm^{-1} resolution. Integrated intensities for different temperatures may be directly compared

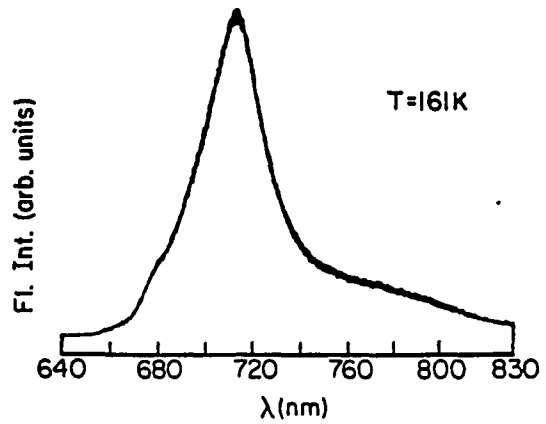

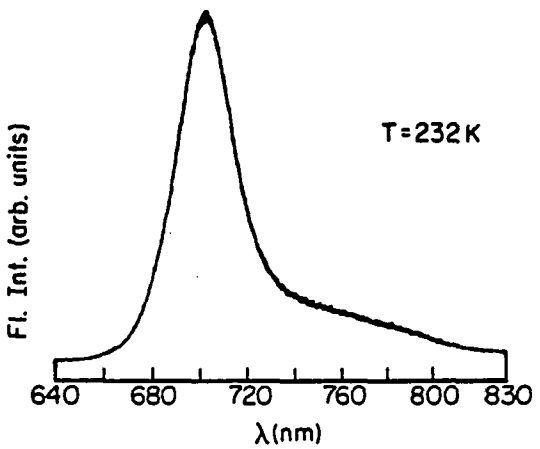

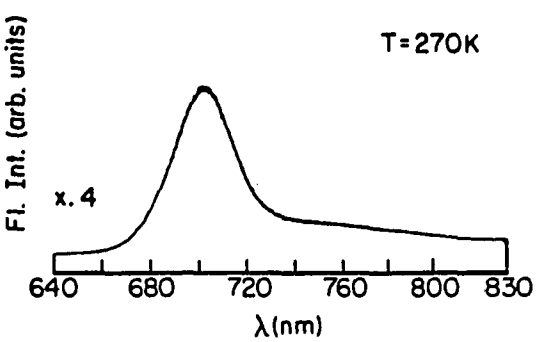

Figure 3. Continued

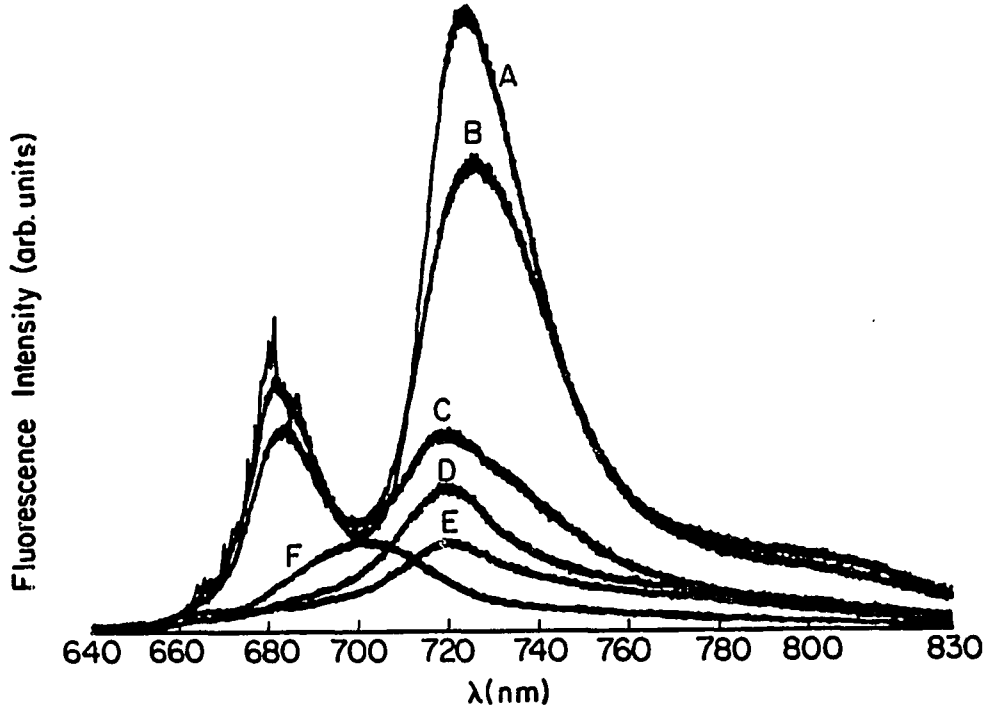

Figure 4. Temperature dependence of the dimer fluorescence in DMF. A = 5 K, B = 91 K, C = 140 K, D = 176 K, E = 201 K and F = 270 K. See Fig. 3 caption

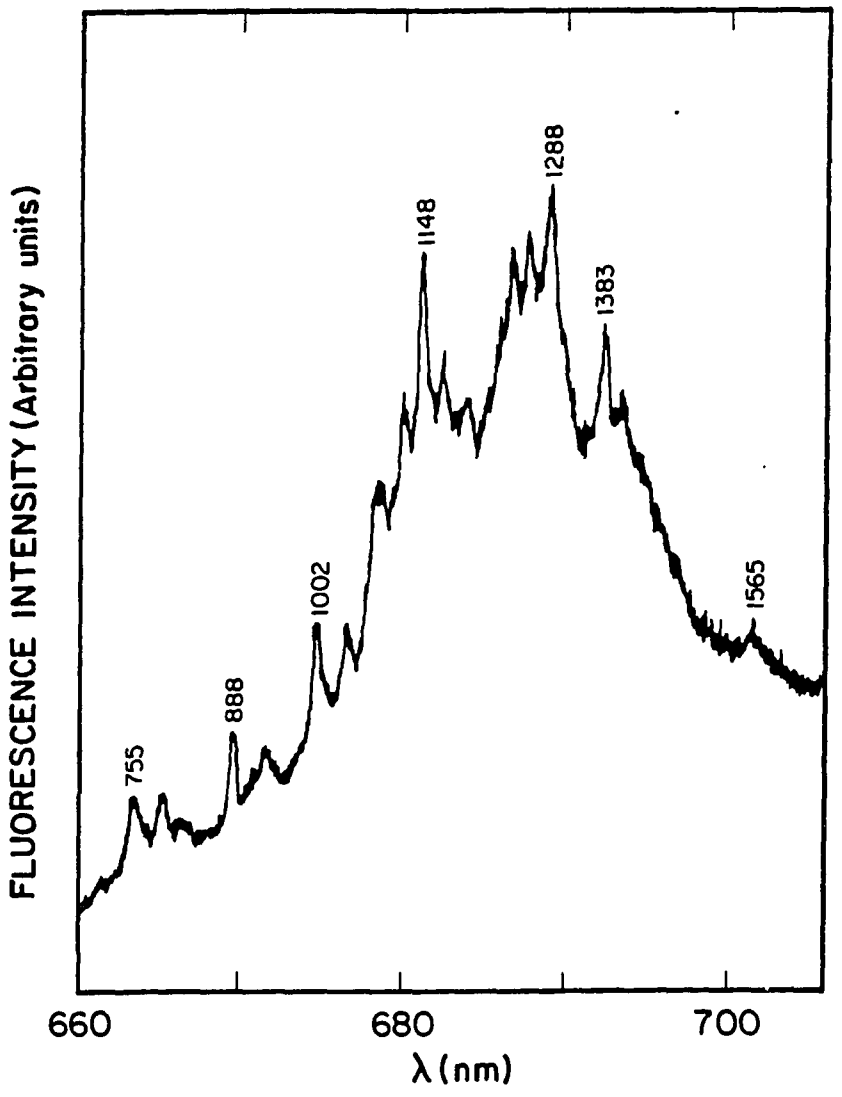

Figure 5. Fluorescence line narrowed spectra associated with the 685 nm emission. In toluene, 5 K, 8 cm^{-1} resolution

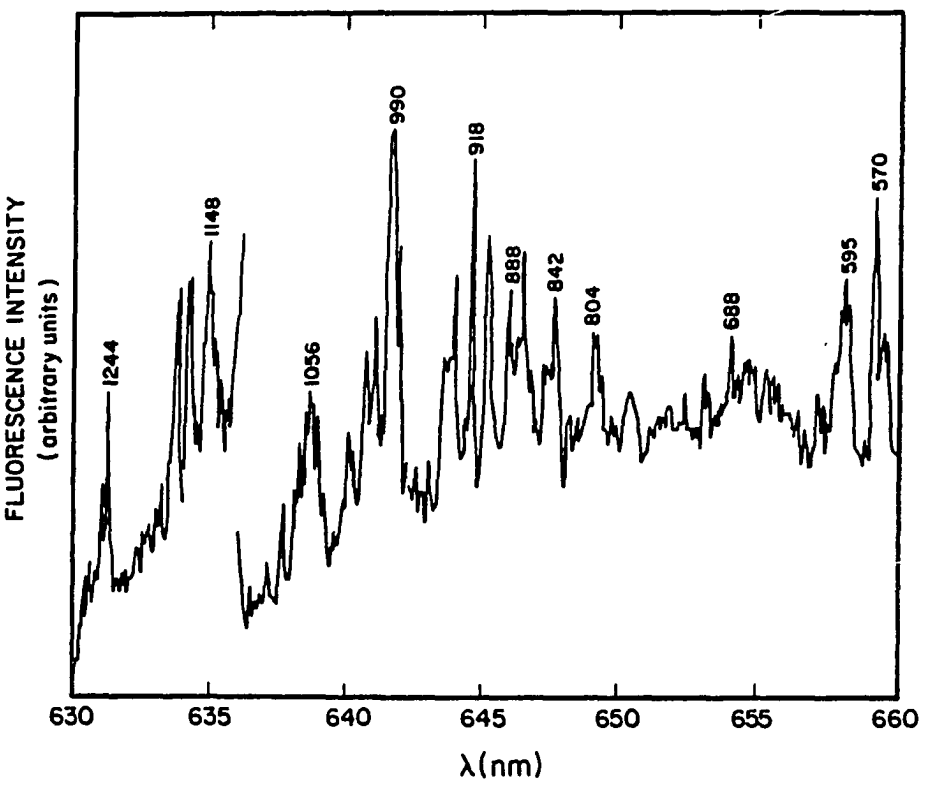

Figure 6. Line narrowed fluorescence excitation spectra. Observation at 685 nm, T = 5 K, 2 cm^{-1} resolution

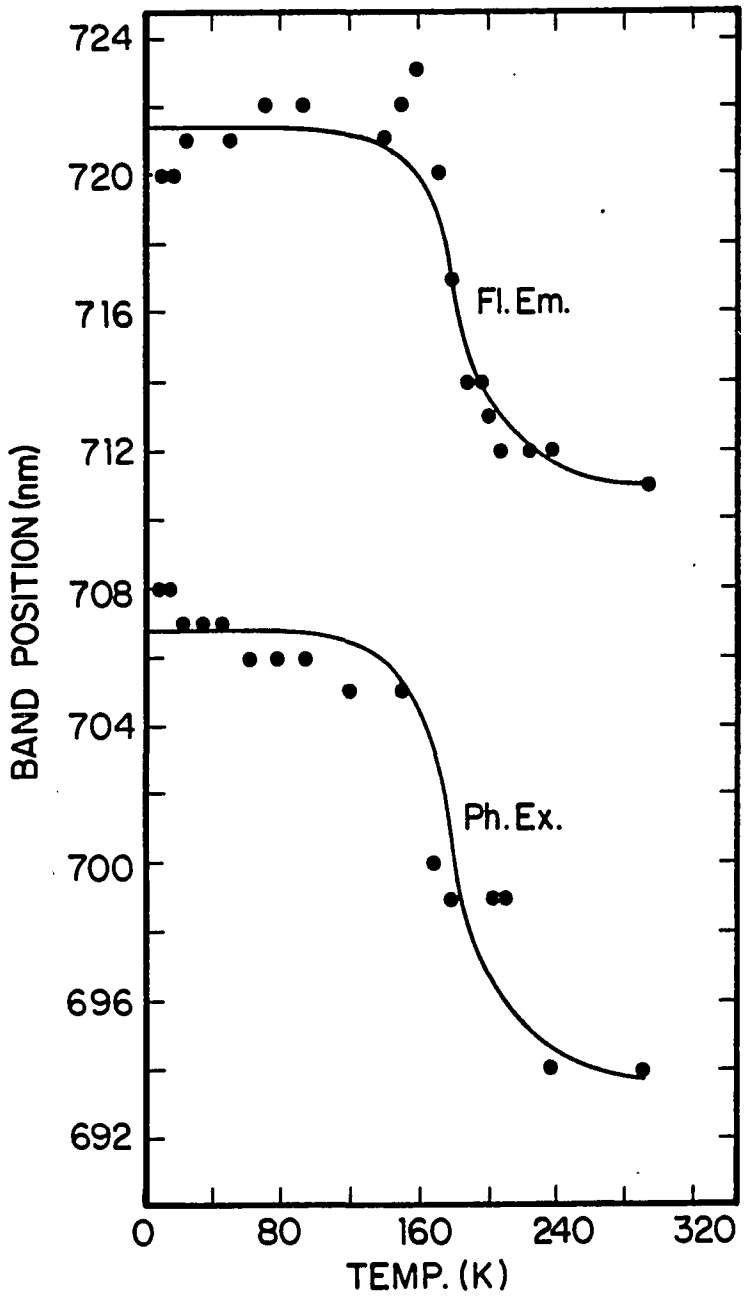

Figure 7. Temperature dependence of the fluorescence (720 nm) and photoexcitation (observation at 730 nm) band positions in toluene

DISCUSSION

Temperature-dependent Absorption and Fluorescence Spectra

The results of the preceding section establish that the (685, 705) nm absorption bands are due to the two electronic states responsible for the (685, 720) nm fluorescence bands. The possibility that one of the two absorption bands is due to an impurity (monomer or dimer) can be ruled out since the HPLC and ^{1}H-NMR analyses of the extensively purified dimer yield a limit for an impurity concentration that is no greater than 5% [16]. Deconvolution [24] of the low T absorption spectrum in Fig. 2 yields a 685:705 integrated intensity ratio of about unity. This is inconsistent with either of the two components being due to an impurity (at a level of < 5%) since the measured molar extinction coefficient is consistent with a Q_y transition (~50,000 at room T). Furthermore, the T-dependent fluorescence data for toluene and MTHF show that the loss of 685 nm fluorescence intensity for $T \geq T_f$ is compensated by a gain in the 720 nm fluorescence intensity, vide infra. This is not consistent with the behavior of an isolated impurity. The T-dependent fluorescence behavior also argues against the 705 nm absorption band being due to an aggregate(s) of the dimer (analogous to aggregates of Chl monomers [25,26]). Furthermore, the solvent purification procedure and the addition of ~1% pyridine (an excellent ligand for Mg) should preclude aggregate formation especially since dilute solutions (~10^{-5} M) were used in the experiments. Typically, aggregation requires much higher concentrations, on the order of 10^{-2}-10^{-3} M [25-27].

We proceed now to consider the possibility that a <u>single</u> dimer conformation (e.g., as in Fig. 1) can account for the T-dependent absorption and fluorescence data. To do so requires a consideration of the exciton model for the dimer whose constituent monomers possess Q_y-transition moments which are anti-parallel (180° out-of-phase). We denote the two dimer states by $P_{\pm}$ (+ and - indicating symmetric and antisymmetric with respect to the dimer symmetry axis) and the Davydov splitting by 2 V. In the absence of symmetry

breaking (e.g., due to the solvent), only the P_- state carries oscillator strength and, furthermore, it is this state that lies lower in energy since $V > 0$ [28]. Clearly, the presence of two absorption bands cannot be reconciled with this model. Consider next that solvent-induced symmetry breaking scrambles P_+ and P_- to an extent that endows them with comparable oscillator strengths or that the conformation of the dimer is not that shown in Fig. 1. This single conformation would be one for which the monomer transition dipoles are not anti-parallel (or parallel) so that both P_+ and P_- carry oscillator strength [29]. There are several difficulties with both of these possibilities. First, it is well documented for organic crystals that [30-32] relaxation from an upper exciton (Davydov) level to a lower energy exciton level occurs on a picosecond or subpicosecond time scale even at very low T. Very recently, a decay time of 260 fsec at 1.6 K has been measured for an upper exciton level of the 7-bacteriochlorophyll *a* containing protein subunit of the light harvesting complex from Prosthecochloris aestuarii [33]. The theory for such relaxation has been extensively developed [34-37] and shows that the relaxation is induced by low frequency intermolecular aggregate modes which modulate the resonance energy transfer integrals. In the absence of these modesw or perturbing solvent modes, such relaxtaion is forbidden [38]. There is no precedent for the suggestion that the observation of the 685 nm fluorescence at low T is due to very slow (~nsec) decay of the 685 nm exciton level to the 705 nm level. Second, the observation that the 685 nm level abruptly begins to decay at $T \sim T_f$ is difficult to reconcile in terms of existing theories for inter-exciton level relaxation. Third, if the 685 and 705 nm absorption bands are exciton components of a single dimer configuration, then it is necessary to explain why the 705 and 685 nm levels shift and do not shift (respectively) appreciably with temperature. That is, the Davydov splitting is T-dependent but the energy of the upper component is T-independent. This could occur if the expected shift for the upper component was cancelled by the T-dependence of the dispersion energy. However, this possibility is viewed as extremely remote.

Thus, we conclude that the T-dependent fluorescence and absorption data cannot be understood in terms of a single conformation of the dimer shown in Fig. 1. Consequently, a model in which two stable conformations (A and B) of the dimer exist is

explored next. The 685 and 705 nm absorption bands will be considered to be the Q_y-origin bands of A and B. Possible conformer structures will be considered later, section IV. B. Hypothetical potential energy curves for the ground and excited states of the dimer are given in Fig. 8 (solid curves). The potential well minima for conformer B are shifted relative to each other because of the Stokes shift associated with the 705 nm state. For each of the solvents used the integrated absorption intensity remains constant as the temperature increases from the low T limit (where the 685 and 705 nm components are resolved) to room T (where only a single absorption band is apparent). The spectra for all solvents, e.g., Fig. 2, show that as T increases past ~T_f, the 705 nm band blue shifts until it merges with the 685 nm band. The data in Fig. 7 for toluene indicate that at room T the 705 nm band has shifted to ~694 nm. Within our experimental uncertainty, the 685 nm band does not appear to shift with temperature. It was argued above that the 705 nm state or conformer B emits at 720 nm. Furthermore, the 720 nm fluorescence band is present at all temperatures. All three factors indicate that both A and B are stable conformers at room T. The low temperature absorption spectra then establish that conformers A and B have comparable concentrations (making the reasonable assumption that their oscillator strengths are similar). Deconvolution of the low T absorption profiles in terms of two Gaussians showed that 685 and 705 nm absorption bands are equal in intensity (± 30%) for toluene, MTHF and DMF. However, the fluorescence spectra obtained with λ_{ex} = 632.8 nm show that the 720 nm fluorescence is 3-5 times more intense than the 685 nm fluorescence at low T, Table I. This excitation wavelength should excite A and B with nearly equal probability, Fig. 2. Obvious (but unsubstantiated) arguments involving differences in oscillator strengths and radiationless decay constants for A and B could be presented to explain the greater fluorescence intensity from B.

We consider now the T-dependence of the 685 nm fluorescence band. For all solvents the intensity was constant from T~5 K to T_g, where T_g is the glass transition temperature, Table I. As the temperature was increased above T_g, the fluorescence intensity rapidly diminished. By T~T_f (Table I), the 685 nm fluorescence was not detectable. As discussed earlier, the diminution of this fluorescence for toluene and MTHF

is compensated by a gain in the intensity of the 720 nm emission. Thus, it appears that large amplitude solvent motion is required for relaxation from the 685 nm state of A to the 705 nm state of B. If one assumes that for $T \geq T_g$ the two conformers in their excited state are in thermal equilibrium, the T-dependence of the 685 nm fluorescence intensity leads to $\Delta' = 360$ and 475 cm^{-1} for MTHF and DMF, respectively, cf. Fig. 8. Considering for the moment that in Fig. 8 $\Delta = 0$ and noting that the 685 and 705 nm absorption bands are separated by ~ 400 cm^{-1}, it follows that Δ' = (400 + 1/2 Stokes shift) for the case where $\omega' \sim \omega$, Fig. 8. The Stokes shift is ~300 cm^{-1}, Table I, so that a calculated value for Δ' is 550 cm^{-1}. Improved agreement with the experimental values for MTHF and DMF can be achieved by allowing for $\Delta < 0$ and/or $\omega' < \omega$. Indirect evidence for $\omega' < \omega$ is that the low T FWHM of the 705 nm absorption band (from deconvolution) is about 100 cm^{-1} narrower than the FWHM of the 720 nm fluorescence band in all solvents used.

To conclude this section we consider the T-dependent fluorescence spectra for DMF shown in Fig. 4. Although the behavior for the 685 nm fluorescence band is similar to those for toluene and MTHF, the T-dependence of the 720 nm band is distinctly different. That is, the latter band undergoes a significant decrease in intensity as T is increased above ~120 K (T_g = 129 K). By room T its intensity decreased by about a factor of ten. This interesting behavior is best discussed in the context of the recent time domain studies, section IV. C.

Possible Dimer Conformations

The data presented above indicate that relaxation from conformer A to B occurs with a rate competitive with fluorescence as T approaches T_g. At $T \sim T_f$, the relaxation rate has significantly increased to the point where fluorescence from A is no longer observable. Detailed considerations of the dimer structure, Fig. 1, indicate that the most plausible intra-dimer vibrational coordinate for conformational relaxation is "bicycling" by the two single bonds joined to the vinyl group linkage. The dihedral angle between the olefinic linkage and the macrocycles shown in Fig. 1 is ~50°. A computer molecular model program

(BIOGRAF) was used to gauge the steric limitations imposed by the α-, vinyl and 1-methyl protons on bicycling. The 12-C and 2-C and ethylenic carbons were used to define the dihedral angle discussed throughout this paper (the chlorophyll carbons being numbered in the standard manner [4]). It was found that dihedral angles between ~50° and ~140° satisfied the van der Waal's requirements for the above protons with the macrocyclic planes in a parallel configuration. It is important to note that π-electron delocalization between the two macrocycles via the vinyl group would be minimized for the 90° position and that this configuration could lead to formation of a TICT state (twisted intramolecular charge transfer state). We return to this point in section IV. C but note now that such a state could be expected to experience a significant stabilization in a high polarity solvent such as DMF.

Calculations of the potential energy minima along the bicycling coordinate would require consideration of atom-atom interactions and the π-electron stabilization energy associated with partial conjugation across the bridge between the two macrocycles (for both the ground and excited electronic states). In the absence of such calculations it is, nevertheless, clear that more than one thermally accessible conformation is entirely plausible, consistent with the conclusion of the preceding section that the dimer exists in two conformations (A and B) in all solvents utilized. The correlation between the onset of relaxation of conformer A with the glass transition temperature, T_g, is convincing evidence for the importance of large amplitude solvent motion for configurational change in the dimer. However, the excited state energies of A and B (685 and 705 nm states) and the Stokes shift for B are not very sensitive to solvent polarity, Table I. But, again, solvent polarity has a profound effect on the radiationless decay of the 705 nm state at higher temperatures.

Radiationless Decay of the 705 nm State of Conformer B

The data presented here establish that for a solvent of sufficiently high polarity such as DMF (ε = 37), an efficient radiationless decay channel for the 705 nm state of

conformer B (emission at 720 nm) is accessed. This observation provides a connection with the picosecond transient absorption, fluorescence quantum yield and stimulated emission studies of Johnson et al. [16] (referred to hereafter as JSW), which were performed at room T with a series of solvents of different polarity. At room T JSW were only able to monitor the 720 nm emission band. They observed a two order of magnitude decrease in fluorescence quantum yield from toluene ($\varepsilon = 2$, $\phi_{fl} = 0.18$) to DMF ($\varepsilon = 37$, $\phi_{fl} = 0.002$), $\lambda_{ex} = 425.0$ nm. A stimulated emission feature was observed in the transient absorption spectra which coincides with the 720 nm fluorescence maximum. Excitation was at 610 nm (an important fact for what follows). The stimulated emission observed by JSW exhibited a rise time (τ_s) which was solvent dependent, varying from $\leq$1.5 psec for DMF to 18 psec for toluene (the least polar solvent used).

In what follows, the two conformer model for the dimer suggested in this paper is shown to provide a qualitative explanation for the data of JSW when relaxation of the 705 nm state into a charge-transfer (CT) state is invoked. Such a state was discussed by JSW. However, in view of the data presented here, this model was realized to present certain difficulties. For example, the rise time (τ_s) was assumed to arise from the decay of the upper exciton level of the dimer shown in Fig. 1 to the dipole allowed lower exciton level (P_-). The former (P_+) is dipole forbidden, in the absence of solvent perturbations, and it was difficult to understand why excitation at 610 nm should preferentially excite P_+ rather than P_+. Excitation of the latter would lead to prompt stimulated emission (excitation at 610 nm is lower than the onset of absorption due to Q_x transitions). No prompt stimulated emission was detected [16].

Within the two conformer (685, 705 nm) model, the τ_s data can be understood as follows. The $\lambda_{ex} = 610$ nm utilized by JSW provides ~1600 cm^{-1} vibrational excitation for conformer A absorbing at ~685 nm, Table I. From the point of view of maximal vibronic Franck-Condon factors, this is an optimal region for chlorophyllic species [18,39]. On the otherhand, an additional ~250 cm^{-1} of vibrational energy is provided for the excited state of B which should lead to a decrease in the Franck-Condon factor by about a factor of 10 [39]. Thus, $\lambda_{ex} = 610$ nm preferentially excites conformer A by an amount governed by

this factor. Therefore, it may be concluded that the stimulated emission rise time is a direct measure of the rate of relaxation from conformer A to B at room T.

To account for the marked dependence of the 720 nm fluorescence lifetime on solvent polarity, we follow JSW and suggest that solvents with sufficiently high polarity stabilize a CT state to an extent which places it sufficiently close to the 705 nm state to allow for its decay. Such a CT state is schematically shown in Fig. 8 as the dashed potential energy curve. We hasten to add that the CT state needn't lie lower in energy than the 705 nm state of B for efficient relaxation of the latter into the former, as recently discussed by Won and Friesner [40] in connection with charge separation in photosynthetic reaction centers. On the otherhand the CT state can't lie too far above 705 nm, as is apparently the case for nonpolar solvents such as toluene. A quantitative discussion of this point requires knowledge of the exchange interaction between the 705 nm state (which may be assumed to be excitonic) and the CT state as well as the relevant electron-vibration coupling strengths of the two states [38]. These are not known. However, the weak dependence of the Stokes shift of the 705 nm state on solvent polarity establishes that this shift is primarily a consequence of configurational displacement within the dimer, as suggested by Fig. 8. The good correlation between the fluorescence quantum yield and lifetime data presented by JSW establishes that the 685 nm state does not decay directly into the CT state but indirectly via the 705 nm state. On the basis of the electrochemical data presented by JSW, one can roughly estimate that the hypothetical CT state would lie about 1000 cm^{-1} above the 705 nm state. JSW were not able to observe fluorescence from the proposed CT state. This suggests that this state is dark or that it emits in the ir (> 900 nm).

A possible candidate for the CT state is a TICT state of the type mentioned in Section IV. B. and associated with the 90° dihedral angle. Very often TICT states are observed to exhibit fluorescence whose maximum depends sensitively on solvent polarity, viscosity and temperature [41,42]. However, there are several examples of compounds for which convincing evidence for a nonemissive TICT state has been presented [43-45].

In summary, we have established that relaxation from the 685 nm dimer state of conformer A to the corresponding state of B at 705 nm onsets at $T \sim T_g$ in solvents of widely differing polarity. Thus, large amplitude solvent motion is required for relaxation from A to B to occur on the nsec to picosecond time scale. At the same time the energies of the above two states do not depend strongly on solvent polarity. Molecular modeling suggests that the two conformations of the dimer are related by motion along the bicycling coordinate discussed in section IV. B. It is further demonstrated that a radiationless decay channel for B's 705 nm state opens at $T \sim T_g$, but only in solvents of sufficiently high polarity, e.g., DMF. The fact that this channel in DMF is closed at $T \leq T_g$ indicates that solvent motion is required for the formation of a new excited state dimer configuration, which acts as a precursor for decay into a CT state. If the CT state is a TICT state, this new configuration would be one for which the dihedral angle is ~90° (see Section IVB). For this model, the dihedral angle for B would be intermediate in value between 90° and 50° since direct decay from the 685 nm state of A (dihedral angle ~50°) into the CT state (dihedral angle ~90°) does not occur. Decay occurs from conformer A to the CT state only through the 705 nm state of B.

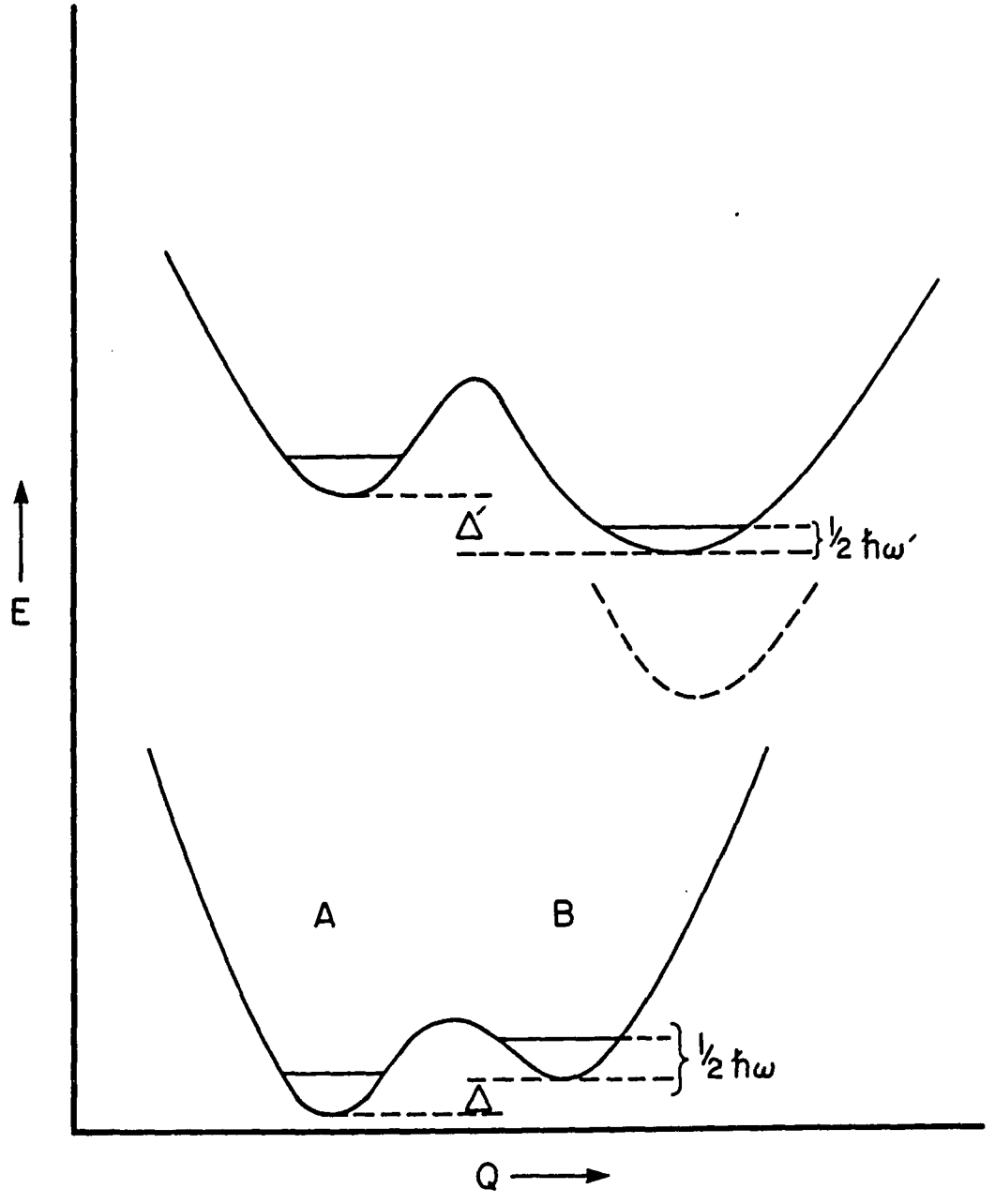

Figure 8. Hypothetical potential energy curves for two conformers of the dimer

CONCLUDING REMARKS

The T-dependent data presented here establish that the methyl pyrochlorophyllide *a* dimer exists in two conformations, A and B. It is suggested that the picosecond stimulated emission (720 nm) rise time (τ_s) data [16] reflect excited state relaxation from conformer A to B at room temperature. To better understand the dependence of this relaxation on solvent (τ_s= 18 psec for toluene, ≤1.5 psec for DMF) will require the measurement of τ_s as a function of temperature for different pumping wavelengths. The solvent dependence observed at room T might reflect solvent dynamics or the fact that the barrier height in the excited state, Fig. 8, is determined, in part, by solvent-dimer interactions. The observation that the relaxation onsets (becomes competitive with fluorescence) for T~T_g proves that solvent dynamics can be expected to be rate limiting at lower temperatures in the range $T_g \leq T \leq 300$ K. This needn't be the case at room temperature.

In addition to the excited Q_y states of A and B, a third excited state (CT) has been implicated as a decay channel for the Q_y (705 nm) state of B in solvents of sufficiently high polarity. The observation that this channel opens (is competitive with fluorescence) for T~T_g suggests that large amplitude solvent motion is the first step of the relaxation dynamics. It will be important in future studies to measure the T-dependence of the 705 nm state emission (at 720 nm) lifetime in high polarity solvents. Although the association of the third excited state with a CT state (a TICT state was considered) is reasonable, it is not proven. It is conceivable, for example, that radiationless decay ($S_0 \Rightarrow S_1$) from the excited state conformation of B achieved by solvent motion ($T \geq T_g$) would be polarity-dependent.

The reason why the Stokes shift (linear electron-phonon coupling) is moderately large for conformer B (but small for A) is not clear. The absence of fluorescence line narrowing for B's 720 nm emission is consistent with strong electron-phonon coupling. The Stokes shift, given approximately by $2S\omega$ where ω is a mean phonon frequency, is about 300 cm^{-1} in all solvents measured. If we take ω~30-50 cm^{-1}, then S~5-3. Since the

Franck-Condon factor for the zero-phonon transition is exp(-S), S-values in this range would render this transition quite highly Franck-Condon forbidden. In future studies it will be important to perform nonphotochemical hole burning [46] on the 705 nm absorption band (and the 685 nm band for comparison) in different glassy solvents in order to determine ω and whether this effective mode frequency is associated with an intra-dimer (e.g., bicycling) or a solvent coordinate.

Finally, we comment that while there are some similarities between the spectroscopic, electronic structural and photophysical properties of the synthetic dimer and the special pair of photosynthetic bacterial reaction centers, the ability of the former to assume different conformations may set it apart from the special pair in which conformational changes are, as yet, unobserved. Nevertheless, the synthetic dimer presents very interesting possibilities for future studies on the static and dynamic roles of solvents in intramolecular conformational changes and the interaction of excitonic and CT states.

ACKNOWLEDGEMENT

The Ames Laboratory is operated for the U.S. Department of Energy by Iowa State University under Contract No. W-7405-Eng-82. The research at the Ames Laboratory was supported by the Director for Energy Research, Office of Basic Energy Sciences. The Argonne work was supported by the Division of Chemical Sciences, Office of Basic Energy Sciences, U.S. Department of Energy under Contract No. W-31-109-ENG-38. S.G.J. would like to acknowledge Mr. Daniel S. Zamzow and Dr. Ryszard Jankowiak of Ames Laboratory for technical assistance and Prof. Keith Woo of Iowa State University for helpful discussions regarding structural aspects.

REFERENCES

1. Deisenhofer, J.; Epp, O.; Miki, K.; Huber, R.; Michel, H. J. Mol. Biol. 1984, 180, 385.
2. Allen, J. P.; Feher, G.; Yeates, T. O.; Rees, D. C.; Deisenhofer, J.; Michel, H.; Huber, R. Proc. Natl. Acad. Sci. USA 1986, 83, 8589.
3. Chang, C. H.; Tiede, D.; Tang, J.; Smith, U.; Norris, J.; Schiffer, M. FEBS Lett. 1986, 205, 82.
4. Katz, J. J.; Hindman, J. C., In Biological Events Probed by Ultrafast Laser Spectroscopy, Alfano, R. R., Ed.; Academic Press: New York, 1982, p 119.
5. Wasielewski, M. R., In Light Reaction Path of Photosynthesis, Fong, F. K., Ed.; Springer-Verlag: West Berlin, 1982, p 234.
6. Boxer, S. G. Biochim. Biophys. Acta 1983, 726, 265.
7. Fong, F. K. Proc. Natl. Acad. Sci. USA 1974, 71, 3692.
8. Shipman, L. L.; Cotton, T. M.; Norris, J. R.; Katz, J. J. Proc. Natl. Acad. Sci. USA 1976, 73, 1791.
9. Wasielewski, M. R.; Smith, U. H.; Cope, B. T.; Katz, J. J. J.A.C.S. 1977, 99, 4172.
10. Wasielewski, M. R.; Studier, M. H.; Katz, J. J. Proc. Natl. Acad. Sci. USA 1976, 73, 4282.
11. Boxer, S. G.; Closs, G. L. J.A.C.S. 1976, 98, 5406.
12. Pellin, M. J.; Wasielewski, M. R. Nature 1979, 278, 54.
13. Yuen, M. J.; Closs, G. L.; Katz, J. J.; Roper, J. A.; Wasielewski, M. R.; Hindman, J. C. Proc. Natl. Acad. Sci. USA 1980, 77, 5598.
14. Bucks, R. R.; Netzel, T. R.; Fujita, I.; Boxer, S. G. J. Phys. Chem. 1982, 86, 1947.
15. Agostiano, A.; Butcher, K. A.; Showell, M. S.; Gotch, A. J.; Fong, F. K. Chem. Phys. Lett. 1987, 137, 37.
16. Johnson, D. G.; Svec, W. A.; Wasielewski, M. R. Israel J. Chem. 1988, 28, 193.

17. Personov, R. I. In Spectroscopy and Excitation Dynamics of Condensed Molecular Systems, Agranovich, V. M. and Hochstrasser, R. M., Eds.; North-Holland: Amsterdam, 1983, p 555.

18. Avarmaa, R. A.; Rebane, K. K. Spectrochimica Acta 1985, 41A, 1365.

19. Fünfschilling, J.; Williams, D. F. Photochem. Photobiol. 1977, 26, 109.

20. Avarmaa, R. A.; Rebane, K. K. Chem. Phys. 1982, 68, 191.

21. Jankowiak, R. J.; Cooper, R. S.; Zamzow, D. S.; Small, G. J.; Doskocil, G.; Jeffrey, A. M. Chemical Research Toxicology 1988, 1, 60.

22. Lutz, M. In Advances in Infrared and Raman Spectroscopy, Clark, R. J. H. and Hester, R. E., Eds.; Wiley Heydon: London, 1984, Vol. 11, p 211.

23. CRC Handbook of Chemistry and Physic, Weast, R. C., Ed.; CRC Press: BocaRaton, 1979.

24. This was performed with a computer varying the positions, full width at half maximum and relative intensities of two gaussians to fit the origin contribution to the Q_y absorption band.

25. Amster, R. L. Photochem. Photobiol. 1969, 9, 331.

26. Cotton, T. M.; Loach, P. A.; Katz, J. J.; Ballschmiter, K. Photochem. Photobiol. 1978, 27, 735.

27. Brody, S. S.; Broyde, S. B. Biophys. J. 1968, 8, 1511.

28. Calculations performed using the dipole-dipole approximation yielded V = 120 cm^{-1} for the conformation in Figure 1.

29. Davydov, A. S. Theory of Molecular Excitons; Plenum:New York, 1971.

30. Craig, D. P. and Walmsley, S. H.Excitons in Molecular Crystals; W. A. Benjamin: New York, 1968.

31. Port, H.; Rund, D.; Small, G. J.; Yakhot, V. Chem. Phys. 1979, 39, 175.

32. Johnson, C. K.; Small, G. J. In Excited States, Lim, E. C., Ed.; Academic Press: New York, 1982, Vol. 6, p 97.

33. Johnson, S. G.; Small, G. J. Chem. Phys. Lett. 1989, 155, 371.

34. Craig, D. P.; Dissado, L. A. Chem. Phys. Lett. 1976, 44, 419.

35. Clark, M .; Craig, D. P.; Dissado, L. A. Mol. Cryst. Liq. Cryst. 1978, 44, 309.

36. Toyozawa, Y. J. Lumin. 1970, 1/2, 732.

37. Yarkony, D.; Silbey, R. J. Chem. Phys. 1976, 65, 1042.

38. Freed, K. J.A.C.S. 1980, 102, 3130.

39. Gillie, J. K.; Small, G. J.; Golbeck, G. H. J. Phys. Chem. 1989, 93, 1620.

40. Won, Y.; Friesner, R. A. J. Phys. Chem. 1988, 92, 2214.

41. Rettig, W. Angew. Chem. Int. Ed. Engl. 1986, 25, 971.

42. Heldt, J.; Gormin, D.; Kasha, M. Chem. Phys. Lett. 1988, 150, 433.

43. Jones, G.; Jackson, W. R.; Halpern, A. M. Chem. Phys. Lett. 1980, 72, 391.

44. Jones, G.; Jackson, W. R.; Choi, C.-Y.; Bergmark, W. R. J. Phys. Chem. 1985, 89, 294.

45. Lippert, E.; Rettig, W.; Bonacic-Koutecky, V.; Heisel, F.; Miehé, J. A. Adv. Chem. Phys. 1987, 68, 1.

46. Small, G. J., In Spectroscopy and Excitation Dynamics of Condensed Molecular Systems, Hochstrasser, R. M., Ed.; North-Holland: Amsterdam, 1983, p 515.

ADDITIONAL RESULTS AND DISCUSSION

A small number of hole burn experiments were performed on the dimer. A more extensive study had been planned, however, appropriate burning wavelengths proved unobtainable with our laser system at that time. For these experiments the solvent was not one of the three featured in paper I in this section but was n-bromo butane. This is a relatively nonpolar solvent which was purified prior to the experiment and contained 1% (by vol.) pyridine. The absorption spectra displayed two absorbing species, 685 nm and 705 nm, at T=1.6 K similar to the other three solvents used in this study. The hole burning experiments were conducted at T=1.6 K.

Figure 1 shows a typical hole (λ_B=684.40 nm). The percentage change in optical density (ΔOD) is 14% at λ_B. The hole was read using a double beam absorption apparatus with a read resolution of 0.2 cm^{-1}. The laser used for the experiments was a Coherent 699 ring laser (pumped by an CW Argon ion laser) which was operated in single frequency mode (linewidth 20 MHz). The holewidth, corrected for read resolution, is 0.6 cm^{-1}. It is doubtful that this width represents twice the homogeneous width for the 685 nm component, The linewidth obtained may not be determined by excited state dynamics alone as experimental conditions could interfere with this. The burn power was 190 mW/cm^2 and the burn time was 180 s. In order to obtain γ_{homo} a shorter burn time and lower burn intensity should be utilized to circumvent power broadening and saturation effects which will lead to hole broadening [59]. Ideally a ΔOD of no more than 5% should be used to obtain accurate dynamical information. In addition to these experimental considerations the overlap of the absorption profiles of the 685 nm and 705 nm components makes the assignment of the hole to a particular component questionable.

The narrow ZPH could be due to either a vibrational level in the 705 nm state (~450 cm^{-1}) or zero point decay for the 685 nm component's excited state. The absorption in this region is dominated by the 685 nm component and thus the ZPH and corresponding pseudo-phonon side band hole (PSBH) lying to lower energy are assigned to the 685 nm component. No other satellite holes were observed. Franck-Condon factors for Chl *a* S_1

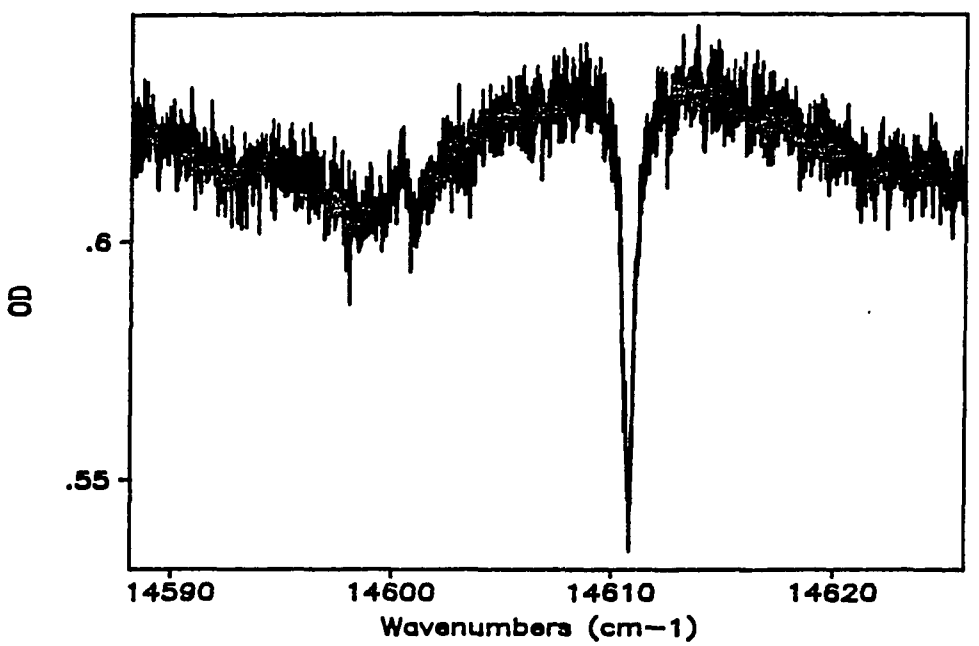

Figure 1. Hole burned spectra for dimer in n-bromo butane, T=1.6 K. λ_B=684.4 nm. Res.=.2 cm^{-1}

vibrational modes are ≤.02 [60] (Chl *a* in antenna of PSI-200) and the F-C factors are thought to be similar for this molecule. Therefore it is extremely unlikely that this ZPH is due to the 705 nm state.

The pseudo-PSB lies ~13 cm^{-1} to lower energy and is a result of the burning of sites (whose zero-phonon frequencies lie lower than ω_B) which absorb ω_B via their phonon sideband. Phonons for chlorophyllic molecules in protein systems have 17-30 cm^{-1} phonons [60-62] associated with them; the value determined here is very close to this range and represents a chlorophyll dimer-solvent low frequency mode (phonon). Weak electron-phonon (e-p) coupling is indicated for the 685 nm transition. This is collaborated by the very small Stokes shift observed in the fluorescence spectra of the 685 nm component for toluene, MTHF and DMF solutions of this molecule [63] and the prescence of sharpline fluorescence features on a broad fluorescence band for these three solvents [63]. The Stokes shift is ~$2S\omega_m$ and with ω_m=13 cm^{-1} and an estimated S<1 (weak coupling) the Stokes shift would be neglegible. It was not possible to obtain S (Huang-Rhys factor) directly.

It seems reasonable that the phonon frequency, ω_m, for the 705 nm component would be similar to that for the 685 nm component, ~13 cm^{-1}. This provides a more accurate method of estimating the e-p coupling strength (S) of the 705 nm component than that given previously [63], S=3-5 and ω_m=50-30 cm^{-1}. With the Stokes shift of the 705 nm component, conformer B, being 300 cm^{-1} [63], S can be esimated to be approximately 11. This would represent a case of very strong e-p coupling and a zero-phonon transition whose Franck-Condon factor, exp(-S), would render it as a highly forbidden transition. The observation of a featureless fluorescence band corresponding to emission from conformer B [63] confirms the presence of strong coupling (absence of line narrowing) observed with a variety of excitations [63].

The large value obtained for S, 11, could be interpreted as indicating a shift in the excited state potential well relative to the ground state well. The coordinate considered here would be that defined by the bicycling motion that has been proposed to occur in the excited state. A large range of values for the dihedral angle were considered as possible for

this molecule based on computer modelling and steric interactions [63]. This explanation would not invoke any C-T character for the excited state (720 nm) which fluoresces. It does not address the temperature dependent decay of the 720 nm fluorescence, as observed for DMF [63] (see Fig. 3) which may or may not involve a C-T state.

The magnitude of S, 11, is similar to that observed for charge-transfer states of π-molecular donor-acceptor complexes [64]. This would assign the 720 nm fluorescence as that emanating from a C-T state. This assignment, however, would be in contradiction with the interpretations put forth previously in regard to the picosecond transient absorption and fluorescence measurements of Johnson et al. [58]. Their results were interpreted in terms of the more polar solvents stabilizing a C-T state which then "bled-off" the excited state population with the C-T state being either dark or IR emitting. The manner in which the proposed C-T state is mixed with the excited state of the dimer is still not known. It may be possible that more than one C-T state could exist with the lowest energy C-T state lying lower than the excited state well of conformer B (705 nm). The curve crossing for this state and the excited state of conformer B could be such that thermal activation is necessary to cross the barrier to populate the C-T state. An activation energy is calculated later in this section. This more accurate estimate of S points out the uncertainties that are still present in the potential energy diagram proposed for this unusual molecule [63]. The general notion of stabilizing a C-T state with more polar solvents (higher ε, dielectric constant) and hence lowering its energy [63,65], so that it can mix more readily with the first excited state of the molecule, can itself be questioned. The concept of the polarity of a solvent needs to be examined more closely to do this.

When the polarity of the solvent is sufficiently high it has a stabilizing effect on the charge transfer state of a molecule. The dielectric constant (ε) is the measure of polarity employed here. The temperature dependence of this quantity is important to discuss since our data were gathered over a wide temperature range (5-300 K). ε can be defined using the Debye expression:

$$(\varepsilon-1)/(\varepsilon+2) = N/3 \times \{\alpha+\mu^2/(3kT\varepsilon_o)\} \qquad (1)$$

Where α is the polarizability, μ is the dipole moment of the solvent, and N is Avogadro's constant. As the temperature of the solvent decreases from room temperature to the glass transition temperature (T_g) or to the freezing point (T_m) ε increases by as much as a factor of 5 for polar solvents [66-69] over this temperature range. In particular, for DMF ε=38 at T=293 K and ε=58 at T=213 K [66]. For nonpolar or weakly polar solvents such as toluene (ε=2.4) or MTHF (ε=7) the temperature dependence of ε is neglegible and the molecular polarizability, α, becomes more important in determining ε.

In general, ε for polar solvents assumes a smaller value when $T<T_g$ which is similar to that for a nonpolar solvent when $T<T_g$ [70]; the values for ε would vary somewhat upon the values for α, which are not well known for all solvents. The physical reasoning for this is that in a glass the solvent dipoles are randomly oriented and unable to reorient themselves while in the glassy state. The stabilizing abilities of a polar solvent, e.g., DMF and MTHF, are effectively reduced when $T<T_g$ thus leading to the observation of less dramatic differences in the interactions between a regular excited state of the dimer and a C-T state in the three solvents used. These differences would be much more pronounced when $T=T_g$ (i.e., when solvent molecules once again are mobile). The effect of the solvent's physical and spectral properties of the chlorophyll dimer can be clearly seen when DMF is used as the solvent.

Figure 2 is a plot of the position (nm) of the 720 nm fluorescence band versus T (K) for the dimer in DMF. The smooth curve is drawn through the points. This plot is very similar to that obtained for toluene [63]. This smooth curve displays a feature that the curve for toluene does not, a bimodal shape with two inflection points! These inflection points are ~130 K and ~210 K. The glass transition and melting transition temperatures are 129 K and 212 K, respectively. A similar plot for MTHF, which has an intermediate polarity between toluene and DMF, shows this behavior but to a lesser extent than DMF. For DMF and MTHF temperature dependent photo-excitation spectra were not obtained, but it is credible that these data would, if plotted in a manner similar to the fluorescence band position, behave in a manner like toluene. In other words, the two plots, band

position of fluorescence and photo-excitation features versus T, would mimic one another in shape and position of inflection points. The toluene data indicated only one inflection point at approximately 180 K, the T_m point.

This plot, for DMF, can help in determining the nature of the 720 nm fluorescence band. This band was assigned as Stokes shifted fluorescence from conformer B, the 705 nm absorbing component. The possibility of this state having C-T character was considered earlier in this section and by Johnson et al. [58,63]. Consider the data just presented and the question is: is this behavior indicative of a solute or a solvent dominated action? Remember, our solvent, in this case DMF, can be considered small compared to our chlorophyll dimer(which has four pyridine molecules ligated to it) in terms of physical dimensions. The change in the viscosity of our solvent between 5 K and just above the T_m should be a fairly gradual process and thus any physical (motional) process involving the solvent itself should also change gradually, such as rotating to align its dipole. A solute molecule, however, would need to experience configurational changes in a large number of solvent molecules, which comprise the solvent cage surrounding it, before it could undergo a large amplitude motion.

Whatever is responsible for the blue shift (higher energy) in the fluorescence band position of the 720 nm band is a solute (dimer) determined process. The rather abrupt change observed for the fluorescence band position is caused by a geometry change of the solute (dimer) molecule which is able to undergo a bicycling motion (see ref. [63]) about the ethylenic bridge when enough solvent molecules are mobile (i.e., when the "cage" relaxes). Realistically, this motion is most likely a concerted process with the dimer and the solvent each participating to some extent. This motion, as evidenced by the fluorescence shifting to the blue, is more prevalent for the smaller solvent molecules (DMF < MTHF < Toluene). Unfortunately, the polarity of the these solvents is also in the same order (although reversed) as their physical size which makes this conclusion tenative. It would be a test for this proposal to use either a polar molecule that was very large physically or a nonpolar molecule that was very small physically. Of course the added

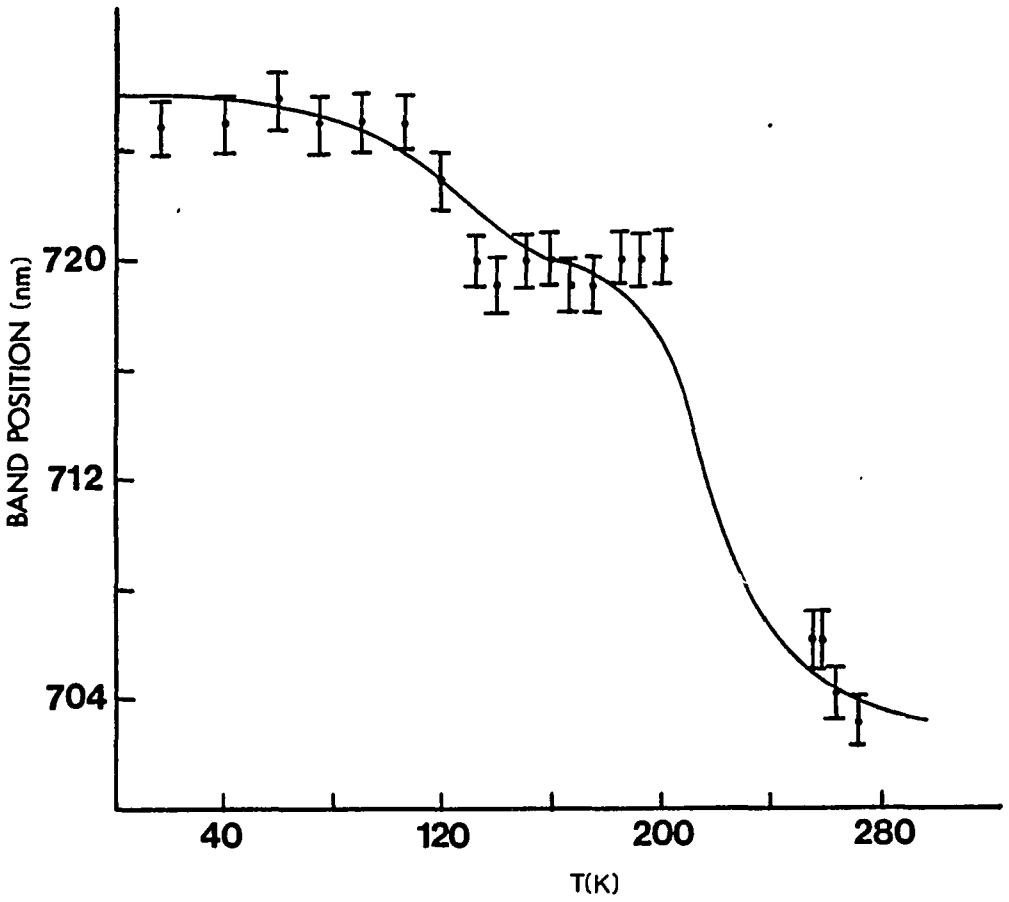

Figure 2. Temperature dependence of the fluorescence (720 nm) band position in DMF

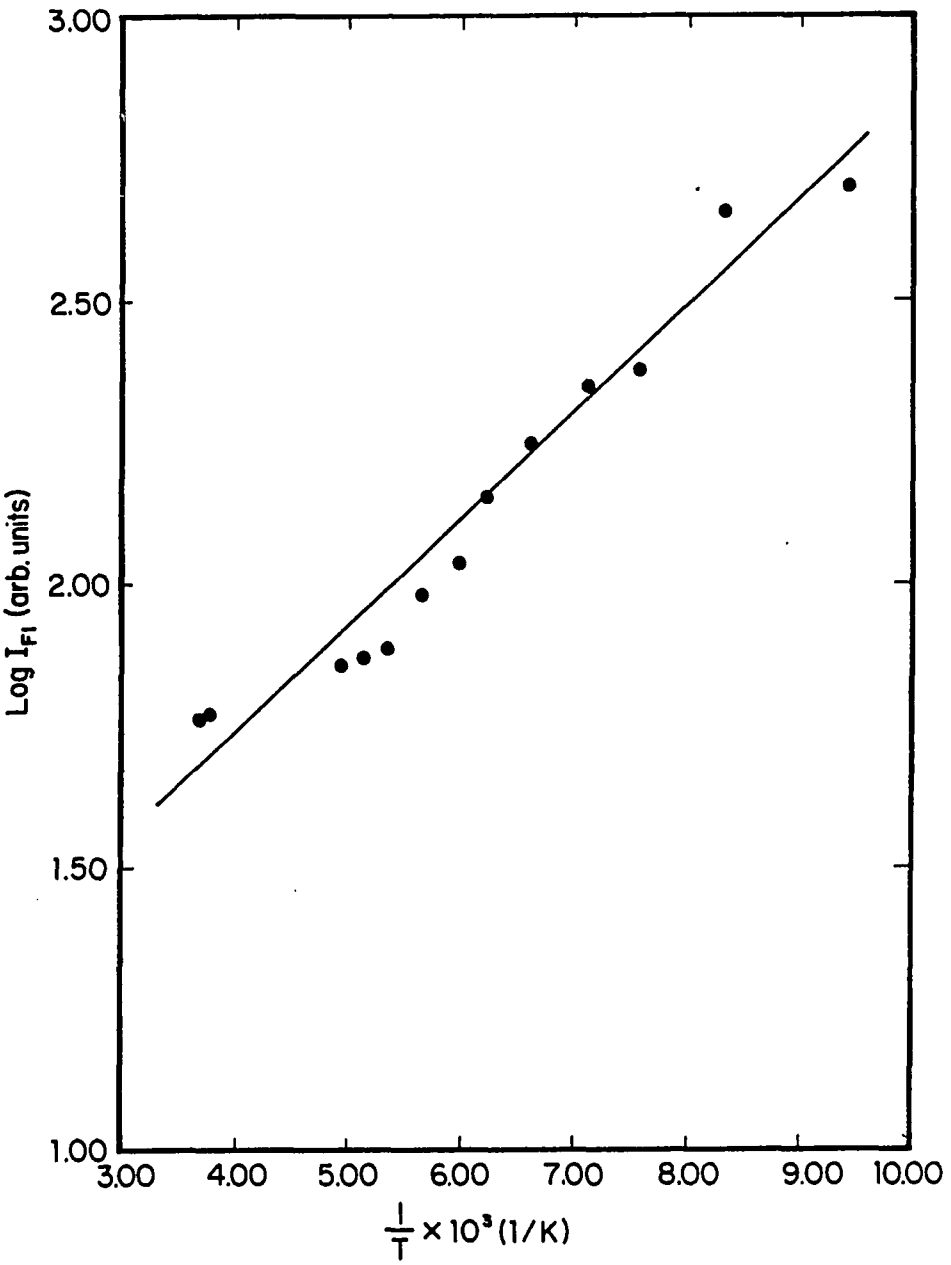

Figure 3. Temperature dependence of the integrated intensity of the 720 nm fluorescence band in DMF

constraint of the solvent being nonhydrogen bonding, to preclude aggregation, would make this choice somewhat more difficult.

Figure 3 presents the plot of log of integrated fluorescence intensity for the 720 nm band (DMF) versus 1/T (1/K). A line has been drawn through the points to illustrate their linearity. The integrated intensity has been corrected for the addition of 685 nm fluorescence intensity. The range of temperatures encompasses that region where the fluorescence intensity of the 720 nm band undergoes decay. A similar type of plot for the decay of the 685 nm fluorescence in DMF and MTHF yielded values for Δ' for these solvents. Δ' being the difference in the zero point energies for the first excited state potential energy wells for the two conformers of the dimer. There is no firm experimental evidence for an additional excited state potential well, yet (two are known to exist). Johnson et al. [58] estimated that a C-T state lies approximately 1000 cm^{-1} higher in energy based on electrochemical data. This is low enough to interact with the regular excited state based on the calculations of Won and Friesner [71,72] for the primary electron donor of photosynthetic bacteria, where a C-T state that lies 2000 cm^{-1} higher in energy than the PED can mix with the state to cause ultrafast decay. Also the "entities" here can not be assumed to be in thermal equilibrium, as was the case for the two excited states of conformer A and B in calculating a value for Δ'.

An activation energy, E_a, can be calculated from the data in Fig. 3, the quantum yield of fluorescence at room temperature and fluorescence lifetime [58]. The quantum yield of fluorescence can be expessed as:

$$\phi_{fl}(T) = \{k_{fl}/(k_{fl} + A\exp(-E_a/kT))\} \qquad (2)$$

Where $\phi_{Fl}(T)$ is the temperature-dependent quantum yield of fluorescence, k_{Fl} is the fluorescence rate ($1/\tau_{Fl}$) and E_a is the activation energy for the process under consideration. The $\phi_{Fl}(T=300\ K)=.002$ and $\tau_{Fl}=1.5$ ps [58]. By scaling the integrated fluorescence intensity at T=300 K to any other temperature the quantum yield at that

temperature can be obtained and by making the reasonable assumption that τ_{nat} does not change in the temperature range considered (100-300 K) k_{Fl} can be obtained. $\tau_{nat} = \tau_{Fl} + \tau_{NR}$, where τ_{NR} encompasses all nonradiative processes (i.e., intersystem crossing, internal conversion). It is therefore possible to obtain E_a by ratioing two quantum yields at different temperatures. The pertinent equation obtained by solving equation 2 as stated above is:

$$E_a = -kT_1T_2/(T_1-T_2) \times \ln\{ [k^1_{fl}(\phi^1_{NR}/\phi^1_{fl})] / [k^2_{fl}(\phi^2_{NR}/\phi^2_{fl})]\} \qquad (3)$$

Where $\phi_{NR}=1-\phi_{Fl}$ and the superscripts 1 and 2 refer to at $T=T_1$ or T_2. The activation energy calculated is .80+.10 kcal/mol (280 cm^{-1}). No explanation for this relatively small activation energy is proposed at this time.

Although some is known about this unusual molecule and its excited state dynamics through the results presented here and elsewhere [58,63] further experiments are necessary to fully understand what processes are taking place. A series of picosecond transient absorption and stimulated emission studies done at a variety of temperatures between 5 K and 300 K with several solvents of different polarity would yield the information necessary to further refine the model for the excited state dynamics proposed here.

REFERENCES

1. O'Malley, P. J.; Babcock, G. T. Proc. Natl. Acad. Sci. USA 1984, 81,1098.
2. Wasielewski, M. R.; Norris, J. R.; Crespi, H. L.; Harper, J. J. Am. Chem. Soc. 1981, 103, 7664.
3. Wasielewski, M. R.; Norris, J. R.; Shipman, L. L.; Lin, C.-P.; Svec, W. A. Proc. Natl. Acad. USA 1981, 78, 2957.
4. Watanabe, T.; Kobayashi, M.; Hongu, A.; Natazato, M.; Hiyama, T.; Murata, N. FEBS Lett. 1985, 191, 252.
5. Phillipson, K. D.; Sato, V. L.;Sauer, K. Biochem. 1972, 11, 4591.
6. Norris, J. R.; Uphaus, R. A.; Crespi, H. L.; Katz, J. J. Proc. Natl. Acad. Sci. USA 1971, 68, 625.
7. Norris; J. R., Druyan, M. E.; Katz, J. J. J. Am. Chem. Soc. 1973, 95, 1680.
8. Deisenhofer, J.; Epp, O.; Miki, K.; Huber, R.; Michel, H. J. Mol. Biol. 1984, 180, 385.
9. Deisenhofer, J.; Epp, O.; Miki, K.; Huber, R.; Michel, H. Nature (London) 1985, 318, 618.
10. Michel, H.; Epp, O.; Deisenhofer, J. EMBO J. 1986, 5, 2445.
11. Chang, C. H.; Tiede, D. M.; Tang, J.; Smith, U.; Norris, J.; Schiffer, M. FEBS Lett. 1986, 205, 82.
12. Allen, J. P.; Feher, G.; Yeates, T. O.; Rees, D. C.; Deisenhofer, J.; Michel, H.; Huber, R. Proc. Natl. Acad. Sci. USA 1986, 83, 8589.
13. Yeates, T. O.; Koyima, H.; Chirino, A.; Rees, D. C.; Allen, J. P.; Feher, G. Proc. Natl. Acad. Sci. USA 1988, 85, 7993.
14. Yuen, M. J.; Closs, G. L.; Katz, J. J.; Roper, J. A.; Wasielewski, M. R.; Hindman, J. C. Proc. Natl. Acad. Sci. USA 1980, 77, 5598.
15. Boxer, S. G.; Closs, G. L. J. Am. Chem. Soc. 1976, 98, 5406.
16. Wasielewski, M. R.; Studier, M. H.; Katz, J. J. Proc. Natl. Acad. Sci. USA 1976, 73, 4282.

17. Shipman, L. L.; Cotton, T. M.; Norris, J. R.; Katz, J. J. Proc. Natl. Acad. Sci. USA 1976, 73, 1791.

18. Pellin, M. J.; Wasielewski, M. R.; Kaufmann, K. J. J. Am. Chem. Soc. 1980, 102, 1868.

19. Wasielewski, M. R.; Smith, U. H.;Cope, B. T.; Katz, J. J. J. Am. Chem. Soc. 1977, 99, 4172.

20. Hindman, J. C.; Kugel, R.; Wasielewski, M. R.; Katz, J. J. Proc. Natl. Acad. Sci. USA 1978, 75, 2076.

21. Pellin, M. J.; Kaufmann, K. J.;Wasielewski, M. R. Nature (London) 1979, 278, 54.

22. Wasielewski, M. R.; Svec, W. A. J. Org. Chem. 1980, 45, 1969.

23. Huber, M.; Lendzian, F.; Lubitz, W.; Trankle, W.; Mobius, K.; Wasielewski, M. R. Chem. Phys. Lett. 1986, 132, 467.

24. Hofstra, U.; Schaafsma, T. J.;Sanders, G. M.; Van Dijk, M.; Van Der Plas, H. C.; Johnson, D. G.; Wasielewski, M. R. Chem. Phys. Lett. 1988, 151, 169.

25. Bucks, R. R.; Netzel, T. L.; Fujita, I; Boxer, S. G. J. Phys. Chem. 1982, 86, 1947.

26. De Wilton, A. C., Koningstein, J. A. J. Phys. Chem. 1983, 87, 185.

27. Thibodeau, D. L.; Koningstein, J. A. J. Phys. Chem. 1989, 93, 7713.

28. Thibodeau, D. L.; Koningstein, J. A.; Haley, L. V. Chem. Phys. 1989, 138, 265.

29. Agostiano, A.; Butcher, K. A.; Showell, M. S.; Gotch, A. J.; Fong, F. K. Chem. Phys. Lett. 1987, 137, 37.

30. Alfano, A. J.; Showell, M. S.; Fong, F. K. J. Chem. Phys. 1985, 82, 765.

31. Alfano, A. J.; Lytle, F. E.; Showell, M. S.; Fong, F. K. J. Chem. Phys. 1985, 82, 758.

32. Abraham, R. J.; Goff, D. A.; Smith, K. M. J. Chem. Soc. Perkin Trans. I 1988, 2443.

33. Wasielewski, M. R.; Niemczyk, M. P. J. Am. Chem. Soc. 1984, 106, 5043.

34. Wasielewski, M. R.; Niemczyk, M. P.; Svec, W. A. Tetrahedron Lett. 1982, 23, 3215.

35. Wasielewski; Johnson, D. G.; Svec, W. A.; Kersey, K. M.; Minsek, D. W. J. Am. Chem. Soc. 1988, 110, 7219.

36. Kagan, N. E.; Mauzerall, D.; Merrifield, R. B. J. Am. Chem. Soc. 1977, 99, 5484.

37. Cowan, J. A.; Sanders, J. K. M.; Beddard, G. S.; Harrison, R. J. J. Chem. Soc. Chem. Commun. 1987, 55.

38. Gust, D.; Moore, T. A.; Moore, A. L.; Makings, L. R.; Seely, G. R.; Ma, X.; Trier, T. T.; Gao, F. J. Am. Chem. Soc. 1988, 110, 7567.

39. Osuka, A.; Maruyama, K.; Yamazakai, I.; Tamai, N. J. Chem. Soc. Chem. Commun. 1988, 1243.

40. Fujita, I.; Fajer, J.; Chang, C.-K.; Wang, C.-B.; Bergkamp, M. A.; Netzel, T. L. J. Phys. Chem. 1982, 86, 3754.

41. Netzel, T. L.; Kroger, P.; Chang, C.-K.; Fujita, I.; Fajer, J. Chem. Phys. Lett. 1979, 67, 223.

42. Mataga, N.; Yao, H.; Okada, T.; Kanda, Y. Chem. Phys. 1989, 131, 473.

43. Donohoe, R. J.; Duchowski, J. K.; Bocian, D. F. J. Am. Chem. Soc. 1988, 110, 6119.

44. Wasielewski, M. R. Photchem. Photobiol. 1988, 47, 923.

45. Boxer, S. G. Biochim. Biophys. Acta 1983, 726, 265.

46. Meyer, T. J. Acc. Chem. Res. 1989, 22, 163.

47. Katz, J. J.; Hindman, J. C. In "Biological Events Probed by Ultrafast Laser Spectroscopy"; Alfano, R. R., Ed.; Academic Press: New York, 1982; p 119.

48. Norris, J. R.; Scheer, H.; Druyan, M. E.; Katz, J. J. Proc. Natl. Acad. Sci. USA 1974, 71, 4897.

49. Brody, S. S.; Brody, M. Nature (London) 1961, 189, 547.

50. Seely, G. R.; Jensen, R. G. Spectrochim. Acta 1965, 21, 1835.

51. Boxer, S. G.; Lockhart, D. J.; Middendorf, T. R. Chem. Phys. Lett. 1986, 123, 476.
52. Boxer, S. G.; Middendorf, T. R.; Lockhart, D. J. FEBS Lett. 1986, 200, 237.
53. Meech, S. R.; Hoff, A. J.; Wiersma., D. A. Proc. Natl. Acad. Sci. USA 1986, 83, 9464.
54. Meech, S. R.; Hoff, A. J.; Wiersma, D. A. Chem. Phys. Lett. 1985, 121, 287.
55. Tang, D.; Jankowiak, R.; Small, G. J.; Tiede, D. M. Chem. Phys. 1989, 131, 99.
56. Lockhart, D. J.; Boxer, S. G. Biochemistry 1987, 26, 664.
57. Lockhart, D. J.; Boxer, S. G. Chem. Phys. Lett. 1988, 144, 243.
58. Johnson, D. G.; Svec, W. A.; Wasielewski, M. R. Israel J. Chem. 1988, 28, 193.
59. Small, G. J. In Spectroscopy and Excitation Dynamics of Condensed Molecular Systems, Hochstrasser, R. M., Ed.; North Holland: Amsterdam, 1983, p 515.
60. Gillie, J. K.; Small, G. J.; Golbeck, J. H. J. Phys. Chem. 1989, 93, 1620.
61. Johnson, S. G.; Small, G. J. Chem. Phys. Lett. 1989, 155, 371.
62. Jankowiak, R.; Tang, D.; Small, G. J.; Seibert, M. J. Phys. Chem. 1989, 93, 1649.
63. Johnson, S. G.; Small, G. J.; Johnson, D. G.; Svec, W. A.; Wasielewski, M. R. J. Phys. Chem. 1989, 93, 5437.
64. Haarer, D. Chem. Phys. Lett. 1977, 67, 4076
65. Lippert, E.; Rettig, W.; Bonacic-Koutecky, V.; Heisel, F.; Miehe, J. A. Adv. Chem. Phys. 1987, 68, 1.
66. Bass, S. J.; Nathan, W. I.; Meighan, R. M.; Cole, R. H. J. Phys. Chem. 1964, 68, 509.
67. Leader, G. R.; Gormley, J. F. J. Am. Chem. Soc. 1951, 73, 5731.
68. Brody, S. S.; Brodye, S. B. Biophys. J. 1968, 8, 1511.
69. Wright, J. D. Molecular Crystals; Cambridge University Press: Cambridge, 1987.
70. Wong, J.; Angell, C. A. Glass, Structure by Spectroscopy; Marcel Dekker: New York (1976).

71. Won, Y.; Friesner, R. A. J. Phys. Chem. (1987), 84, 5511.

72. Won, Y.; Friesner, R. A. J. Phys. Chem. (1988), 92, 2214.

SECTION II.

PERSISTENT SPECTRAL HOLE BURNING OF A STRONGLY EXCITON COUPLED ANTENNA COMPLEX

INTRODUCTION

The water soluble bacteriochlorophyll-protein complex from *Prosthecochloris aestuarii* was the first chlorophyll containing complex to have its structure determined to atomic resolution (2.8Å) by single crystal x-ray diffraction in 1975 [1]. This structural analysis preceded that of the reaction center (RC) of *Rps. viridis* [2] by nine years, but it has not received the same amount of attention as the RC. The structure of this chlorophyll-protein complex, also called Fenna-Matthews-Olson (FMO) complex, after the investigators who first determined the structure [1] (Fenna and Matthews) and who first crystallized the complex [3] (Olson), consists of 21 Bchl *a* molecules organized into three identical subunits, each containing 7 Bchl *a* molecules (see Figs. 1 and 2). These subunits are related by a three-fold axis of symmetry. The center-to-center distances for chromophores within a subunit is 11.3-14.4 A, while each subunit within the trimer is separated by 24-36 A (edge-to-edge) from the other subunits. Recently the x-ray structure has been improved to 1.9 A resolution [4] and its complete amino acid sequence has been determined [5]. This complex provided several unique opportunities to researchers in the photosynthesis area.

Relatively little high resolution spectroscopy has been performed on this chlorophyll-protein complex, in fact, comparatively little spectroscopy has been applied to this antenna species at all. The first spectroscopic investigation on *P. aestuarii* was performed by Sybesma et al. [6-8] in 1963 and 1964. The room temperature and 77 K fluorescence spectra of whole cells and the isolated Bchl *a* antenna complex were obtained. The kinetics of oxidation of the primary electron donor, P840, were also investigated [8]. At that time the species was still called *Chloropseudomonas ethylica* 2K. Olson [9] later unraveled the confusion concerning the name of the species and it became *Prosthecochloris aestuarii* strain 2K or simply *P. aestuarii*. The confusion actually stemmed from the fact that some early samples [9,10] were a mixture of *Desulfuromonas acetoxidans* and *P. aestuarii*. More recent fluorescence studies have been reported by Karapetyan et al. [11], Swarthoff et al. [12] and van Grondelle et al. [13]. Karapetyan et al.

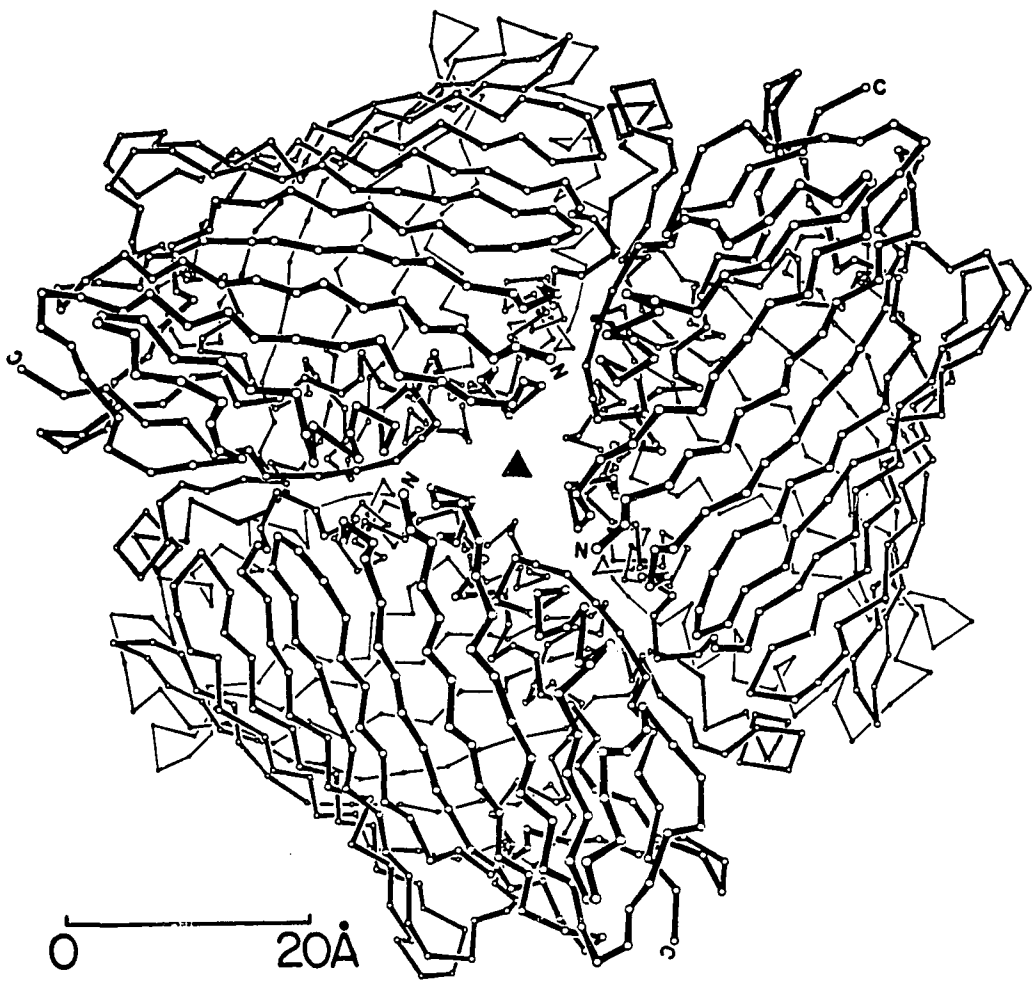

Figure 1. Bacteriochlorophyll-protein complex as viewed down the threefold symmetry axis. The chlorophyll molecules have been removed for clarity and only the protein backbone is represented

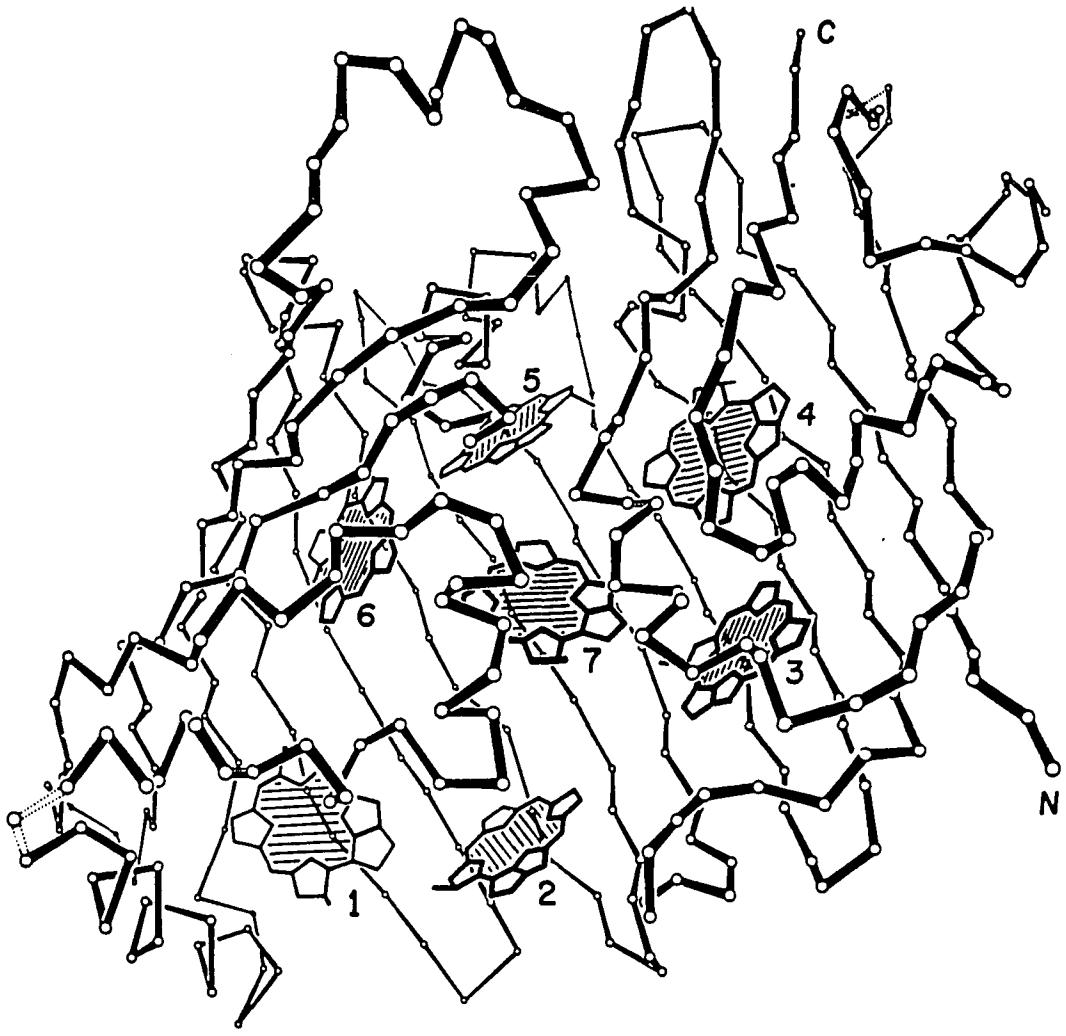

Figure 2. Seven bacteriochlorophyll molecules in their protein environment for one subunit of *P. aestuarii*. The phytyl chains of each chlorophyll have been omitted for clarity

[11] studied the effect of dithionite on the fluorescence properties of whole cells of *P. aestuarii*. Van Grondelle et al. [13] investigated the size of the antenna-protein complex by using singlet-singlet quenching. Swarthoff et al. [12] studied the temperature dependence of the fluorescence of whole cells, as well as, just the antenna complex. All of these studies were consistent in their findings with only one fluorescencè feature, ~830 nm, appearing at low temperature (5 K) and the fluorescence spectrum being more complicated at room temperature (two or more features) [6,7,11-13].

Lutz et al. [14] applied resonance Raman spectroscopy to comment on the extent which ligand (protein) interactions could affect the local environment of the seven Bchl *a* molecules in each subunit. The extent of ligation for each Bchl *a* molecule was estimated as was the extent of hydrogen bonding to each Bchl *a*(via the carbonyl group on the porphyrin macrocycle). In addition, Lutz et al. [14] firmly established that the lowest absorbing electronic transition ($S_1 \leftarrow S_0$) was in fact the Q_y transition.

Swarthoff et al. [15] obtained linear dichroism spectra for both whole cells and the isolated antenna species. The linear dichroism spectra from the isolated antenna species showed very little, if any, LD signal in the Q_x or Q_y spectral regions [15].

Causgrove et al. [16] performed polarized pump-probe spectroscopy at room temperature on the Q_x band of the antenna complex from *P. aestuarii*. They observed that at 603 nm the polarization decays with a mean lifetime of 4.8 ps. Their data were analyzed using an exciton hopping model and one of the known geometries [4] of the complex (hexagonal). The Forster mechanism was utilized in their analysis and this mechanism will be examined more closely latter in this section.

From a theoretical modelling standpoint several groups [17-24] have attempted to explain the structured absorption spectra of the Q_y-manifold and circular dichroism (CD) spectra. Phillipson and Sauer [17] tried fitting the absorption and CD spectra by using a computerized fitting procedure involving only 3 components. The correct number to use would have been 7, for 7 Bchl *a* molecules, but they were operating under the incorrect assumption, which was reasonable at that time, of there being 4 subunits of 5 molecules

each [3,17]. The error of their approach was clear when the x-ray structure was obtained 3 years after they reported their analysis.

Olson et al. [18] attempted a similar fitting of the absorption and CD spectra in 1977. Their analysis resulted in assigning six components instead of seven [18], even though they acknowledged that seven components should be present. Two papers by Whitten et al. [19,20] in 1978 and 1980 presented analyses of the absorption and CD spectra using 4th and 8th derivative spectroscopy. They succeeded in assigning a total of seven components in both the absorption and CD spectra, but did not attempt a theoretical analysis [19,20]. The most complete theoretical treatment of the antenna complex has been that of Pearlstein and coworkers [21-24].

Pearlstein and Hemenger [21] reported on the first theoretical calculations performed on this complex. One of the major difficulties they faced was the assignment of what they termed as the "environmental shift". A very active aspect of the theoretical approaches to this complex is assigning the diagonal energies for each Bchl [21-24]. These are expected to differ due to the differences in the local environment (protein) and conformation for each Bchl. The extended dipole method was used by Pearlstein and Hemenger to calculate the exciton matrix elements [21]. Their fit of the absorption and CD spectra using the conventional geometry for the Bchl *a* molecules was poor [21]. When the lowest electronic transitions for the Bchl *a* molecules, $S_1 \leftarrow S_0$, were assumed to be x-polarized instead of y-polarized agreement between theory and experiment was improved [21]. However, this assumption was shown to be incorrect by Lutz et al. [14] several years latter.

A significantly different approach was proposed by Pearlstein [22] in 1988. He proposed that, in solution, microcrystals (which are known to exist [25]) are formed and that they did so in an equatorial configuration which allowed relatively strong (excitonic) interactions between Bchl *a* molecules belonging to different trimers (see Fig. 3). Such interactions are known to be very weak for hexagonal or trigonal crystals of the trimers [26]. These interactions result in the exciton interaction matrix expanding to 14x14 (two subunits). In addition, Pearlstein allowed for three different diagonal energies for the 7

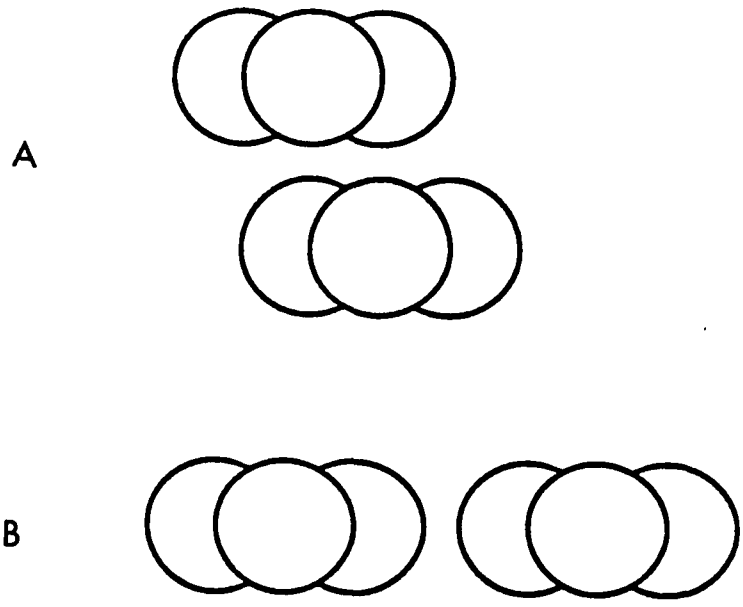

Figure 3. Justaposition of two trimer units of *P. aestuarii*: a.)packing as in the trigonal crystal configuration (or hexagonal), b.)packing in Pearlstein's proposed equatorial configuration

Bchl *a* based on the number of aromatic amino acid residues in contact with each Bchl *a* [22]. Calculations by Pearlstein using this new solution configuration (with his method of assigning the diagonal energies) led to good fit for either the absorption or CD spectra, but not both simultaneously [22,23]. Pearlstein has also examined variations of several of the adjustable parameters (dipole strength, geometry of coupling) in this model [24]. However, agreement between theory and experiment was still unsatisfactory. A quantum chemical approach of determining the diagonal energies has been presented recently by Gudowska-Nowak et al. [27] and results in the 7 Bchl *a* molecules having their Q_y absorption bands between 740 and 840 nm before the exciton interaction "turns on". They examined the effect of the axial ligands (amino acid residues), as well as, the orientations of the metal ions, neighboring amino acid residues and the substituents of the Bchl on the Q_y transition energies. In addition, the intrinsic conformational variations (porphyrin skeletal variations) were investigated and determined to have as great an effect as the above mentioned considerations [27]. At this time Gudowska-Nowak et al. [27] have not calculated the exciton interaction matrix elements (off-diagonal terms).

From a photosynthetic viewpoint this system has provided the opportunity to evaluate the theories that exist to describe electronic excitation transport (EET) in photosynthetic antennas. These theories have been extensively discussed and reviewed in the literature [28-32]. The pebble-mosaic model for EET proposed by Sauer [30,32] was found to be consistent with the structure of the FMO complex. This model described groups of chlorophyll molecules (subunits) which were interacting strongly (excitonically) among themselves but which interacted weakly via the Forster energy transfer mechanism with other subunits. Thus, the EET would take place via a random walk of excitation between subunits of chlorophylls. The excitation would be delocalized within any particular group of chlorophylls, however.

The connotations of "strong" and "weak" describing coupling between molecules or groups of molecules should be explained further. Energy transfer can occur using several different mechanisms [33,34]. The idealized case (vibrational structure of donor and acceptor neglected) of energy transfer from a donor (D) to an acceptor (A) will be

presented first and then three cases where the vibrational structure is considered, however, the coupling matrix element $U=\langle\Psi_D^*\Psi_A|H_c|\Psi_D\Psi_A^*\rangle$ is related differently in each case to the vibrational and electronic spectra of A and D. H_c is the coupling Hamiltonian, and Ψ_D and Ψ_A are the electronic wavefunctions for the donor and acceptor, with the asterisk denoting electronic excitation.

The rate of energy transfer (n_D) from D to A, in the absence of vibrational levels can be approximated,

$$n_D \approx 2\pi|U|h^{-1} \quad \text{if } \Delta E << 4|U| \tag{1}$$

$$n_D \approx 0 \qquad \text{if } \Delta E >> 4|U| \tag{2}$$

With ΔE being the energy difference between the excited electronic states of D and A (the donor is assumed to be the higher lying state).

In the first case strong coupling shall be considered. The donor and acceptor are assumed to have vibrational levels for all three cases presented here. In strong coupling $|U|$ is assumed to be larger than ΔE and the widths of both the A and D excited electronic states (due to pure dephasing). For example, excitation of any level in the vibrational manifold of D^* may be followed by energy transfer to any vibrational levels of A^*. In this case the following rate would result

$$n \approx 2\pi|U|h^{-1} \tag{3}$$

In the second case, that of weak coupling, $|U|$ is considered to be of comparable magnitude or smaller than the electronic bandwidths. In addition, the vibrational levels are sufficiently narrow and resolved so that energy transfer inbetween distinct vibrational levels must be considered. In this case, which is similar to the strong coupling case, U is replaced by V_{ij}, which is the interaction energy between individual vibrational levels of the donor and acceptor. The corresponding energy transfer rate is

$$n \approx \Sigma\, 2\pi |V_{ij}|\, h^{-1} \qquad (4)$$

with summation over all energetically allowed donor and acceptor transitions.

The last case is called very weak coupling. Here U is smaller than the electronic absorption bandwidths and the vibrational manifold exhibits a density that is large (but constant) compared to U. The number of available acceptor states is thus proportional to $|U|$, which results in a $|U|^2$ dependence for the transfer rate,

$$n \approx 32 |U|^2 h^{-1} J \qquad (5)$$

where J is defined as the overlap integral which takes into consideration the vibrational Franck-Condon factors, the density of the vibrational manifold and conservation of energy. In simpler terms, in very weak coupling vibrational relaxation is much faster than the step of transferring the energy between D and A and therefore the probability of back-transfer of the energy is negligible.

For the antenna complex considered here U and ΔE can be estimated to be ~200 cm^{-1} (from Pearlstein [24]) and $\leq$100 cm^{-1} (separation between exciton states, this work), respectively, based on the low temperature absorption spectra. Thus, for a subunit the energy transfer that occurs would fall within the strong or, perhaps, weak coupling regime. However, the energy transfer would not be considered to be in the very weak coupling regime.

This antenna complex whose exact structure is known provides an ideal system in which to investigate EET. With the large quantity of knowledge present in the literature concerning the excited state dynamics of Bchl *a* and the exact structure of this complex, the opportunities to evaluate the current theories of EET, in particular the Sauer pebble-mosaic model, by obtaining high resolution optical spectra several orders better than existing in the present literature were enticing. In addition, this complex has the important advantage of relative simplicity over the RC systems, such as *Rb. sphaeroides* and *Rps. viridis*, in the

study of strongly interacting chromophores. The RC systems are more complicated due to the well acknowledged possibility of interaction with charge transfer states. The technique of spectral hole burning provided a most ideal method to obtain this information.

EXPERIMENTAL METHODS

Samples

Samples of the water soluble antenna-protein complex from *Prosthecochloris aestuarii* were generously provided by Dr. Roger E. Fenna (University of Miami(Fl.), Medical School). The samples were in a buffered solution of water and were diluted with two parts potassium glycerophosphate 75% (in water, K&K Laboratories) to obtain a good glass forming solvent. The concentration was such that an OD of ≤.3 at 814 nm (4.2 K) for a 1 cm path length was obtained. 1 cm (i.d.) polystyrene tubes were utilized and a brass sample holder of local design which provided optical access to the sample was used.

Cryogenic Equipment

The cryogenic apparatus described in section 1 were also used here. In addition, some spectra were obtained at 1.6 K which necessitated pumping on the liquid helium with an auxiliary vacuum pump. When this was performed it was possible to take helium past its lambda point of 2.25 K to a temperature of 1.6 K.

Experimental Apparatus

The apparatus for reading the preburn and hole burned absorption spectra was a Bruker IFS 120 HR Fourier-transform spectrometer. A visible-NIR source consisting of a tungsten lamp (range 3000-25000 cm^{-1}) was used in conjunction with a Si-diode detector (operated at room temperature) to obtain the spectra presented here. Both electronic and optical filters (where necessary) were used to obtain spectra with an optical resolution of upto 1.0 cm^{-1}. Spectra presented here were the average of 20-50 scans.

The burn irradiation was provided by two sources. The first consisted of a excimer pumped dye laser which was described fully in the experimental methods section in chapter

1. The second burn laser was a Ti:sapphire laser (model T-1000, Excel Technology Inc., Bohemia, New York) pumped by a Nd:YLF (model I-1000 and Q-1000, Excel Tech.). The laser system was operated at 1 KHz and provided tunable radiation from 670-1050nm. The laser linewidth was 50 GHz (provided by a Coherent 3 plate birefringent filter assembly) and exhibited a pulse width of 35 ns. Average power arriving at the sample was modulated using neutral density filters.

The fluorescence spectra presented were obtained using the apparatus described in the experimental methods portion of Section I.

PAPER I. SPECTRAL HOLE BURNING OF A STRONGLY EXCITON COUPLED BACTERIOCHLOROPHYLL a ANTENNA COMPLEX

Spectral Hole Burning of a Strongly Exciton Coupled Bacteriochlorophyll a Antenna Complex

S. G. Johnson and G. J. Small

Chemical Physics Letters 1989, 155, 371.

ABSTRACT

Persistent spectral hole burning is reported for the antenna complex of the photosynthetic bacterium *Prosthecochloris aestuarii*. This complex contains subunits which contain seven BChl *a* molecules. The hole burning data are shown to be consistent with an excitonically coupled system. The data also provide the magnitude of the inhomogeneous broadening, a decay time of ~250 fsec for an upper exciton level and the magnitude of the linear exciton-phonon coupling of the optical transition associated with the lowest energy absorption system.

Spectral hole burning of the electronic transitions of chromophores imbedded in solid host media has been observed for a wide variety of organic and inorganic systems [1] and very recently for photosynthetic antenna [2-5] and reaction center complexes [6-8]. However, the technique has not been applied to an organic or biomolecular system in which strong excitonic interactions (few hundred cm^{-1}) between monomers give rise to resolved excitonic structure in the optical absorption spectrum. In this letter we report the first observation of such for the bacteriochlorophyll (BChl) *a*-protein from the green photosynthetic bacterium *Prosthecochloris aestuarii*.

The crystal structure of this protein [9], which has now been refined at 1.9 Å resolution [10], shows that the basic structural unit is a trimer of subunits containing 7 BChl *a* molecules. Nearest neighbor Mg...Mg distances for chromophores within the subunit vary between 11.3 and 14.4 Å and, thus, significant exciton interactions can be expected. These interactions are believed to be important in determining the resolved structure in the absorption spectrum shown in Fig. 1. Spectral fitting procedures have led to the assignment of seven exciton components [11]. However, the agreement between the observed and calculated linear and circular dichroism spectra is poor [11,12]. The difficulty of attaining a firm theoretical understanding of the spectra is compounded by the fact that the BChl *a* monomers of the subunit are energetically inequivalent due to different intramolecular geometries and ligand (protein) interactions [12-14]. Nothing is known about excited state relaxation dynamics within the Q_y-exciton manifold of the subunit.

Using persistent hole spectra we will establish the following: the inhomogeneous line broadening contribution to the absorption component profiles; that the spectra are consistent with a coupled chromophore system; that the exciton-phonon coupling associated with the optical transition is weak; and that the relaxation time of an upper exciton level is ultra-fast (250 fsec). Experimental details will be given elsewhere [15]. Briefly, *P. aestuarii* samples were kindly provided by Roger E. Fenna and experiments performed with a pulsed dye laser (0.2 cm^{-1} linewidth) and a Bruker IFS 120 HR Fourier-transform spectrometer (operated with a 1 cm^{-1} read resolution).

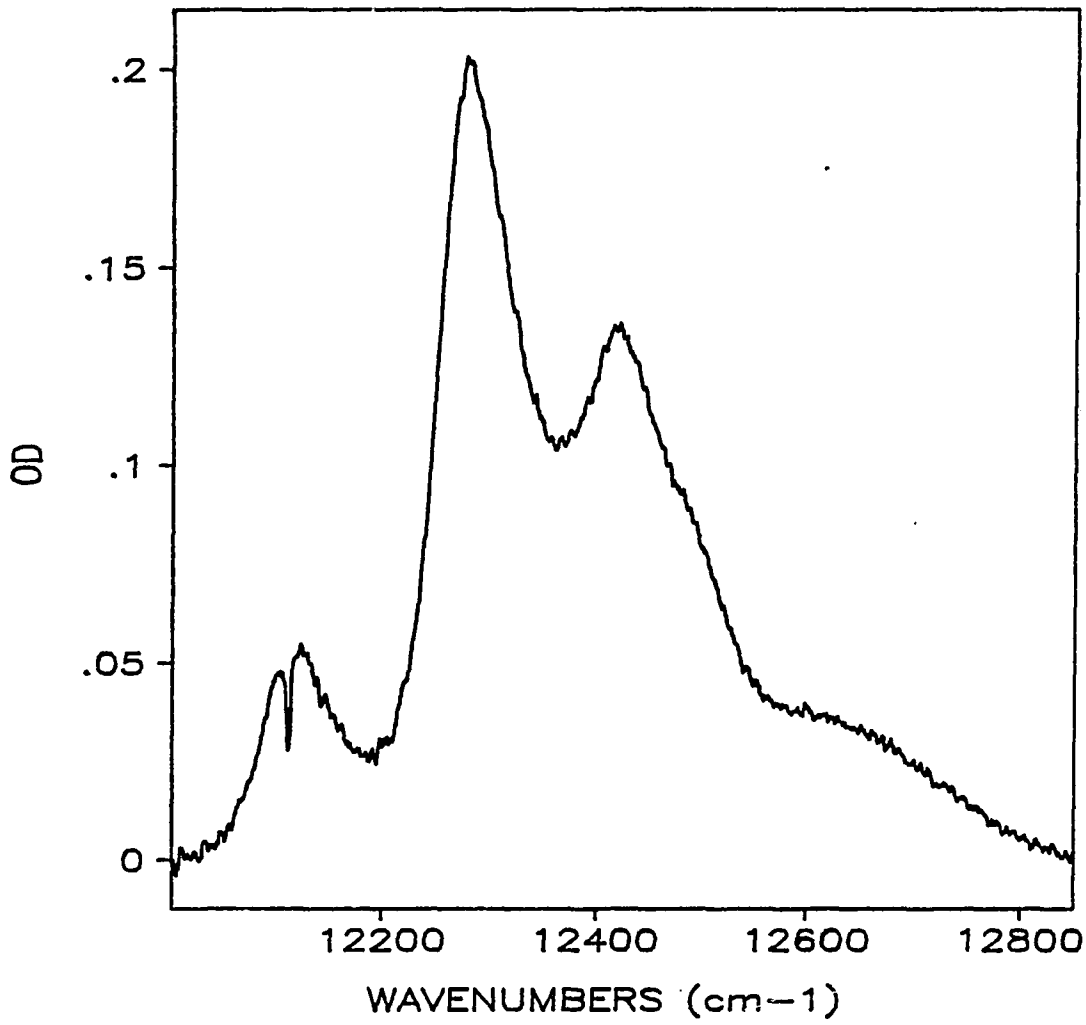

Figure 1. Hole burned spectrum for the antenna-protein complex from *Prosthecochloris aestuarii* at 1.6 K. The burn wavelength λ_B = 825.0 nm. Hole characteristics FWHM = 5.3 cm^{-1} (uncorrected for 1 cm^{-1} read resolution), 40% hole depth. Burn intensity 1 mW/cm^2 for 70 min @ 30 hz (10 ns pulse)

Figure 1 displays a saturated zero-phonon hole (ZPH) burned into the lowest energy 825 nm (12120 cm^{-1}) absorption component. The ZPH is coincident with the burn wavelength (λ_B) of 825.0 nm and represents a peak O.D. change of 40%. Spectra obtained with different λ_B-values within the 825 nm band show that the ZPH tracks λ_B. Therefore, the ~ 90 cm^{-1} FWHM of the 825 nm band is largely determined by inhomogeneous broadening. Such broadening is presumably due to statistical fluctuations in structure from subunit to subunit. Fluorescence line narrowed spectra associated with the 825 nm component have also been obtained [15] which further support the dominance of the inhomogeneous line broadening. Thus, the 825 nm component does not suffer significantly from broadening due to strong linear exciton-phonon coupling, consistent with a recent observation for the Q_y transition of Chl *a* and *b* antenna pigments in photosystem I 200 particles [3]. Figure 2 is the Δ OD spectrum associated with Fig. 1 and the pre-burn absorption spectrum (not shown). The ZPH at 12120 cm^{-1} is clearly evident. Figure 3 shows the burn time dependence of the spectrum in the vicinity of this ZPH. The growth of the ZPH with increasing fluence is apparent. A 30 cm^{-1} pseudo-phonon sideband hole at 12090 cm^{-1} is also apparent despite the small ΔOD changes (≤0.02). The corresponding Huang-Rhys factor (determined from burn time dependent spectra in Fig. 3 and others by the procedure described in ref. 3) is 0.5. Thus, the linear exciton-phonon coupling is weak, as is the case for the Chl *a* core and Chl *a/b* antenna complexes of PSI [2,3]. Protein phonons of ~30 cm^{-1} also characterize these systems [2,3]. The weak linear exciton-phonon coupling is further evidenced by the fluorescence experiments [15] which provide a Stokes shift of 40 cm^{-1} for the 825 nm band. This value is in reasonable agreement with that calculated by the approximate relationship: Stokes shift = $2\omega_m S$, using S = .5 and a ω_m = 30 cm^{-1}. Returning to the 12120 cm^{-1} ZPH of Fig. 2 we note that its FWHM is 5.3 cm^{-1} (uncorrected for read resolution). Narrowing to 4.0 cm^{-1} is observed for shallower holes. However, higher resolution studies as a function of burn fluence and intensity are required in order to determine the minimum width [16]. Thus, we draw no dynamical inferences from the 4 cm^{-1} hole width.

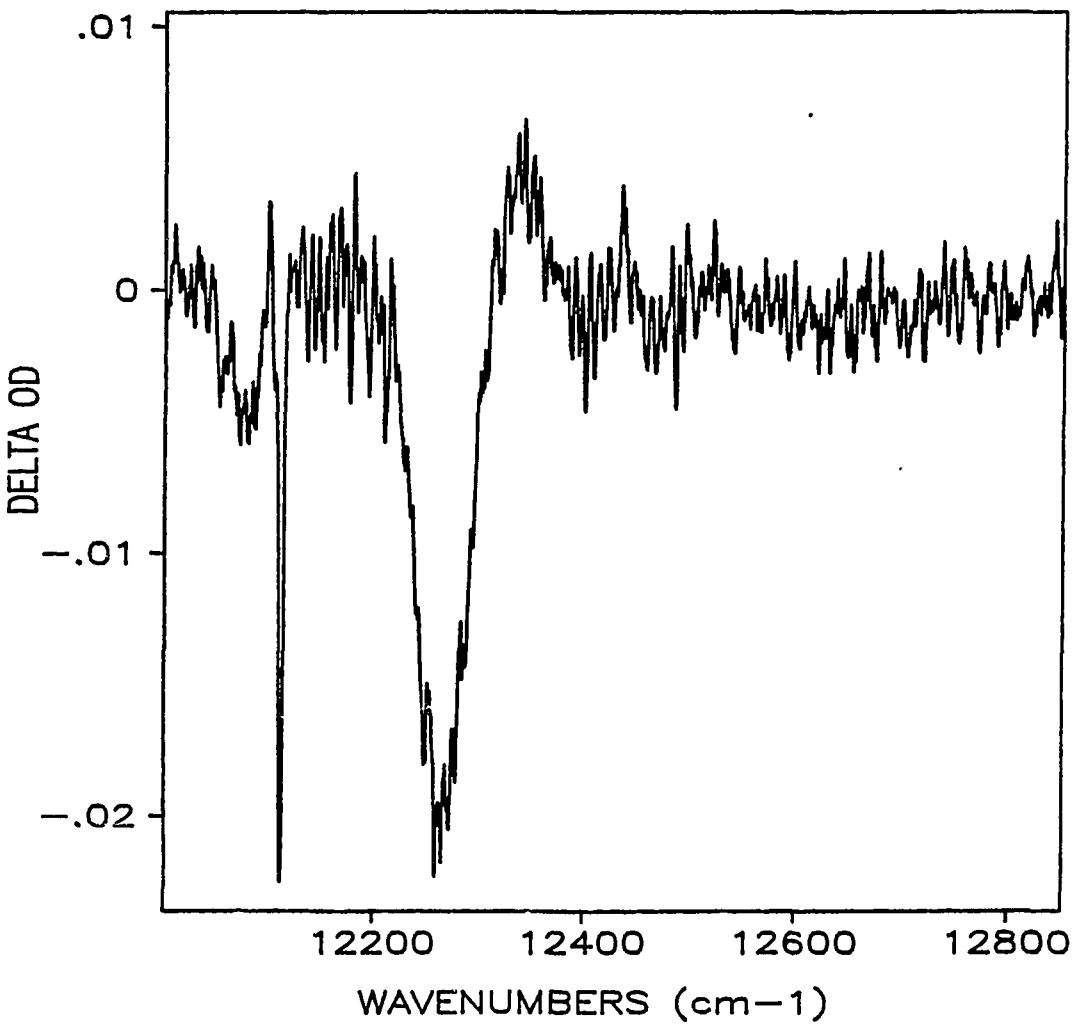

Figure 2. Difference hole burned spectrum of Figure 1 displaying sharp ZPH coincident with λ_B, broad pseudo-phonon sideband hole displaced 30 cm^{-1} to lower energy of ZPH, and satellite hole @ 814 nm

Perhaps the most interesting aspect of Fig. 2 is the observation of the 50 cm^{-1} wide satellite hole located just to the left of 12250 cm^{-1}. This hole, produced with λ_B = 825.0 nm, is centered at the most intense absorption feature of Fig. 1 near 814 nm. If the 814 and 825 nm absorption bands were due to uncoupled (unconnected) but energetically inequivalent BChl *a* monomers in the subunit, the 814 nm satellite hole of Fig. 2 would not be observed. Its observation is consistent with the 814 and 825 nm bands being due to exciton states of the subunit since the delocalization (which leads to exciton behavior) provides connectivity between the states (bands). The peak Δ O.D. of the 814 nm hole in Fig. 2 is 10% (see Figs. 1 and 2) compared with 40% for the 825.0 nm hole. By taking into account the difference in the width of the two holes and the pseudo-phonon sideband hole associated with the 825.0 nm ZPH, it can be seen that the fractional integrated O.D. changes associated with the burning of the 814 and 825 nm bands are roughly equal. Figure 2 and other spectra (e.g., Fig. 4) indicate that an antihole (increase in absorption) occurs at ~12350 cm^{-1} and that it is associated with the 814 nm hole. It is possible that the antihole could be interfered with, to some extent, by a broad hole associated with the second most intense absorption band at 804 nm. Spectra with an improved S/N ratio are required to reach a definite conclusion on this. Observation of the anti-hole is consistent with nonphotochemical hole burning [1]. We note that experiments were performed on the same sample over a period of several days and that during this period the sample was subjected to thermal cycles (1.6-100 K). No photodegradation was observed based on the 1.6 K absorption spectra obtained following laser irradiation and a thermal cycle. A contribution to the hole spectra from a photochemical mechanism would not, of course, alter the principal conclusions (see Abstract).

Since inhomogeneous line broadening exists in this system and because the correlation between the distributions of excitation energies for the 825 and 814 nm components is unknown, no interesting dynamical inferences can be drawn from the 50 cm^{-1} width for the 814 nm hole of Fig. 2 (although there is line narrowing since the width of the 814 nm absorption band is ~100 cm^{-1}). To study the dynamics of the 814 nm

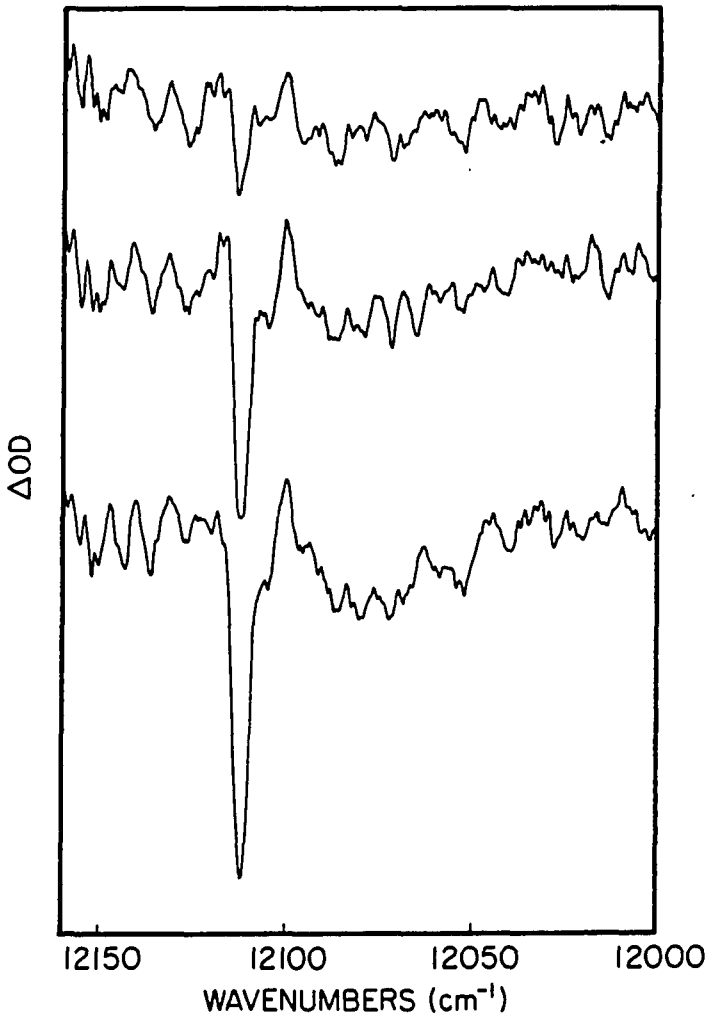

Figure 3. Burn time dependence of the hole spectrum in the vicinity of 825 nm. Burn times (from top to bottom) are 3, 16 and 70 min. The OD scale is equivalent for the three spectra. Burn intensity same as for Figs. 1 and 2. λ_B = 825.0 nm

exciton component, it is necessary to burn directly into this component. This has been done for several λ_B-values. Importantly, the hole position and width is independent of λ_B to within experimental uncertainty. An example of a spectrum is shown in Fig. 4. The hole width is 40 cm^{-1}, which is not so different from the 50 cm^{-1} value obtained from Fig. 2. The difference may be due to incomplete correlation of the type necessary to have yielded a 40 cm^{-1} hole width in Fig. 2. Our results from hole burning into the 825 nm component indicate that [17] the 40 cm^{-1} width is due to homogeneous broadening and, therefore, that the population decay time of the 814 nm exciton is ~ 250 fsec. This ultra-fast decay is presumably due to downward scattering to a lower exciton level(s) which is accompanied by phonon emission. It has been suggested that [11] a weakly absorbing exciton level is located midway between the 814 and 825 nm level but we view this assignment as tentative. The above type of scattering can arise from the linear and higher order terms in the expansion of the resonance energy transfer integrals about the equilibrium geometry of the subunit excited state [18]. That is the weak coupling energy transfer theories (e.g., Förster), which appear to be appropriate for subunit to subunit "hopping" transfer [19], are not applicable since the exciton states are already diagonal with respect to the intermolecular potential energy (static lattice). The picosecond pump-probe depolarization studies of Causgrove et al. [19] indicate that subunit to subunit excitation transport occurs at room T in ~ 14 psec. Our results show that ~ 100 fsec time resolution will be required to resolve exciton relaxation within a subunit.

With reference to Fig. 4, we note that a satellite hole at 825 nm is not discernible from the burn at 814 nm. Given the 40 cm^{-1} width of the 814 nm hole, the difference between the peak ODs at 814 and 825 nm and the incomplete site excitation energy correlation (vide supra), the anticipated peak ΔOD for the 825 nm satellite hole is ~0.003. With the S/N ratio of Fig. 4, this ΔOD change is too small to be detected. Future studies in which deeper primary holes are utilized are planned.

Very recently Pearlstein [20] has proposed a third structure (hexagonal and trigonal structures exist for crystals of P. aestuarii) for the protein trimer in solution in which the trimers pack in an equatorial configuration. This configuration allows for strong

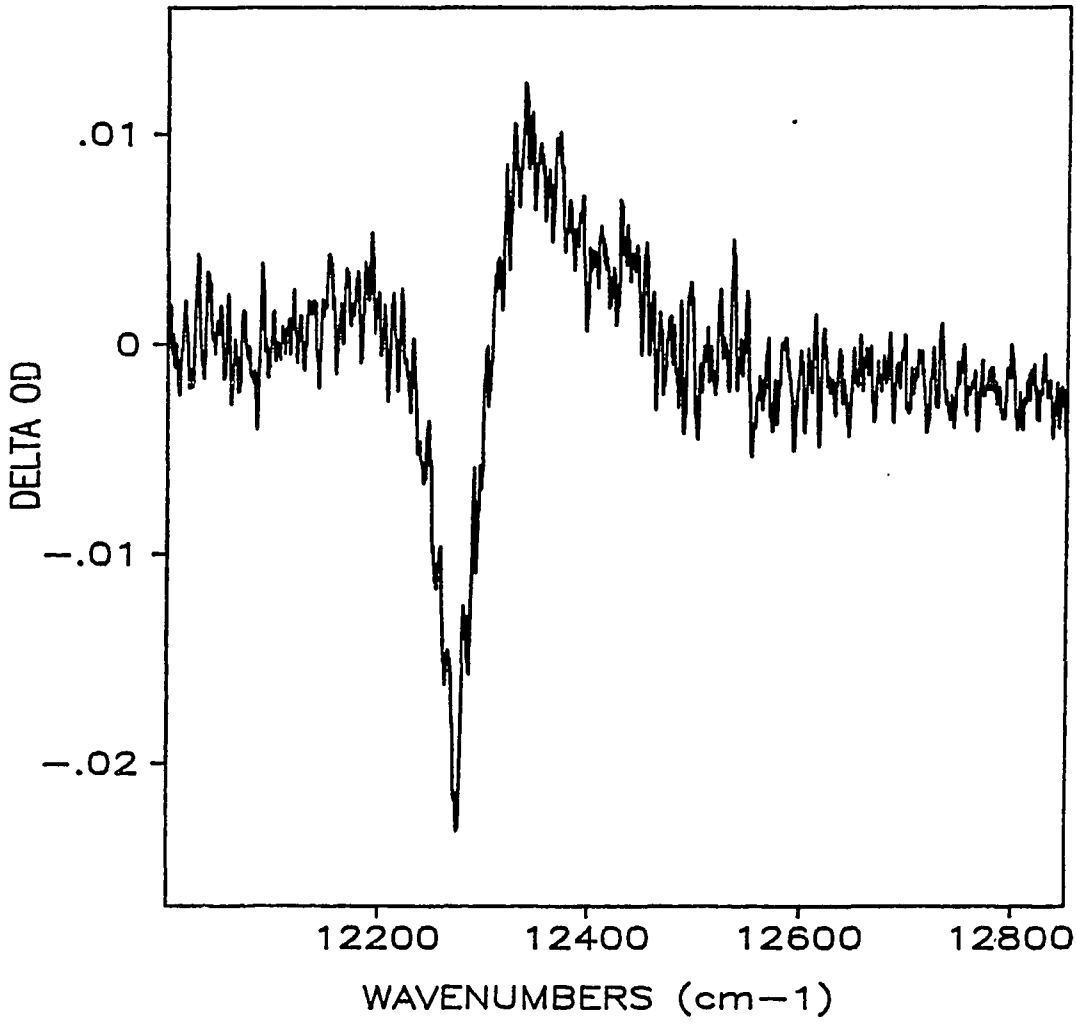

Figure 4. Difference hole burned spectrum with λ_B = 814.0 nm, 1.6 K. Hole characteristics FWHM = 40 cm^{-1}, 10% hole depth. Burn intensity 4 mW/cm^2 for 20 min @ 30 hz (10 nsec pulse)

interactions between BChl *a* molecules belonging to different trimers. Improved agreement between the calculated and observed absorption spectrum was obtained [20]. Polarized hole burning experiments with a single frequency dye laser are planned which will hopefully yield data that are useful for testing of the proposed structures.

ACKNOWLEDGEMENTS

Ames Laboratory is operated for the U.S. Department of Energy by Iowa State University under contract No. W-7405-Eng-82. This research was supported by the Director for Energy Research, Office of Basic Energy Science. Professor Roger Fenna is gratefully acknowledged for providing the samples of *Prosthecochloris aestuarii*. We also wish to thank Professor Walter Struve for useful discussions.

REFERENCES

1. Moerner, W. E., Ed. Persistent Spectral Holeburning: Science and Applications, Topics in Current Physics 44, Springer-Verlag: New York, 1988.
2. Gillie, J. K.; Hayes, J. M.; Small, G. J.; Golbeck, J. H. J. Phys. Chem. 1987, 91, 5524.
3. Gillie, J. K.; Small, G. J.; Golbeck, J. H. J. Phys. Chem. 1989, 93, 1620.
4. Mauring, K.; Renge, I.; and Avarmaa, R. FEBS Lett. 1987, 223, 165.
5. Köhler, W.; Friedrich, J.; Fischer, R.; Scheer, H. Chem. Phys. Lett. 1988, 143, 169.
6. Boxer, S. G.; Middendorf, T. R.; Lockhart, D. J. FEBS Lett. 1986, 200, 237.
7. Gillie, J. K.; Fearey, B. L.; Hayes, J. M.; Small, G. J.; Golbeck, J. H., Chem. Phys. Lett. 1987, 134, 316.
8. Vink, K. J.; DeBoer, S.; Plijter, J. J.; Hoff, A. J.; Wiersma, D. A., Chem. Phys. Lett. 1987, 142, 433.
9. Matthews, B. W.; Fenna, R. E. Acc. Chem. Res. 1980, 13, 309.
10. Tronrud, D. E.; Schmid, M. F.; Matthews, B. W. J. Mol. Biol. 1986, 188, 443.
11. Whitten, W. B.; Olson, J. M.; Pearlstein, R. M. Biochim. Biophys. Acta 1980, 591, 203.
12. Olson, J. M.; Ke B.; Thompson, K. H. Biochim. Biophys. Acta 1976, 430, 524.
13. Pearlstein, R. M.; Hemenger, R. P., Proc. Natl. Acad. Sci. 1978, 75, 4920.
14. Philipson, K. D.; Sauer, K. Biochemistry 1972, 11, 1880.
15. Johnson, S. G.; Small, G. J., submitted to J. Phys. Chem.
16. Thijssen, H. P. H.; Völker, S. Chem. Phys. Lett. 1985, 120, 496.
17. Because the 40 cm^{-1} hole is much wider than the holes associated with the 825 nm band, the 40 cm^{-1} width cannot be due to pure dephasing. Furthermore, ZPH widths of ~0.05 cm^{-1} have been observed by antenna pigments of PSI, see refs. 2 and 3.

18. Johnson, C. K.; Small, G. J. In Excited States, Lim, E. C., Ed.; Academic Press: New York, 1982, Vol. 6

19. Causgrove, T. P.; Yang, S.; Struve, W. S., J. Phys. Chem. 1988, 92, 6790.

20. Pearlstein, R. M. In Photosynthetic Light-Harvesting Systems, Scheer, H., Schneider, S., Eds.; Walter de Gruyter & Co.: Berlin, 1988, p 566.

ADDITIONAL RESULTS AND DISCUSSION

Additional hole burning experiments were performed on the antenna complex from *P. aestuarii* using a Ti:sapphire laser pumped by a Nd:YLF. This laser system has been described in the experimental methods section of this chapter. The results presented here, in the form of two tables, are consistent with those in Paper I of this section, but are much more extensive. In addition to the hole burning experiments, line narrowed fluorescence spectra were obtained. All experiments described here were performed at 4.2 K. There were no noticeable differences in the hole spectra obtained at 1.6 K [35] and 4.2 K. The hole spectra will be discussed first with the results summarized in Table I.

By irradiating in the highly structured Q_y absorption profile at a variety of wavelengths (829-794 nm) a total of eight holes were observed (see Table I). These holes, depending on the burn frequency, were determined to be of either excitonic nature or due to downward energy transfer. As has been previously noted the structured absorption spectra is generally acknowledged to be the result of strong (excitonic) interactions between the Bchl *a* molecules. This idea has been further confirmed here by the observation to higher energy (higher energy than λ_B) of excitonic satellite holes. The position of these holes providing the best means to date of unraveling the underlying structure of the low temperature absorption spectra. By burning directly into these excitonic components it was possible to obtain their excited state decay times (see Table I). It was reassuring to observe that the decay times for the lowest energy components exhibited were considerably slower than the higher energy exciton states in accord with the theory of strongly coupled states [28,29].

The fluorescence line narrowed spectra obtained by exciting into the vibronic progression for S_1 electronic state were very useful for several purposes. First, the assignment of the low frequency intramolecular vibrational modes of S_1 was possible and these are summarized in Table II. Secondly, the degree of inhomogeneous broadening present in the lowest energy exciton component (the only component that would fluoresce) was confirmed. Lastly, it was possible to calculate the Stokes shift, from the difference in

the absorption and fluorescence maxima, which further supported the assignment of an excitonic component at an energy lower than 825 nm (827.1 nm).

Both the hole spectra and the fluorescence spectra presented here were consistent with the antenna complex from *P. aestuarii* being a strongly coupled chromophore system [28,29]. The hole spectra provide for the first time the decay times from S_1 of the exciton components for this complex. It would be interesting to perform ultrafast pump-probe depolarization experiments on the Q_y spectral region at 4.2 K with time resolution sufficient to resolve the decay times indicated here. Such experiments would provide confirmation of the results presented here.

It is of special note that eight exciton components were determined within the Q_y spectral region. This complex consists of a trimer of subunits each containing seven Bchl *a* molecules. Due to differing protein interactions and relative geometries it was thought that a maximum of seven absorption features existed. The observation of eight components brings into question the long held belief that the aggregations of trimers, which are known to exist in solution [25], form in hexagonal or trigonal arrangements. Such arrangements are known to hold the trimers far enough apart to discourage strong coupling between chlorophylls in different trimers. The data presented here supports the theory of Pearlstein [22-24] who proposed that the trimers aggregated in an equatorial fashion in solution which allowed strong coupling between chlorophylls in different trimers. It was acknowledged by Pearlstein [22-24] that at least some of the 14 (2x7) excitonic states would be very weakly absorbing, and therefore, perhaps, undetectable using the technique of spectral hole burning. It is significant, however, that hole burning is the only technique applied to this system (and reported on) that has been able to resolve the underlying exciton components in the Q_y spectral region.

Table I. Exciton components indicated by hole burning

Component	Wavelength (nm)/(cm^{-1})	Excited State Decay Time[a]
1	827.1 (12090)	≥20. ps[b]
2	824.4 (12130)	≥20. ps
3	816.3 (12250)	100 fs
4	813.0 (12300)	100 fs
5	807.8 (12380)	100 fs
6	804.8 (12425)	100 fs
7	801.3 (12480)	100 fs
8	793.6 (12600)	100 fs

[a] Decay time of S_1 electronic state as measured by burning directly into that state.

[b] Decay times obtained from homogeneous widths. See text for details.

Table II. Vibrational Modes for Lowest Energy State

Excited State Freq. (cm^{-1})[a]	Ground State Freq. (cm^{-1})[b]
199	199
209	
216	
273	264
286	290
320	313
350	361
368	379
415	426
456	452
484	479
493	
510	
522	

[a]Excited state (S_1) vibrational frequencies this work.

[b]From resonance Raman (see ref. 14).

REFERENCES

1. Fenna, R. E.; Matthews, B. W. Nature (London) 1975, 258, 573.
2. Deisenhofer, J.; Epp, O.; Miki, K.; Huber, R.; Michel, H. J. Mol. Biol. 1984, 180, 385.
3. Olson, J. M.; Koenig, D. F.; Ledbetter, M. C. Arch. Biochem. Biophys. 1969, 129,42.
4. Tronrud, D. E.; Schmid, M. F.; Matthews, B. W. J. Mol. Biol. 1986, 188, 443.
5. Daurot-Larroque, S. T.; Brew, K.; Fenna, R. E. J. Biol. Chem. 1986, 261, 3607.
6. Sybesma, C.; Vredenberg, W. J. Biochim. Biophys. Acta 1963, 75, 439.
7. Sybesma, C.; Olson, J. M. Proc. Natl. Acad. Sci. USA 1963, 49, 248.
8. Sybesma, C.; Vredenberg, W. J. Biochim. Biophys. Acta 1964, 88, 205.
9. Olson, J. M. Int. J. System. Bact. 1978, 28, 128.
10. Shaposhnikov, V. V.; Kondratieva, E. N.; Federov, V. D. Nature (London) 1960, 187, 167.
11. Karapetyan, N. V.; Swarthoff, T.; Rijgersberg, C. P.; Amesz, J. Biochim. Biophys. Acta 1980, 593, 254.
12. Swarthoff, T.; Amesz, J.; Kramer, H. J. M.; Rijgersberg, C. P. Isr. J. Chem. 1981, 21, 332.
13. van Grondelle, R.; Hunter, C. N.; Bakker, J. G. C.; Kramer, H. J. M. Biochim. Biophys. Acta 1983, 723, 30.
14. Lutz, M.; Hoff; A. J.; Brehamet, L. Biochim. Biophys. Acta 1983, 679, 331.
15. Swarthoff, T.; de Grooth, B. G.; Meiburg, R. F.; Rijgersberg, C. P.; Amesz, J. Biochim. Biophys. Acta 1980, 593, 51.
16. Causgrove, T. P.; Yang, S.; Struve, W. S. J. Phys. Chem. 1988, 92, 6790.
17. Phillipson, K. D.; Sauer, K. Biochemistry 1972, 11, 1880.
18. Olson, J. M.; Ke, B.; Thompson, K. H. Biochim. Biophys. Acta 1976, 430, 524.
19. Whitten, W. B.; Nairn, J. A.; Pearlstein, R. M. Biochim. Biophys. Acta 1978, 503, 251.

20. Whitten, W. B.; Olson, J. M.; Pearlstein, R. M. Biochim. Biophys. Acta 1980, 591, 203.

21. Pearlstein, R. M.; Hemenger, R. P. Proc. Natl. Acad. Sci. USA 1978, 75, 4920.

22. Pearlstein, R. M. In Photosynthetic Light-Harvesting Systems, Hugo, S., Ed.; Walter de Gruyter: Berlin, 1988, p 555.

23. Pearlstein, R. M. In Chlorophylls, Hugo, S., Ed.; CRC Press: Boca Raton, 1990, in press.

24. Pearlstein, R. M. Biochim. Biophys. Acta 1990, submitted for publication.

25. Whitten, W. B.; Pearlstein, R. M.; Phares, E. F.; Geacintov, N. E. Biochim. Biophys. Acta 1978, 503, 491.

26. Mattews, B. W.; Fenna, R. E.; Remington, S. J. Ultrastruct. Res. 1977, 58, 316.

27. Gudowska-Nowak, E.; Newton, M. D.; Fajer, J. J. Phys. Chem. 1990, submitted for publication.

28. van Grondelle, R. Biochim. Biophys. Acta 1985, 811, 147.

29. Geacintov, N. E.; Breton, In CRC Critical Reviews in Plant Sciences; CRC Press:Boca Raton, 1987, Vol. 5, p 1.

30. Sauer, K. In Bioenergetics of Photosynthesis, Govindjee, Ed.; Academic Press: New York, 1975, p 115.

31. Pearlstein, R. M. Photochem. Photobiol. 1982, 35, 835.

32. Sauer, K. Acc. Chem. Res. 1978, 11, 257.

33. Forster, T. Ann. Physik. 1948, 2, 55.

34. Wilkinson, F. Adv. Photochem. 1964, 3, 241.

35. Johnson, S. G.; Small, G. J. Chem. Phys. Lett. 1989, 155, 371.

SECTION III.

TRANSIENT PHOTOCHEMICAL HOLE BURNING STUDIES OF REACTION CENTERS FROM *Rhodobacter sphaeroides*

INTRODUCTION

The molecular assembly responsible for initiating charge separation in photosynthesis is called the reaction center (RC). The more general aspects of photosynthesis including the organization of the photosynthetic unit and various other details of the electron transport chain have been described in the general introduction, so here the focus will be on the RC. The RC consists of a primary electron donor (PED), accessory pigments and proteins. For the specific RC studied here, that of the purple photosynthetic bacteria *Rhodobacter sphaeroides*, the PED is a special pair of bacteriochlorophyll *a*(Bchl *a*) molecules and there are four accessory pigment molecules, two Bchl *a* and two bacteriopheophytin *a* (BPheo *a*) molecules. The following symbols are commonly used for the PED and accessory pigments: PED- P, Bchl- B_L, B_M, and BPheo- H_L, H_M. The subscripts will be defined later when the structure of the RC is discussed, but briefly they refer to the protein subunits that the pigments are attached to. A detailed description of the RC will also be given later in this section. H_L is the intermediate electron acceptor for the RC in the process of charge separation. Charge separation is initiated by the absorption of a photon by the the PED ($P^* \leftarrow P$)and the promotion of the PED to its first excited state. This promotion can also be accomplished by the transfer of energy from the accessory pigments as will be discussed later in this section. Following excitation of P^*, the charge separated species $P^+B_LH_L^-$ forms in picoseconds via the reaction, $P^*B_LH_L \Rightarrow P^+B_LH_L^-$.

The dynamics of the charge separation reaction, $P^*BH \Rightarrow P^+BH^-$, are not well understood. Answers to two crucial questions regarding the initial step of charge separation as it takes place in reaction centers photosynthetic bacteria are being sought actively. The first question is what is the role of B, the Bchl *a* monomer on the L-side, in the formation of the charge separated state, P^+BH^-? The second question is even more fundamental than the first, what is the nature or structure of P^*, the excited state of the primary electron donor in the RC? Before the high resolution spectroscopy performed on this RC is reviewed it is pertinent to have a better appreciation for the physical dimensions

and geometry of the RC. This information was provided by the technique of single crystal x-ray diffraction and has recently been judged worthy of a Nobel prize in chemistry [1].

The x-ray diffraction experiments of Deisenhofer et al. [2,3] led to the determination of the structure of crystals of the photosynthetic bacteria *Rhodopseudomonas viridis* at 3.0 Å resolution. Michel had demonstrated the ability to grow crystals of the RC of *Rps. viridis* two years prior to this time [4]. The structure determination for *Rb. sphaeroides* was accomplished by two groups of researchers (Allen et al. [5] and Chang et al. [6]) utilizing the coordinates from *Rps. viridis* and the Patterson search (molecular replacement) method. The most precise structural determination for *Rb. sphaeroides* is that of Allen et al. [7] with a resolution of 2.8 Å. Several excellent review articles have appeared on this subject [1,8,9].

The RC of *Rb. sphaeroides* consists of six pigment molecules (4 Bchl *a* and 2 BPheo *a*), two quinone molecules (ubiquinone), one non-heme iron, and three protein subunits (L, M and H). The pigment molecules and quinones are arranged in a fashion such that approximate C_2 symmetry exists (see Fig. 1). Two Bchl *a* are at the top of the RC and are closely associated (center-to-center distance ~7 Å). Closest to this special pair of bacteriochlorophylls are two other molecules of Bchl *a*. These are ~10 Å from the closest member of the special pair and related to one another by ~C_2 symmetry. These two molecules are commonly referred to as voyeur or monomer Bchl *a* (B_L, B_M). After the voyeur Bchl *a* molecules are the two BPheo *a* molecules (H_L, H_M) which are ~16 Å from the closet member of the special pair. These are related by two-fold symmetry, as are the quinones that are next in line (~30 Å from the special pair). The non-heme iron is situated at the bottom of the RC, as featured in Fig.1, and lies along the ~C_2 symmetry axis. The voyeur Bchl *a* and BPheo *a* molecules are referred to as accessory pigments. The RC of *Rps. viridis* is very similar to that of *Rb. sphaeroides* and differs only in the following ways: Bchl *b* replaces Bchl *a*, BPheo *b* replaces BPheo *a*, menaquinone replaces the L-side bound ubiquinone and a cytochrome molecule is bound to the protein on top of the RC.

The subscripts L and M refer to the protein subunit which makes up the majority of the RC (in terms of mass) and which fixes the chromophores at their respective positions.

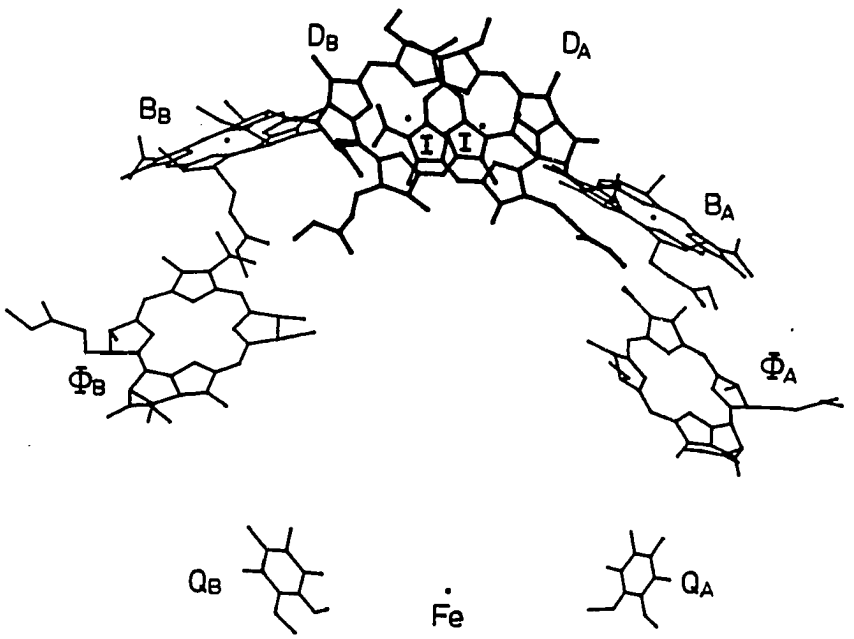

Figure 1. Pigment structure for RC of *Rb. sphaeroides* R-26. Special pair at the top and non-heme iron and quinones at the bottom. See text for further details

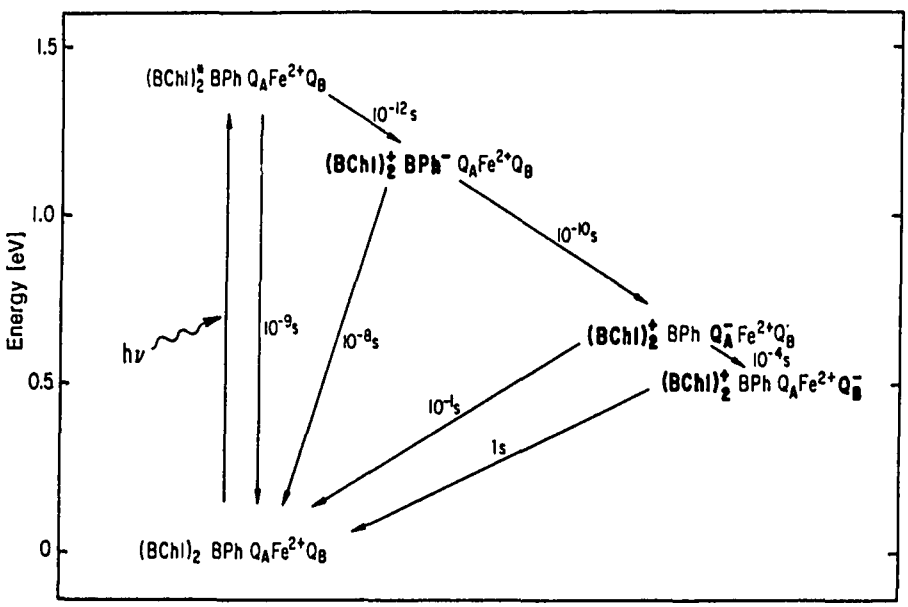

Figure 2. Charge separation and electron transfer reactions as they occur in the RC. The times are order of magnitude estimates for room temperature values. Subscript A is equivalent to L and B to M

The three protein subunits comprising the RC each have a mass of ~30-40 kDa. X-ray diffraction shows the presence of 11 transmembrane helices with the L and M subunits in close contact and forming, between them, a cylindrical core (elliptical in shape with axes ~30 Å and ~70 Å) [8]. The central core region is composed of 4 α-helices. The RC of *Rps. viridis* crystallizes in tetragonal shaped crystals with unit cell dimensions a=b=223.5 Å, c=113.6 Å and one RC (~145 kDa) in each cell [1]. The total length of the RC being ~130 Å with elliptical cross sections of 30 Å and 70 Å [1]. The RC of *Rb. sphaeroides* is acknowledged to be of similar size and shape.

Most importantly, spectroscopic evidence [10] has shown that electron transfer proceeds only down the L-side of the RC (see Fig. 2). This is remarkable since identical pigments occupy each "arm", L and M, of the the RC and they, as well as, the protein subunits, L and M, are related by ~C_2 symmetry [1-9]. There are subtle differences in the amino acid residues in the protein subunits that bind to the pigments [11,12]. Site-specific mutagenesis experiments [13-16] have investigated the effect of changing these residues on the electron transfer and charge separation kinetics. The deciphering of the protein's role in energy and electron transfer is one aspect where high resolution optical spectroscopy has been shown to be effective in giving additional information [9,17,18]. Techniques such as ultrafast and hole burning spectroscopies have been particularly effective in determining early time (fs⇒ns) events involved in energy and electron transfer in photosynthesis [19,20-27]. The role of theoretical calculations in modelling the electronic structure of the RC states is an active one and has focussed considerable attention on the initial act of charge separation.

There are two general schools of thought as to the role of B in the formation of P^+BH^-. Either B acts as an intermediate electron acceptor in the reaction (i.e., $P^*BH \Rightarrow P^+B^-H \Rightarrow P^+BH^-$) or B participates in a superexchange mechanism in which a state with 'B' character acts as a virtual state in the reaction $P^*BH \Rightarrow P^+BH^-$. Both of these proposals have been theoretically considered and reported on [28-32], but no firm consensus has been reached. Marcus [28] considered both mechanisms recently in terms of being consistent with the kinetic and singlet-triplet energy splitting data and concluded that the two step

model fit better with the available experimental evidence. However, ultrafast measurements by Breton et al. [19,33] on RC of *Rb. sphaeroides* and *Rps. viridis* with 100 fs resolution showed no indication of B^- forming (no bleach of the B band). Although, more recent ultrafast results [34] have provided a source of controversy in this matter. The ultrafast data will be discussed in detail later in this section.

Won and Friesner [29] have found that the superexchange mechanism can adequately account for the electron transfer kinetics and singlet-triplet energy splitting if an internal charge transfer(C-T) state of the special pair is incorporated into the theoretical model. Marcus [28] did not make use of an internal charge transfer state in his calculations. Bixon et al. [30] supported the superexchange mechanism for the RC of *Rb. sphaeroides* but did not utilize a C-T state. This field of research is active from both theoretical and experimental viewpoints and has been the subject of several review articles [31,32,35].

The model of Won and Friesner [29] brings up the second question proposed above, that concerning the nature of the state P^*. A basic point of controversy is what , if any, amount of charge transfer character to assign to P^*. Early experimental evidence based on hole burning [20-23], accumulated photon echo [22,23] and Stark effect spectroscopy [36-39] suggested that P^* could possess significant charge transfer character. Theoretical calculations by Won and Friesner [40-42], which utilized vibronic coupling of P^* to a "nearly resonant" C-T state, were able to provide satisfactory fits to the unstructured photochemical hole spectra of Boxer et al. [20,21]. The C-T state was thought to lie $\leq$2000 cm^{-1} from the special pair transition ($S_1 \leftarrow S_0$) and an exchange coupling strength of $\geq$80 cm^{-1} was found necessary to account for the lack of a zero-phonon hole in the spectra of Boxer et al. [20,21]. Two low frequency vibrational modes, 50 and 100 cm^{-1}, were utilized by Won and Friesner for the vibronic coupling of P^* to the C-T state. No specific molecular motion was attributed to these modes.

The more recent hole burning experiments of Tang et al. [24,25] and Johnson et al. [26,27] which clearly show a zero-phonon hole(ZPH) in the photochemical hole profiles for the RC of *Rps. viridis* and *Rb. sphaeroides* are in contradiction with the theoretical

predictions of Won and Friesner [40,41] which allowed for ultrafast dephasing from P^* and thus no ZPH would be observable. Their theory has recently been modified to account for the observation of a weak ZPH by allowing for a variable exchange coupling strength [31]. A more reasonable approach to the modeling of the hole spectra, as well as, the more general question of the nature of P^*, $P870^*/P960^*$, has been proposed by Hayes and Small [43,44].

The model proposed by Hayes and Small [43,44] is reviewed and expanded upon in detail in the additional results and discussion section in this chapter, so its merits will be only briefly outlined here. The anomalously large width of the hole spectra and absorption profiles of P870/P960 (Boxer et al. [20,21]) were explained in terms of coupling to protein phonons (linear electron-phonon coupling) and inhomogeneous broadening [44]. The coupling strength was thought to be moderately strong, S~4-5, based on the data of Boxer et al. [20,21] and inhomogeneous broadening of 150-350 cm^{-1} was indicated. No coupling to a C-T state was utilized. This model successfully accounted for the data of Boxer et al. [20,21], as well as, the thermal broadening data of Hayes et al. [44] for both *Rb. sphaeroides* and *Rps. viridis*. The role of C-T character in the excited state of the primary electron donor, $P870^*/P960^*$, can not be completely excluded, however, based on experimental evidence from Stark data [36-39].

Time regime experiments performed on RC of *Rb. sphaeroides* by Martin et al. [45] yielded several important pieces of information. Their experiments were performed with ~100 fs time resolution at room temperature using excitation directly into the P870 absorption band. The changes in the absorption spectrum were monitored at a variety of wavelengths both to the red (as far as 1240 nm) and to the blue (as far as 545 nm). The results of their experiments were that instantaneous (≤100 fs) bleaching of P870 occurred, as well as, instantaneous induced absorption gain (over a broad spectral range, 600-1300 nm) and stimulated emission from $P870^*$, when P870 was directly excited with a laser [45]. The stimulated emission of $P870^*$ was observed to decay with a lifetime of 2.8±.2 ps [45] as was the induced absorption gain. Changes in the other portions of the spectrum, Q_y bands of BPheo *a* and Bchl *a*, were observed to occur in ≤100 fs and decay with time

constants of 2.8 ps. The observation of the photo-reduction of pheophytin in 2.8 ps and the observation of absorption gain at centered ~1240 nm with a time constant of 2.8 ps indicating P^+ formation led to assignment of the time, 2.8±.2 ps as that for the $P^*B_LH_L \Rightarrow P^+B_LH_L^-$ reaction. No bleaching of the Bchl *a* monomer band was reported, only an electrochromic shift of this feature (occurring with a 2.8 ps time constant) [45]. The local electric field of P^+BH^- leads to a shift of the absorption spectra of B. Earlier time regime studies [46-48] had led to a great deal of controversy concerning the degree of involvement of B_L in electron transfer. These studies were hampered by either laser pulses of inappropriate length (33 ps) or suspect data analysis [46,47]. The studies of Martin et al. [45] (the highest resolution at that time, 1986) determined no involvement unless it occurred in ≤100 fs. Similar experiments performed on RC of *Rps. viridis* yielded identical results (instantaneous bleaching, ≤100 fs, and formation of $P^+B_LH_L^-$ in 2.8±.2 ps) [49]. The experiments on *Rps. viridis* differed somewhat in that excitation into the BPheo *b* and Bchl *b* bands was also performed and energy transfer was observed to occur in ≤100 fs [49]. Similar experiments were performed on RC of *Rps. viridis* by Wasielewski and Tiede [50] with .45 ps time resolution and they determined a 6.0 ps time constant for the initial charge separation step at room temperature.

Ultrafast experiments by Breton et al. [33] at room temperature and with ~150 fs time resolution on RC of *Rb. sphaeroides* using excitation into the BPheo *a* and Bchl *a* (Q_y) bands yielded similar results to those of Martin et al. [45]. Instantaneous (≤150 fs) energy transfer to P870 from either $B_{L,M}$ or $H_{L,M}$ was observed, however when excitation and observation were within the Q_y of $B_{L,M}$ a transient bleach which recovered in ~400 fs was noted [33]. This phenomenon was reported to occur in *Rps. viridis* as well by Breton et al. [49]. This was not interpreted as evidence for involvement of B_L in electron transfer (i.e., $P^+B_L^-H_L$ was not considered to be indicated) instead several other explanations were considered. The most plausible explanation proposed [33] was that ~10% of the Bchl *a* monomer molecules relaxed to the ground state in ~400 fs ($B^* \Rightarrow B$) without transferring energy to P870, while the remaining fraction (.90) transferred their energy to P870. The observation of the dependence of the quantum yield of charge

separation (ϕ_{CS}) upon excitation wavelength seemed to corroborate this explanation with ϕ_{CS}=.93 (for excitation into the Bchl *a* monomer band) and ϕ_{CS}=1.0 (for P870 excitation) [51].

The experiments on RC of *Rb. sphaeroides* were also performed at T=10 K with 100 fs time resolution and reported by Breton et al. [19]. The initial charge separation step ($P^*BH \Rightarrow P^+BH^-$) was stated as occurring in 1.2±.1 ps [19]. Results for RC of *Rps. viridis* were reported in the same paper and a time constant of .7±.1 ps for the initial charge separation step was reported [19]. The 400 fs transient bleach in the Bchl monomer region was also observed for RC from both species at 10 K [19]. The earlier explanation, stated above, for the observation of the 400 fs transient bleach was confirmed and supported by Breton et al. [19]. In addition, experiments were performed on RC of *Rb. sphaeroides* treated with borohydride (which either removes B_M or turns it into the corresponding pheophytin) and these indicated that this 400 fs transient was not due to B_M alone [19].

More recent experiments by Holzapfel et al. [34] on RC of *Rb. sphaeroides* conducted at room temperature with 80 fs time resolution have created a new controversy concerning the presence or not of an intermediate electron acceptor (before H_L). They excited within the P870 absorption band and probed to higher energy. Their data (in early time, ≤10ps) were fit using two time constants of 3.5 and .9 ps instead of just one of 2.8 ps. They fit transient absorption spectra at several different wavelengths effectively with this model [34], with the first step occurring in 3.5 ps and the second step in .9 ps. The charge separation and electron transfer processes occurred as $P^*BH \Rightarrow P^+B^-H \Rightarrow P^+BH^-$ based on their analysis [34]. The rapid depletion of P^+B^-H allowed for a maximum ~15% of this species to be created at any one time and this was thought to explain the lack of observation of the photo-reduction of the B_L previously [34]. Frequency regime studies, in particular hole burning experiments, have provided excellent complementary information to the ultrafast measurements in the area of the initial act of charge separation and the nature of the excited state of the special pair.

Transient photochemical hole burning (PHB) experiments have been performed on RC of *Rb. sphaeroides* [20,22] and *Rps. viridis* [21,23] as early as 1985. Boxer et al.

[20,21] used PVOH films of both RC while Meech et al. [22,23] utilized RC suspended in glycerol/water (2:1). These studies, which shall be reviewed here, in combination with the time regime measurements, discussed earlier, gave rise to a great controversy concerning the initial step of charge separation. Both of these groups of researchers, independently, observed similar results for the PHB studies, the formation of broad (FWHM=350-500 cm^{-1}) holes when they irradiated within the P_- band of the RC [20-23]. In the case of *Rps. viridis* both groups reported unstructured holes (FWHM=350-400 cm^{-1}) whose maxima did not depend upon the position of the burn laser (i.e., the hole maxima was stationary) for λ_B=830-980 nm (Meech et al. [23]) and λ_B=975-1013 nm (Boxer et al. [21]). In the case of RC of *Rb. sphaeroides* Boxer et al. [20] reported unstructured holes (FWHM=400-500 cm^{-1}) whose maxima shifted (~200 cm^{-1}) depending upon λ_B (860-895 nm). Meech et al. [22] also reported unstructured holes for RC of *Rb. sphaeroides*, however, they reported no movement of the hole maxima with varying λ_B (865-890). This discrepancy can be explained, as will be shown later in this section, in terms of a solvent effect upon the low temperature absorption spectra of P_- [52]. It is relevant to point out that Meech et al. [22,23] utilized difference transmission spectra while Boxer et al. [20,21] used difference absorption spectra for their respective analyses. The distinction between these two methods of data presentation being, under most conditions, considerable [26,27], as will be made clear later in this section. Regardless, of this fact their interpretation of their results were very similar.

Without the observation of a ZPH, even though the lasers used for the hole burning experiments exhibited moderately narrow linewidths of 2-4 cm^{-1}, the holewidths (~400 cm^{-1}) were interpreted as homogeneous and indicative of an ultrafast excited state lifetime, ~25 fs [20-23]. This time was corroborated by Meech et al. [22,23] by the use of accumulated photon echo experiments which indicated a process occurring ≤100 fs. Both groups [20-23] proposed that this could indicate decay into a C-T state from which the charge separated state P^+BH^- was formed. Boxer et al. [20,21] also proposed a second possible explanation for the broad holes which was that the special pair exhibited strong linear electron-phonon coupling (so that a ZPH was totally suppressed) and

inhomogeneous broadening. With the second proposal, Boxer et al. [21] indicated the strong possibility that the excited state (S_1) for P870 possessed significant charge-transfer character.

Thus together with picosecond measurements performed on RC of *Rps. viridis* [19,49,50] and *Rb. sphaeroides* [19,33,45] the early holeburning measurments [20-23] led to a great deal of controversy concerning the excited state of P870/P960, as well as, the formation of the charge separated state P^+BH^-. The contrast between the ~25 fs and 1 ps times indicated by the frequency [20-23] and time [19,33,45,49,50] regime measurements, respectively, was a prime motivating factor for initiating new hole burning studies on P870 of *Rb. sphaeroides* and P960 of *Rps. viridis*. The hole burning experiments of Tang et al. [24,25] performed on RC of *Rps. viridis* in several different hosts in 1988 and 1989 indicated that an extremely weak ZPH could be observed. The width of this feature, ~10 cm^{-1}, indicated a ~1 ps excited state decay time for $P960^*$. This agreed well with the time regime measurements [19,49,50], but was at odds with the hole burning studies of Boxer et al. [21] and Meech et al. [23]. In addition to the ZPH Tang et al. [24,25] observed three other features (holes) which they labelled X, Y and Z. The X hole (upon which the ZPH was superimposed when appropriate λ_B was used) had a FWHM of ~120 cm^{-1} as did the Y hole which was ~120 cm^{-1} to higher energy. Y was assigned as the first quanta of a low frequency vibrational mode of state X, ω^1_{sp}. The Z hole, which was ~300 cm^{-1} higher in energy in relation to the X hole, was assigned as an electronic state coupled to X with charge transfer character. This Z state was thought to contribute significantly to the absorption profile of P960.

The rather complex analysis of the PHB spectra of *Rps. viridis* by Tang et al. [24,25] has been recently simplified [26,27,52] due to the obtaining of difference absorption hole spectra (only difference transmission spectra had been available earlier). The newer data [26,27,52] on P960 indicate that the coupling to a low frequency intermolecular vibrational mode (~135 cm^{-1}) and moderately strong linear electron-phonon coupling (S~2) to protein phonons provides complete agreement with the PHB spectra, the absorption spectra and the

ultrafast measurements without coupling to a C-T state. The newer studies on P960 were done concurrently with the studies on P870 of *Rb. sphaeroides* presented here.

The confusion generated by the seemingly contradictory holeburning results of Boxer et al. [20,21] and Meech et al. [22,23] and the ultrafast measurements by Breton et al. [19,33,49], Martin et al. [45] and Wasielewski and Tiede [50] are clarified by studies performed on RC of *Rb. sphaeroides* and reported here and the studies performed on RC of *Rps. viridis* [26,52].

EXPERIMENTAL METHODS

Samples

The reaction center (RC) samples were graciously provided by Dr. David M. Tiede of Argonne National Laboratory. Fresh RC samples were made by dissolving crystals of *Rb. sphaeroides* in a suitably buffered host. Details of the crystallization procedure can be found in ref. [6]. The host was glycerol:water glass (2:1) with .8% n-octyl-β-D-glucopyranoside detergent, 10 mM Tris, 1 mM EDTA, pH=8.0. RC samples in polyvinyl alcohol films (PVOH) (~.1 mm thick) were also used. The optical density (OD) of the primary donor state absorption was less than .5 for the samples used in this study. Care was taken to eliminate exposure to light when the sample was at room temperature.

Cryogenic Equipment

The samples were placed in a 1 cm (i.d.) path length polystyrene tubes in a brass sample holder of local design which allowed optical access to the sample. The cryostat and temperature monitoring appartus for the experiments, which were conducted at ≥4.2 K, have been described in detail in the experimental methods section of Section 1.

Experimental Apparatus

A block diagram of the experimental apparatus is shown in Figure 3. Transmission spectra were obtained using a 1 m McPherson 2061 monochromator (F=7.0, providing a linear dispersion of .833 nm/mm and blazed for the red). The slit width of the monochromator was varied as was called for in the experiment. The probe light was provided by a tungsten-halogen lamp (600 W) which was dispersed by the monochromator. The probe light upon exiting the monochromator was focussed through the sample and onto a mechanical shutter (Uniblitz 26L, Vincent Assoc. Inc.) was used to exclude the burn

laser from the detection system. The detection was accomplished using a cooled Hamamatsu R316-02 photomultiplier tube (enhanced S-1 response). Measurements were made using a Stanford Research SR250 boxcar averager interfaced with an IBM-PC compatible computer. Both shutter and boxcar averager were triggered off a single pulse from the zero drift control of the laser. The laser was operated at 16 Hz (or less in certain circumstances) to allow for the adequate charge recombination time of 21 ms for the species P^+BHQ^-.

The burn laser was a excimer (Lambda Physik EMG102) pumped dye laser (Lambda Physik FL2002) with a laser linewidth of .2 cm^{-1} and a pulse width of 10 ns. Using DCM laser dye (Exciton) the dye laser output was Raman shifted (H_2 gas) to provide tunable radiation in the region of interest (850-920 nm) for the experiments which involved burning directly into P870. LDS 722 was used for the pheophytin holeburning experiments (no Raman shifting was necessary). Pulse energies were ≤.4 mj (attenuated with neutral density filters where necessary) focussed into a .3 cm x 1. cm spot.

The boxcar gate was delayed ~2 ms from the laser pulse due to the rise time of the mechanical shutter being ~1.5 ms. A laser-off transmission spectra was obtained and then a laser-on spectra so that a delta transmission (ΔT) hole spectra could be directly obtained. By subtracting the logarithms of the transmission spectra a delta absorbance (ΔA) spectra could be obtained. Care was taken to bleach no more than 20% of the transmittance of P870 to avoid effects due to saturation. Higher burn powers resulted in upto ~80% change in transmittance. By varying the gate delay and obtaining ΔA spectra it was possible to obtain the lifetime of the charge separated bottleneck state P^+BHQ^- (21±3ms) (T=4.2 K) [19].

In the case where linearly polarized spectra were necessary a Glan/Thompson prism was inserted into the probe beam, normal to the beam path, and an optical glass polarizer (Polarcor, Corning electronic materials) was inserted in the laser beam path (to "clean up" its vertical polarization). The Glan/Thompson prism could then be rotated (90^0) to provide parallel and perpendicular linearly polarized hole spectra.

The spectra obtained were stored on diskette and analyzed using Spectra Calc (Galactic Industries Corp.) and outputed to a HP 7475A plotter (Hewlett Packard Co.).

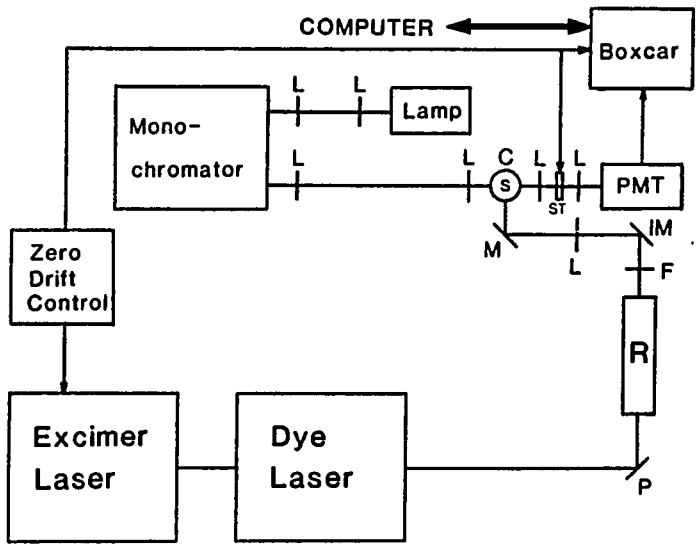

Figure 3. Block diagram of experimental apparatus. L=lens, M=mirror, IM=infrared mirror, ST=mechnical shutter, R=Raman shifter, S=sample, P=prism, C=liquid helium cryostat, F=filter, PMT=photomultiplier tube

ADDITIONAL RESULTS

In this section transient photochemical hole burned (PHB) spectra for the RC of *Rb. sphaeroides* in glycerol/NGP and PVOH/NGP will be presented. Although the hole spectra will encompass the entire Q_y spectral region, the focus will be primarily on the Q_y band of P870 in this section. Figure 4 presents the 4.2 K absorption spectra of the Q_y region of RC for both solvents. The peaks are labelled in the conventional manner [52] with H_L and H_M indicating the unresolved pheophytin bands and B_L and B_M the unresolved bacteriochlorophyll monomer bands. These assignments should be thought of as approximate since electronic structure calculations have suggested that coupling of the six pigment states may occur [53]. The low energy shoulder on the bacteriochlorophyll monomer band (810 nm) is thought to be analogous to the low energy shoulder state present at 850 nm in the absorption spectra of RC of *Rhodopseudomonas viridis* which is suspected to be P_+, the upper exciton component of the special pair by Vermeglio et al. [54].

The PVOH host has two very apparent effects on the absorption of the RC. First a larger degree of inhomogeneous broadening for each spectral feature is noted. Secondly, the absorption of P870 is blue shifted significantly, ~200 cm^{-1}. This second effect is noted for RC of *Rps. viridis*, as well when comparing glycerol and PVOH hosts [52]. The glycerol host provides the smallest amount of inhomogeneous broadening to the spectrum [52]. It may be possible to reduce Γ_I further by using minimally strained RC crystals, but given the high OD of currently available crystals [55] experiments would need to be done in the reflection mode.

The low energy shoulder on the P870 band is visible in the glycerol host but not in the PVOH host. The shoulder is emphasized in Fig. 5 which is a 4.2 K absorption spectrum of P870 (glycerol/NGP) with a second derivative as an insert. This is due to the lesser amount of inhomogeneous broadening imparted by the glycerol host. This feature, whose nature will be discussed latter in this section, is also noted for *Rps. viridis* in several

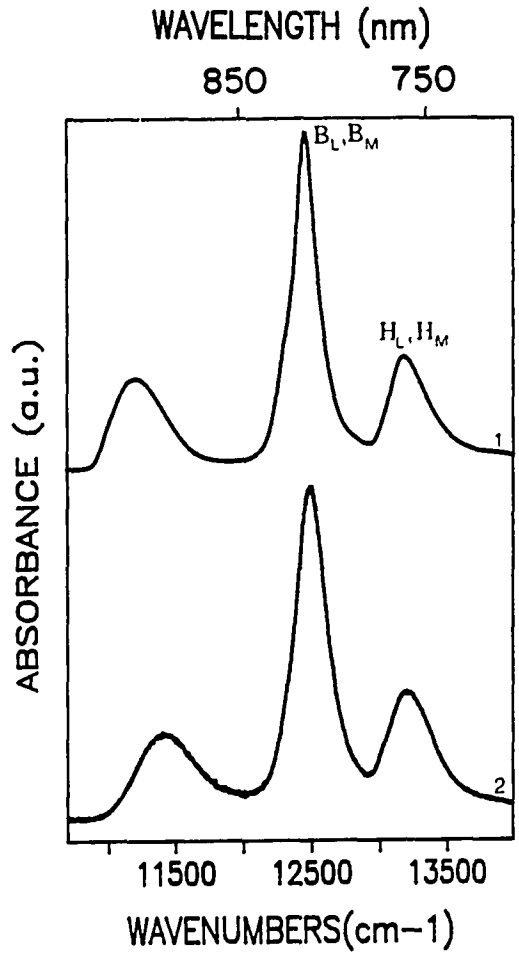

Figure 4. Absorption spectra of the Q_y region, T=4.2 K: *Rb. shaeroides* A.) glycerol/NGP (FWHM=470 cm^{-1}), B.) PVOH/NGP (FWHM=550 cm^{-1})

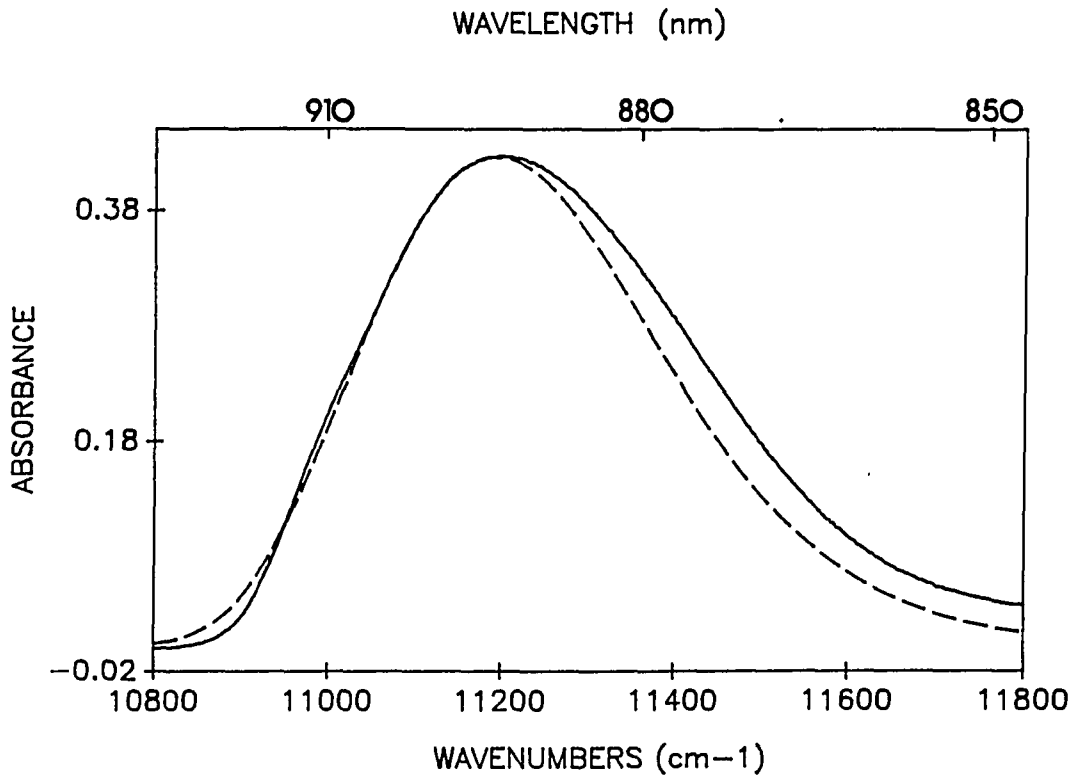

Figure 5. Calculated and experimental absorption spectra for P870. Parameters for calculated spectrum (----): Γ (one phonon profile width)= 30 cm^{-1}, ω_m (mean phonon frequency)= 30 cm^{-1}, S (Huang-Rhys factor)=2.2, Γ_I (inhomogeneous line broadening)=170 cm^{-1}, ω_{sp}=115 cm^{-1}, S_{sp}=1.5. See text for details

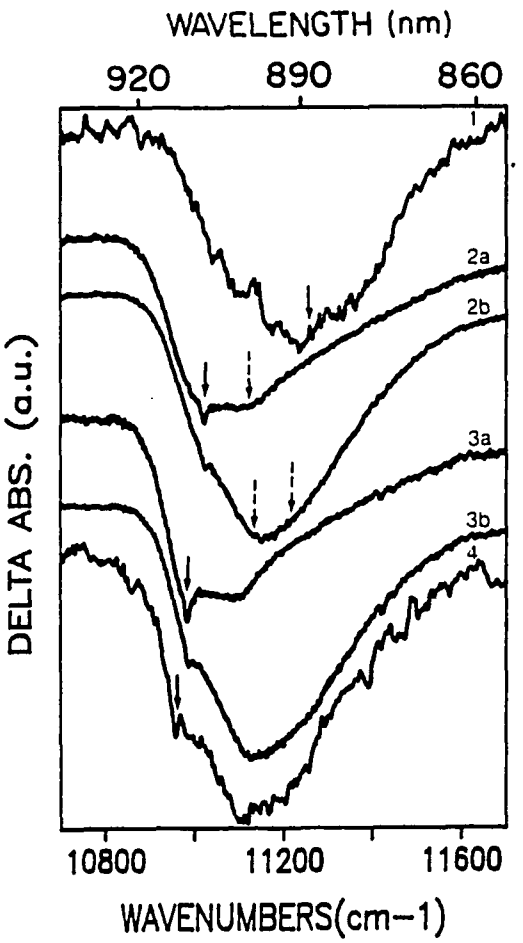

Figure 6. Hole burned spectrum for P870, T=4.2 K. Solid arrows locate λ_B = 890, 907, 910, and 912 nm for spectra 1-4. All spectra are ΔA except for 2a and 3a which are ΔT spectra corresponding to 2b and 3b, respectively. Resolution ≤ 8 cm^{-1}. Dashed arrows in 2a and 2b indicate approximate positions of ω^1_{sp} and ω^2_{sp} satellites

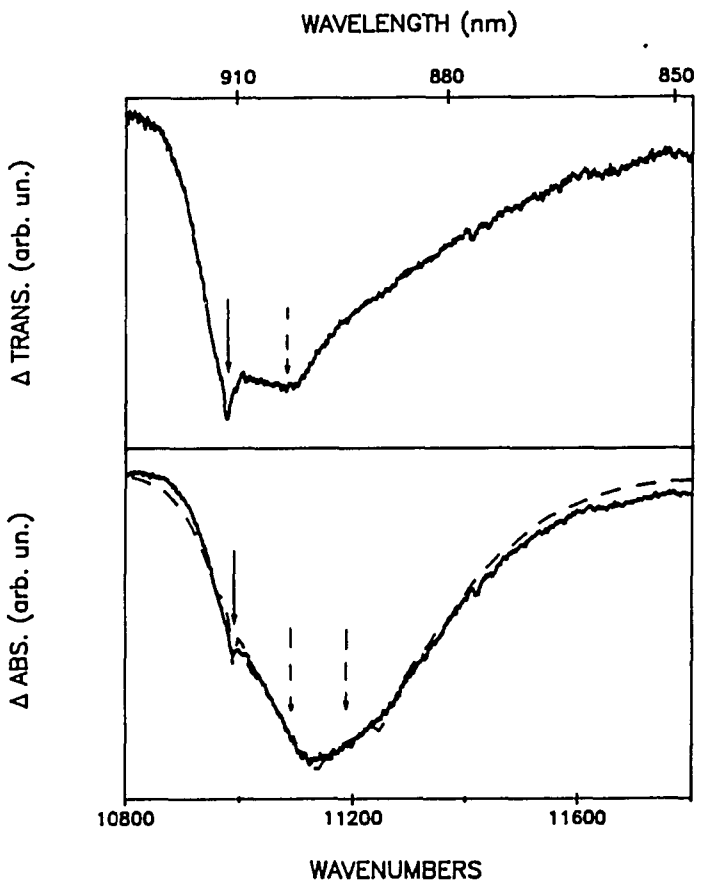

Figure 7. Calculated and experimental hole spectra for P870 (lower frame, ΔA), λ_B=912. nm. See Fig. 5 caption and text for details. Upper frame is ΔT

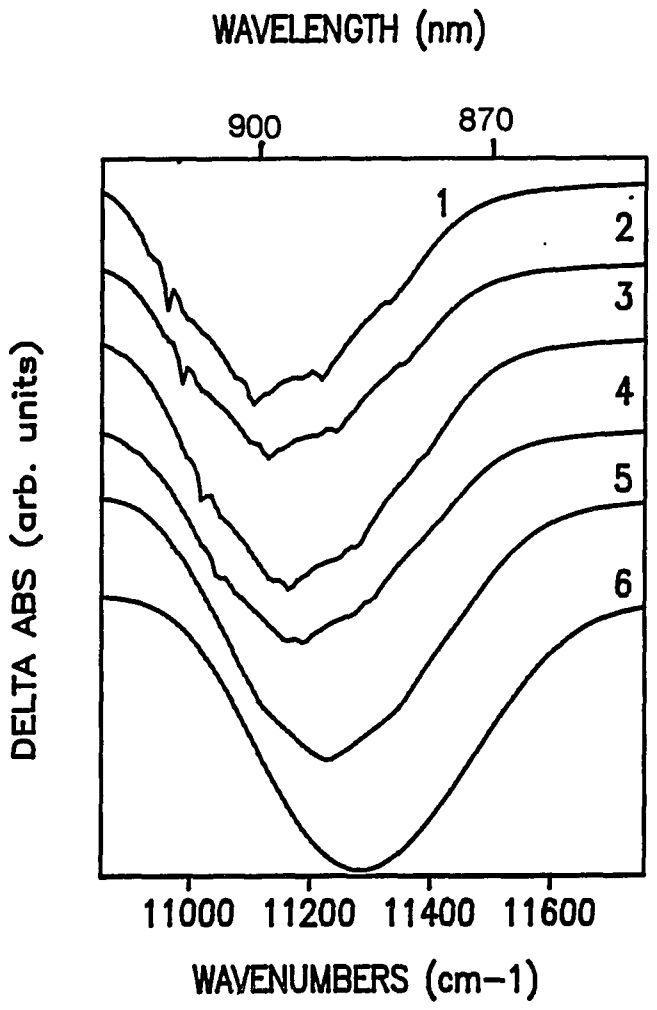

Figure 8. Calculated hole burned spectra for P870 using the same parameters as in Fig. 5. λ_B= 1.) -50 cm^{-1}, 2.) -25 cm^{-1}, 3.) 10 cm^{-1}, 4.) 35 cm^{-1}, 5.) 220 cm^{-1}, 6.) 615 cm^{-1}. λ_B given relative to maximum of zero site distribution (SDF). Maximum of SDF, 11013 cm^{-1}

different host-detergent systems [24,25]. The feature will be shown to be an intrinsic part of the absorption spectrum of the RC [26].

Transient PHB Spectra of P870

Figure 6 presents four ΔA (absorbance) transient hole spectra for Rb. sphaeroides (glycerol/NGP), T=4.2 K. Two ΔT (transmission) spectra are also presented to demonstrate the improved resolution possible in the transmission mode when the sample's optical density is high enough. A narrow zero phonon hole (ZPH) is evident in the spectra where λ_B (burn wavelength) was located near the center of the ω^0_{sp} band. This ZPH is gradually lost as λ_B is shifted higher in energy as is predicted in the theory of strong linear electron-phonon coupling and inhomogeneous line broadening [44].

The ΔA spectra obtained with λ_B=910.0 and 907.0 nm show hole spectra rich in structure. In addition to the ZPH and the hole corresponding to ω^0_{sp} (the shoulder state observed in absorption) a broad hole (400 cm^{-1}) is present which can be seen to consist of a progression of vibronic holes ~120 cm^{-1} in frequency. The first quanta, ω^1_{sp}, is actually more prominent than ω^0_{sp}. The dashed arrows in Fig. 6 indicate the first and second quanta of this vibrational mode, ω^1_{sp} and ω^2_{sp}, in the hole spectra. Similar structured hole spectra were obtained for *Rps. viridis* [26] (incl. a ZPH) showing the progression of a ~135 cm^{-1} vibrational mode with the first quanta, ω^1_{sp}, being more intense than ω^0_{sp}, and three quanta are clearly visible, ω^1_{sp}, ω^2_{sp}, and ω^3_{sp}. The ZPH observed here can give information concerning the excited state decay time for P870 ($P870^*$) and this aspect will be addressed in the next subsection.

It is clear that moderately strong coupling (S_{sp}≈1) to a vibrational mode (ω_{sp}) is necessary to account for the underlying structure observed in the absorption spectra and hole spectra for P870. From the weakness of the ZPH observed moderately strong linear electron-phonon coupling (S≈2) to a protein phonon is also indicated. The proposal of ultra-fast (fs) decay of $P870^*$ to a C-T state made by Won and Friesner [40,41] and others [20-23] finds no support from the spectra presented here, since this type of behavior would

preclude the observation of a ZPH. The theory of Hayes and Small [43,44] was developed to fit the unstructured P870 and P960 hole spectra of Boxer et al. [20,21] and in those circumstances the mean phonon approximation was used (with coupling to a single protein phonon). It is obvious here that both a protein phonon, ω_m, and a second low frequency vibrational mode, ω_{sp}, must be utilized. The intramolecular vibrational modes for Bchl *a* have Franck-Condon factors ≤.02 [56] and thus are not considered intense enough to warrant consideration in understanding the principal features of the hole spectra. The modifications to the theory of Hayes and Small [43,44] are straightforward and shall be shown here.

Using the mean phonon frequency approximation Hayes et al. [44] express the low temperature absorption profile of a single site as

$$L(\Omega-\nu) = e^{-S}\ell_0(\Omega-\nu) + \sum_{r=1}^{\infty} \frac{S^r e^{-S}}{r!}\ell_r(\Omega-\nu - r\omega_m) \qquad (1)$$

where ν is the zero-phonon transition frequency and ω_m is the mean frequency for phonons which couple to the electronic transition. S is the Huang-Rhys factor and the Franck-Condon factors for the r=0,1,2,... phonon transition are governed by the Poisson distribution $\{S^r e^{-S}/r!\}_r$. The Franck-Condon factor for the zero-phonon transition is e^{-S}, and its profile is Lorentzian (l_0) with a FWHM=γ, which is the homogeneous linewidth of the zero-phonon line. The lineshape for the one-phonon profile is l_1 and is centered at $\upsilon+\omega_m$ with a FWHM of Γ. The one-phonon profiles for electronic transitions of molecules in glassy hosts carry a width of ~30 cm^{-1} typically, and the profiles for antenna Chl *a* and *b* confirm this [56]. To a good approximation the profile can be taken to be Gaussian. Eq. 1 is valid for coupling to pseudo-localized phonons or a distribution of host phonons governed by a suitable density of states. For the latter case and a phonon profile governed by a Gaussian, the width of the r-phonon profile, centered at $(\upsilon+\omega_m)$ is given by $\Gamma_r=r^{1/2}\Gamma$. For preliminary fits of the P870 hole spectra presented here Lorentzians for l_r ($r\geq1$) were

used [26,52] with widths governed by the Gaussian values, $r^{1/2}\Gamma$ in order to derive an analytic expression for the hole profile. Subsequently, a method was found to incorporate the use of Gaussians in the expression for the phonon lineshapes without increasing the computing time unreasonsably. The most realistic phonon lineshape was found to be a convolution of the two lineshapes with a Gaussian half ($\leq\upsilon+\omega_m$) and a Lorentzian half ($\geq\upsilon+\omega_m$), with the Lorentzian width being Γ. For simplicity the derivation is done using Lorentzian lineshapes for the phonon profiles.

Eq. 1 can be modified to include coupling to the ω_{sp} mode:

$$L(\Omega-\nu) = \sum_{j=0}^{\infty} \frac{S_{sp}^{j} e^{-S_{sp}}}{j!} \left[e^{-S} \ell_0^j(\Omega-\nu - j\omega_{sp}) + \sum_{r=1}^{\infty} \frac{S^r e^{-S}}{r!} \ell_r^j(\Omega-\nu - r\omega_m - j\omega_{sp}) \right] \quad (2)$$

where S_{sp} is the Huang-Rhys factor for ω_{sp}. The assumption that the electron-phonon coupling (S) is independent of the ω_{sp}-mode occupation number j is made in deriving Eq. 2. In addition ω_m and Γ are to be considered independent of j. However, the homogeneous linewidths γ_j of the zero-phonon functions l_0^j may differ due to, for example, rapid vibrational relaxation of the ω_{sp} ($j\geq1$) levels.

For disordered hosts a Gaussian distribution of zero-phonon transition frequencies of width Γ_I is the appropriate choice, but in order to obtain an analytic expression for the hole profile a Lorentzian is utilized, $N_0(\upsilon-\upsilon_m)/N$ when N is the total number of absorbers and υ_m is the mean zero-phonon frequency. The fits featured here have been accomplished using a Gaussian distribution of zero-phonon transitions by making use of an approximation, however, the derivation will be completed using a Lorentzian lineshape for this quantity for simplicity. The absorption spectrum is calculated as the convolution of this distribution function with the single site absorption profile $L(\Omega-\upsilon)$. The absorption cross-section, laser intensity and photochemical quantum yield are defined as σ, I, ϕ, respectively. Following a burn for time τ

$$N_\tau(\nu - \nu_m) = N_0(\nu - \nu_m)e^{-\sigma I\phi\tau L(\omega_B - \nu)} \qquad (3)$$

where ω_b is the laser burn frequency and $L(\omega_B\text{-}\upsilon)$ is given by Eq. 2. To obtain the absorption spectrum, $A(\tau)$, following the burn one must convolve Eq. 3 with $L(\Omega\text{-}\upsilon)$ and integrate over υ. For notational simplicity, Eq. 1 rather than Eq. 2 is used in what follows. The modifications of the resulting hole shape function necessary to take into account the ω_{sp}-progression will simply be stated. Thus,

$$A_\tau(\Omega) = \int d\nu N_0(\nu - \nu_m)e^{-\sigma I\phi\tau L(\omega_B - \nu)}L(\Omega - \nu) \qquad (4)$$

For simplicity the short burn time limit is employed so that the exponential can be expanded as $1\text{-}\sigma I\phi\tau L(\omega_B\text{-}\upsilon)$. This approximation need not be made, but the resulting expressions are cumbersome if it is not. The hole spectrum in the short burn time limit is simply

$$A_0(\Omega) - A_\tau(\Omega) = \sigma I\phi\tau \sum_{r,r'=0}^{\infty} \left(\frac{S^r e^{-S}}{r!}\right)\left(\frac{S^{r'} e^{-S}}{r'!}\right) \cdot \int d\nu N_0(\nu - \nu_m)\ell_r(\Omega - \nu - r\omega_m)\ell_{r'}(\omega_B - \nu - r'\omega_m) \qquad (5)$$

One cannot assume that $N_0(\upsilon\text{-}\upsilon_m)$ is constant in Eq. 5 because the holes of interest have widths comparable to Γ_I. Integration of Eq. 5 yields

$$[A_0 - A_\tau](\Omega) = \frac{\sigma\phi\tau}{3(2\pi)^2} \sum_{r,r'=0}^{\infty} \left[\left(\frac{S^r e^{-S}}{r!} \right) \left(\frac{S^{r'} e^{-S}}{r'!} \right) \right]$$

$$\cdot \left[\left\{ \frac{\Gamma_I + \Gamma_r}{(\Omega - \nu_m - r\omega_m)^2 + \left[\frac{\Gamma_I + \Gamma_r}{2} \right]^2} \right\} \left\{ \frac{\Gamma_r + \Gamma_{r'}}{(\Omega - \omega_B + \omega_m(r' - r))^2 + \left[\frac{\Gamma_r + \Gamma_{r'}}{2} \right]^2} \right\} \right.$$

$$+ \left\{ \frac{\Gamma_I + \Gamma_{r'}}{(\omega_B - \nu_m - r'\omega_m)^2 + \left[\frac{\Gamma_I + \Gamma_{r'}}{2} \right]^2} \right\} \left\{ \frac{\Gamma_r + \Gamma_{r'}}{(\Omega - \omega_B + \omega_m(r' - r))^2 + \left[\frac{\Gamma_r + \Gamma_{r'}}{2} \right]^2} \right\}$$

$$\left. + \left\{ \frac{\Gamma_I + \Gamma_{r'}}{(\omega_B - \nu_m - r'\omega_m)^2 + \left[\frac{\Gamma_I + \Gamma_{r'}}{2} \right]^2} \right\} \left\{ \frac{\Gamma_I + \Gamma_r}{(\Omega - \nu_m - r\omega_m)^2 + \left[\frac{\Gamma_I + \Gamma_r}{2} \right]^2} \right\} \right] \quad (6)$$

The qualitative implications of Eq. 6 are discussed by Hayes et al. [44]. In the same paper model calculations with realistic values for Γ, ω_m, γ and Γ_I are given with S varying from .5 (weak coupling) to 8 (strong coupling). In Eq. 6, $\Gamma_0=\gamma$ and $\Gamma_r=r^{1/2}\Gamma$ ($r\geq 1$). For strong coupling ($S\geq 2$) and $\omega_B=\upsilon_m$, the intensity of the ZPH relative to the broad hole is given approximately by e^{-2S}. For this value of ω_B, the ZPH is located near the center of the broad and more intense hole upon which it is superimposed. For $\Gamma_I > S\omega_m$ a burn with ω_B located on the low and high energy sides of the absorption profile produces broad hole profiles that are shifted to the blue (higher energy) and red (lower energy), respectively, of ω_B.

The modifications of Eq. 6 required to take into account the ω_{sp}-progression are as follows: first, an additional double summation Σ $(\exp(-S_{sp})S_{sp}^j/j!)$ $(\exp(-S_{sp})S_{sp}^{j'}/j'!)$ must be included and Γ_r, $\Gamma_{r'}$ replaced everywhere by Γ_{rj} and $\Gamma_{r'j'}$, respectively. Thus, γ_j determines the relaxation frequency of the zero-phonon level associated with the jth member of the ω_{sp}-progression; second the energy denominators are modified by the replacements of $r\omega_m \Rightarrow r\omega_m + j\omega_{sp}$ and $r'\omega_m \Rightarrow r'\omega_m + j\omega_{sp}$.

For the calculations it was found sufficient to terminate the j- and r- sums at 5 and 10, respectively. A large number of the "parameters" (γ, S, ω_m, Γ, S_{sp}, ω_{sp}, Γ_I) are

actually experimentally determined or least estimated to a very good approximatiom. ω_{sp} can be estimated within ~10 cm^{-1} by viewing the hole spectra and S_{sp} (the Franck-Condon factor for ω_{sp}) can also be obtained in a similar manner. γ and S are obtained from the ZPH and noting the relative intensity of the ZPH with respect to the ω_{sp} hole, respectively. ω_m has very recently been determined directly using temperature dependent hole spectra [27]. S and ω_m can also be estimated by making use of the fluorescence spectra and the approximate relationship, Stokes shift$\approx 2S\omega_m$. The Stokes shift for *Rb. sphaeroides* is ~140 cm^{-1} [57]. Γ_I can be estimated by the absorption spectrum and the following relationship, $\Gamma_{abs}=\Gamma_I+S\omega_m+S_{sp}\omega_{sp}$. In addition, the amount of inhomogeneous broadening plays a pivotal role in the movement of the hole maxima with varying ω_B. Qualitatively, the increase in homogenous broadening stated for the RC in PVOH is clearly indicated by the increased movement of the hole maxima (see Fig. 10) versus the glycerol host. The hole maxima for RC in glycerol shifts ~180 cm^{-1} while in PVOH the maxima shifts ~220 cm^{-1}. The point being that these "parameters" are not free to assume any possible values to ensure a "good fit", they must be consistent with the experimental data in all accords.

The calculated hole spectra are presented in Figs. 7 and 8. The parameter values are listed in the figure captions. Figure 5 features a calculated spectra near $\omega_B=\upsilon_m$ (center of zero-phonon distribution) and the experimental hole spectrum for comparison. The fit can be seen to be quite good. Figure 8 presents a complete set of hole spectra obtained by varying ω_B. The characteristics of this group are very similar to the experimental spectra in Fig. 6. The gradual loss of the ZPH as λ_B is shifted higher in energy due to the increasing probability for multi-phonon excitation (nonline narrowing) is shown as is the gradual loss of structure in the broad hole as λ_B shifts toward the blue. These traits are in accord with the experimental data (Fig. 6). The PVOH hole spectra (Fig. 10), although they do not show structure, do increase in width ~100 cm^{-1} as λ_B shifts to the blue. Allowance was made for sub-ps decay of ω_{sp} ($j\geq 1$) levels with j^{-1} (Fermi-Golden rule prediction with cubic intermolecular anharmonicity).This dependence is necessary to

account for the lack of ZPHs in the ω_{sp}^1, ω_{sp}^2 ... holes. Attempts to observe such narrow features were made with no success. The additional dephasing for ω_{sp} was 200 fs.

The absorption spectra calculated with the same parameters as the hole spectra was plotted in Fig. 5. The fit on the low energy side and the peak are quite good. The fit on the high energy side shows that more absorption intensity is present than can be accounted for using a two mode approximation. Even though the Franck-Condon factors for the intramolecular modes are very small (≤.02) they may add some intensity in the υ_m+(300-500 cm^{-1}) region. The composition of the P870 band can be stated as 70% homogeneous ($S\omega_m+S_{sp}\omega_{sp}$) and 30% inhomogeneous (Γ_I).

Zero-phonon Holewidths

For P870 (glycerol/NGP) the average of several narrow range scans (2 cm^{-1} read resolution), with λ_B=907-912 nm, yield a holewidth of 8.5±2.0 cm^{-1} (corrected for read resolution). Two representative holes are presented in Fig. 9 A&B (λ_B=909.0 and 911.0 nm). This holewidth indicates a $P870^*$ decay time of 1.3±.3 ps. This value is in good agreement with the 1.2±.1 ps value obtained at T=10 K by ultrafast measurements [19]. Additionally, this agreement makes the statement that vibrational relaxation in the excited state of P870 ($P870^*$) occurs < 1ps. This is due to the fact that the ultrafast experiments prepare $P870^*$ vibrationally excited, while hole burning measures decay from the zero-point. This provides additional justification for providing for sub-ps decay of ω_{sp}^j (j≥1). Similar experiments for P960 of *Rps. viridis* also provided good agreement between holeburning results and time domain values (.8±.1 ps for both [26]). In addition, transient PHB experiments performed on PS II RC yielded a decay time of 1.9±.2 ps [58] which is in good agreement with that obtained by time regime measurements at 15 K [59]. If P870 relaxed to a charge transfer state prior to charge separation there would not be agreement between the holeburning data and the time regime measurements [26].

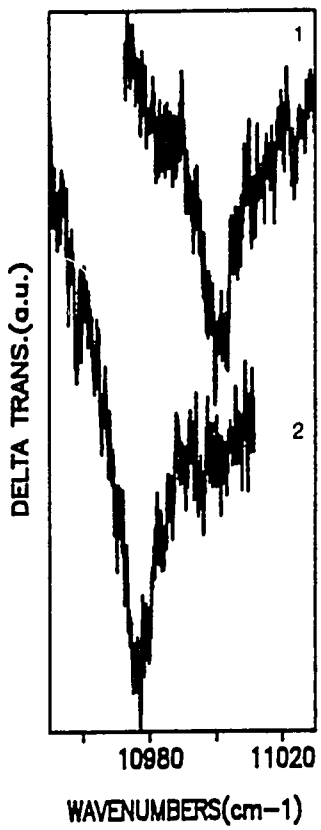

Figure 9. ZPH at 4.2 K for P870: 1.) λ_B=909 nm (11001 cm^{-1}), 2.) λ_B=911 nm (10977 cm^{-1}). Resolution = 2 cm^{-1} for both spectra

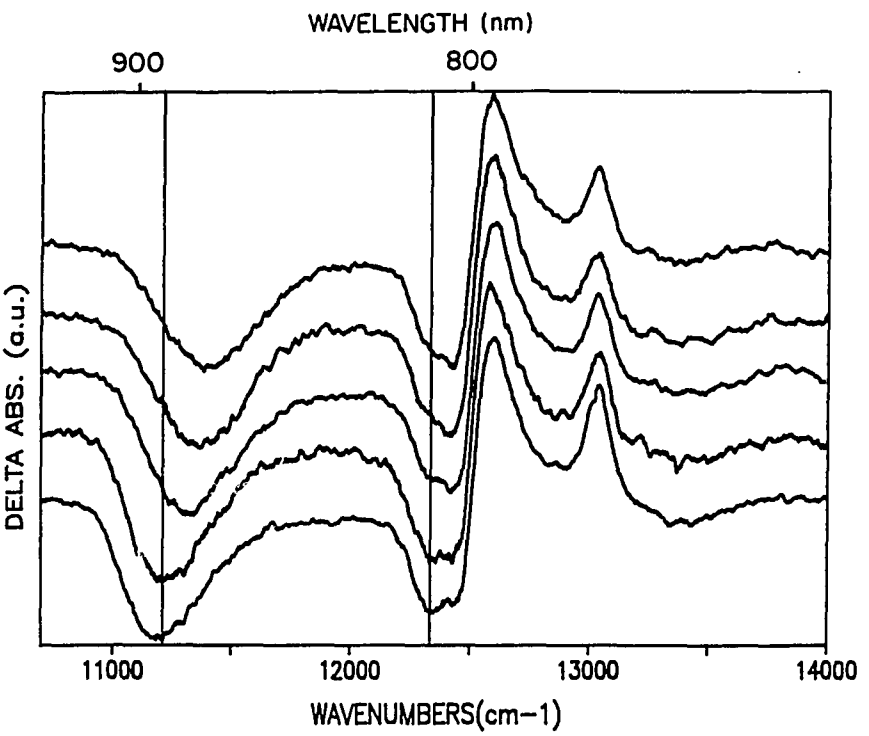

Figure 10. Hole burned spectra for *Rb. sphaeroides* (PVOH/NGP), T=4.2 K, λ_B=860, 875, 885, 900, 905 nm (ordered from top to bottom). Resolution = 8 cm^{-1}

Site Excitation Energy Correlation Effects

Recent nonphotochemical hole burning experiments on the antenna-protein complex from *Prosthecochloris aestuarii* have proven that there is a high degree of site excitation energy correlation between different exciton components of a subunit characterized by strong excitonic interactions [60,61]. With this in mind consider the transient PHB spectra for *Rb. sphaeroides* (PVOH/NGP) in Fig. 10. Only one feature of the Q_y-region of the transient spectra lying higher in energy than P870 exhibits an observable dependence on λ_B. It is the hole or "bleach" [54] that corresponds to the low energy shoulder(LES) of the (B_L,B_M) monomer absorption band. The λ_B-dependence is most pronounced for the PVOH films because of the additional ~100 cm^{-1} of inhomogeneous broadening they provide relative to the glycerol glass hosts. In Fig. 10 the right and left vertical lines are centered at the centroids of the P_- and LES holes of the lowest ω_B-value used. The LES hole for *Rb. sphaeroides* lies at 811.3 nm (12330 cm^{-1}). Transient experiments on the RC of *Rps. viridis* yielded similar results concerning the LES located at 848.0 nm (11790 cm^{-1}). Vermeglio et al. [54] assigned the LES state of *Rps. viridis* to P_+, the upper exciton component of the Q_y-transition of the special pair. It is apparent that that the LES hole tracks λ_B for both *Rb sphaeroides* and *Rps. viridis* in a like manner. Therefore, there exists a significant amount of positive correlation between the site excitation energies of the P_- and LES states. Because of the studies on *P. aestuarii* [60,61] and because of lack of existence of any studies showing any line narrowing on molecular systems that establish any correlation for excited states of different electronic parentage, the results presented here support the assignment of the LES made by Vermeglio et al. [54] and apply it to *Rb. sphaeroides.*

The other bands appearing in Fig. 10 to higher energy are due to electrochromic shifting of the accessory Bchl *a* and BPheo *a* absorption bands which occurs when P^+BHQ^- is produced. It is interesting that these bands exhibit no λ_B dependence. This should not be interpreted as meaning that they do not have any contribution from the special pair (i.e., that they are pure). An alterate explanation is that they could have

ultrafast excited state lifetimes (i.e., that they are homogeneously broadened) due to downward EET processes [27,45,49]. This particular aspect has been investigated using photochemical hole burning and reported on recently [27].

Polarized Hole Burning Studies

The use of polarized photoselection techniques at low temperature to determine relative orientations for pigments in the RC and antennas of photosynthetic bacteria has been taking place for many years, even before a structure of the RC existed [54,62-70]. By using two beams of linearly polarized light, one to effect a photochemical change and a second weaker one to probe the absorption or transmission spectrum, the approximate angle between the pigments could be obtained. Linear dichroism (LD) experiments also provided similar information when the samples were prepared in the appropriate manner [66,69]. An important advantage of the technique of polarized photoselection is that it can be used when the sample is in an amorphous host such as a glass while LD relies on utilizing oriented samples. The results presented here, where a laser is used to site selectively photo-bleach P870 at 4.2 K, are the first reported study of their kind.

The laser provides polarized (in this case vertical) irradiation for the photo-oxidation of P870 and the formation of the charge separated state $P^{+}BHQ^{-}$. The changes in the transmission spectrum are then probed using light that is polarized vertical (parallel) and horizontal (perpendicular). The results of a typical set of spectra are presented in Fig. 11 for RC of *Rb. sphaeroides* in Gly/NGP (λ_B=860 nm). $\Delta A_{||}$ is the hole spectra measured parallel to the burn laser. $\Delta A_{\perp}$ is the hole spectra measured perpendicular to the burn laser. It is an important point that no substantial differences in the polarized spectra ($\Delta A_{||}$ and $\Delta A_{\perp}$) were noted by allowing λ_B to vary across the P870 absorption band (860⇒910 nm) (i.e., the degree of polarization of the P870 band does not vary with λ_B). A quantity of interest when considering the polarized hole spectra in Fig. 11 is the degree of polarization,

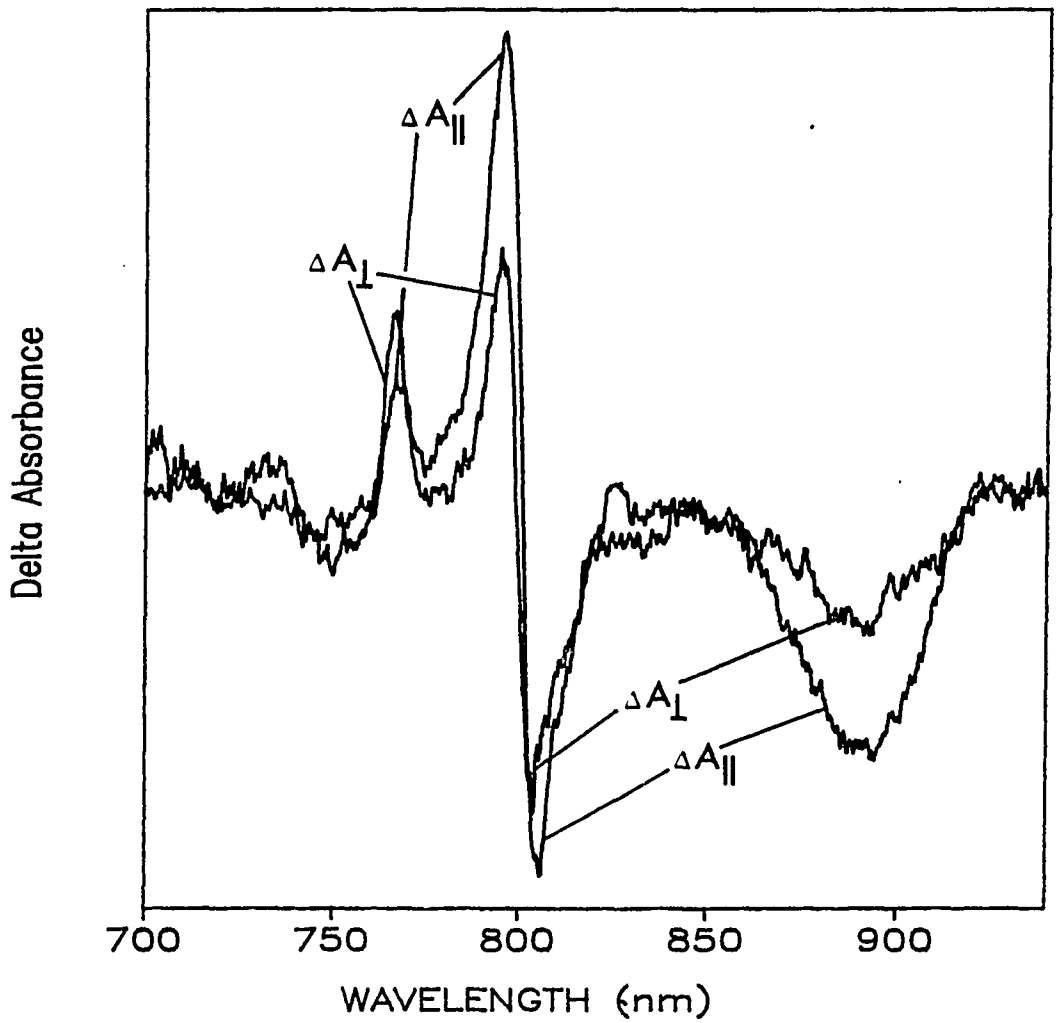

Figure 11. Polarized hole burned spectra ($\Delta A_{||}$ and $\Delta A_{\perp}$) for *Rb. sphaeroides* (Gly/NGP), T=4.2 K, λ_B=860 nm. Resolution, 8 cm^{-1}. See text for details

ρ. It is defined as,

$$\rho = (\Delta A_{||} - \Delta A_{\perp})/(\Delta A_{||} + \Delta A_{\perp}) = (3\cos^2\alpha - 1)/(\cos^2\alpha + 3) \quad (7)$$

Where α is the angle between the excited and detected optical transitions. This is the well known Perrin eq. [71]. For a single transition, such as P870, a perfect value of ρ would be .5. This is the value obtained by allowing α=0 in eq. 7. In terms of the measured hole burned spectra a ratio of $\Delta A_{||}$ to $\Delta A_{\perp}$ should be 3 if a single transition is considered with perfect polarization. A value of .35 was obtained for ρ in Fig. 11 at peak of the P870 bleach (this value is constant within experimental error across the entire P870 band for a given λ_B). This is less than the optimal value of .5 for ρ but it compares favorably with that obtained by other nonsite selective polarized photoselection studies [65,67]. There are several factors that can lead to the observation of a less than ideal degree of polarization including the following: depolarization of the probe and/or burn beams by interaction with the cryostat windows, the degree(%) of bleaching and the presence of more than one state absorbing in the same spectral region. The first reason listed above, depolarization of the burn and/or probe beams, is most likely the cause of the observed discrepancy in Fig. 11 with regard to the degree of polarization. The degree, or percent, bleaching is extremely important because if the transition is bleached too much ρ⇒0 [71]. If the changes in the transmission spectra are confined to ΔT≤20%, as they are here, the maximum amount of information can be obtained from the hole burned spectra. The last reason listed above is perhaps the least probable due to the rather good agreement obtained by Tang et al. [52] and Johnson et al. [26,27] in fitting the P870 absorption and hole profiles with a single transition (with a strong progression of a low frequency dimer mode). However, Johnson et al. [26] did not completely exclude the possible presence of a weakly absorbing charge-transfer state in the same spectral region.

The remaining portion of the spectra, which is due to electrochromic shifting of the accessory pigment bands, is not as easily interpreted because of the many overlapping absorption bands in the 760-820 nm region of the spectrum. The unresolved $B_{L,M}$ band is

at ~800 nm with the unresolved $H_{L,M}$ band at ~760 nm. The voyeur Bchl can be seen to be oriented predominantly parallel to P870 while the pheophytins appear to be oriented mainly perpendicular to P870. When there are overlapping transitions calculation of ρ is relatively meaningless. The relative orientations for the RC pigments obtained by Vermelgio et al. [70] for *Rb. sphaeroides* are in general agreement with the results presented here. Vermeglio et al. [70] determined the following relative orientations based on photoselection experiments using 900 nm (and other wavelengths) of light at a variety of temperatures to bleach P870: pheophytin oriented >70° relative to P870, Bchl oriented ~37° with respect to P870 and the bleaching of a transition at ~805 nm of perpendicular orientation relative to P870. The transition at 805 nm which they refer to has been assigned as P_+ [52], the upper exciton component of P870, and should, if it has oscillator strength, be oriented 90° with respect to P_- (P870). These assignments are in general agreement with those obtained by Gagliano et al. [69] using linear dichroism (LD) and Clayton et al. [68] who utilized both LD and polarized photoselection. The x-ray structure for *Rb. sphaeroides* [5-7] confirmed the above earlier experiments with respect to the relative orientations of the pigments in the RC. The comparison of the pigment structure for the RC of *Rps. viridis* as arrived at via LD data and as determined by single crystal x-ray diffraction resulted in good agreement between the two structures [72].

PAPER I. PRIMARY DONOR STATE MODE STRUCTURE AND ENERGY TRANSFER IN BACTERIAL REACTION CENTERS

PRIMARY DONOR STATE MODE STRUCTURE AND ENERGY TRANSFER IN BACTERIAL REACTION CENTERS

S. G. Johnson, D. Tang, R. Jankowiak, J. M. Hayes,
G. J. Small and D. M. Tiede

Journal of Physical Chemistry 1990, in press.

ABSTRACT

Temperature-dependent photochemical hole burning data for P870 of *Rb. sphaeroides* reaction centers (RC) are reported which lead to a determination for the mean frequency of the protein phonons which couple to the optical transition. Utilization of this frequency, ω_{sp} ~25-30 cm-1, together with improved functions for the single site (RC) absorption lineshape and inhomogeneous broadening are shown to lead to significant improvement in the theoretical fits to the hole and absorption spectra (including those of P960 of *Rhodopseudomonas viridis*). Time-dependent P870 hole spectra are reported which provide additional evidence that the previously observed zero-phonon hole is an intrinsic feature of P870 for active RC. Transient spectra obtained by laser excitation into the accessory Q_y-absorption bands of the RC are presented which show an absence of both line narrowing and a dependence on the location of the excitation frequency. These results, which are consistent with ultra-fast energy transfer processes from the accessory states, are discussed in terms of earlier time domain data.

INTRODUCTION

Recently the underlying structures of the primary donor state (special pair) absorption profiles P870 and P960 of the bacterial reaction centers (RC) from *Rhodopseudomonas viridis* and *Rb. sphaeroides* were revealed by transient photochemical hole burning experiments [1,2]. Both are dominated by a fairly lengthy Franck-Condon progression in an intermolecular special-pair marker mode (ω_{sp}) which exhibits an intensity maximum for the one-quantum transition. For P870 and P960 the theoretical fits to the structured hole spectra led to ω_{sp}-values of ~150 and 125 cm-1 for P960 and P870, respectively [2]. The corresponding S (Huang-Rhys)-factors are S_{sp} = 1.1 and 1.5. The origin (ω^{o}_{sp}) of the ω_{sp}-progression in the hole spectra for P870 and P960 correlates with the low energy shoulder of the low temperature absorption profile which is readily observed for glass solvents that minimize inhomogeneous broadening, Fig. 1. Although the dynamical nature of the marker mode has not been determined, the fact that it is intermolecular [1,2] and that the primary donor state ($P870^{*}$, $P960^{*}$) is believed to possess significant intra-dimer charge-transfer character [3-6], suggest that it is highly localized on the special pair.

The primary donor state also exhibits appreciable coupling to low frequency protein phonons (mean frequency ω_m, Huang-Rhys factor S) as evidenced by the weakness of the zero-phonon hole (ZPH) associated with the ω^{o}_{sp} band. Simulations of the hole spectra presented in refs. 1 and 2 were performed with an analytical expression for the hole profile which takes into account coupling to both the marker mode and protein phonons. This expression is valid in the short burn time approximation [7] and, for example, a zero-phonon excitation frequency distribution function (SDF, width Γ_I) governed by a Lorentzian. Although the principal features of the spectra (including their burn wavelength dependence) could be accounted for, significant deviations occurred on the low energy tails of both the absorption and hole spectra. These deviations were suggested to be due mainly to the utilization of a Lorentzian for the SDF. Although good initial estimates for many of

the theoretical parameters (e.g., ω_{sp}, S_{sp}, S, Γ_I) could be obtained from the spectra, this was not the case for ω_m. Thus, we report here a direct determination of ω_m. This value is used in simulations which avoid the approximations employed in refs. 1 and 2. The results reported here provide significantly improved agreement with experiment. Nevertheless, the basic physical model remains unchanged. The refinement of the values for the physical parameters presented is viewed as important for future studies directed towards determination of the marker mode frequency in the ground electronic state, its dynamical nature and the role of the special pair geometry change in the excited state in primary charge separation.

The ZPH widths reported earlier [1,2] yielded $P870^*$ and $P960^*$ decay times in good agreement with those determined earlier [8,9] by time domain measurements at 10 K, thus proving that there is no ultra-fast electronic relaxation [10,11] from zero-point pf P^* which precedes formation of the charge separated state P^+BPheo^-, where BPheo is bacteriopheophytin. We present here time-dependent hole burning data for P870 which show that the decay kinetics of the ZPH and the broader and more intense hole upon which it is superimposed are the same within experimental uncertainty. This experiment was performed to provide even more convincing evidence [1] that the ZPH is an intrinsic feature of the spectra for functioning RC.

The last part of the paper presents the results of experiments stimulated by the reports that the line narrowing feature of hole burning could be used to study site excitation energy correlation effects between different Q_y-absorption bands of the bacterial reaction centers [1,2]. In these experiments transient spectra for the entire Q_y-region of *Rb. sphaeroides* and Rps. virdis were obtained as a function of laser burn frequency (ω_B) tuned across P870 and P960. Significant positive correlation was observed between the primary donor state absorption band and the band that appears as a low energy shoulder on the BChl monomer band (near 850 and 810 nm for *Rps. viridis* and *Rb. sphaeroides*, respectively). Since such correlation is only expected between states which have similar electronic parentages, it was argued that [1,2] the positive correlation is consistent with the assignment for the "shoulder state" of Vermeglio et al. [12] to the upper dimer component

(P_+) of the special pair. Pertinent to the present paper is the observation that the other features in the transient ΔA hole spectra are invariant to ω_B-tuning. These features are due to electrochromic shifts of the so-called BChl and BPheo monomer bands, the shifts arising form the formation of the P^+Q^- ($Q \equiv$ quinone) state which serves as the bottleneck for the hole burning. We will refer to these bands as accessory. There are two apparent explanations for the invariance: one is that the accessory bands correspond to states that have little contribution from the Q_y-states of the monomers comprising the special pair; the other is that these bands are largely homogeneously broadened. Spectra are presented here which were obtained by burning directly into accessory Q_y-bands. The results are shown to be consistent with the second explanation and support the findings of the femtosecond studies which show that energy transfer from the accessory states occurs in < 100 fsec [8,9].

EXPERIMENTAL

Fresh samples of RC from *Rb. sphaeroides* were prepared by dissolving RC crystals in a suitably buffered host. Details concerning the crystallization procedure can be found in ref. 13. The RC were prepared in glycerol:water glass (2:1) with 0.8% n-octyl-β-D-glucopyranoside detergent (NGP), 10 mM Tris, 1 mM EDTA, pH = 8.0. The optical density (OD) of the samples utilized in this study was 0.25 at the peak of the primary donor state absorption.

The experimental apparatus is described fully in ref. 1. Briefly, burn irradiation (linewidth 0.2 cm-1) was provided by Raman shifted (H2 gas) output of an excimer-pumped dye laser, Lambda Physik EMG 102 and FL-2002, respectively. A pulse repetition rate of 16 Hz or less was used. A Stanford Research SR 250 boxcar averager was utilized to obtain the gated spectra (gate width of 150 μs). The ΔT (transmission) spectra were obtained by subtracting laser-on and laser-off spectra. ΔA (absorbance) spectra were obtained by subtracting the logarithms of the laser-off transmission spectra and the laser-on transmission spectra. Samples were mounted and cooled in a Janis model 8-DT super vari-temp liquid helium cryostat. Temperature measurements were made with a Lakeshore Cryotronics DTC-500K calibrated silicon diode.

For the study of the temporal decay of the P870 hole profile the position of the 150 μs observation window was varied relative to the laser pulse by adjusting the gate delay of the boxcar. Delay times of 2, 5, 10, 15 and 20 ms were employed. A decay time of 21 ± 2 ms for the P^+Q^- bottleneck state had been determined earlier [14].

RESULTS

Simulations and Temporal Evolution of the P870 and P960 Hole Profiles

The theory of Hayes and Small [15] for the hole profile, which is valid for arbitrarily strong linear electron-phonon coupling, was developed to interpret the first hole burned spectra reported for P870 and P960 [16,17]. These important early experimental results demonstrated that there is a significant homogeneous broadening contribution to the absorption profiles but that the maximum of the single broad (~400 cm-1) hole exhibits a weak dependence on the location of ω_B within the primary donor absorption profile. Since the marker mode progression was not observed, Hayes et al. [7] utilized a single mean phonon frequency approximation to account for the results of refs. (16,17). The single site (RC) absorption profile has the form

$$L(\Omega-\nu) = e^{-S}\ell_0(\Omega-\nu) + \sum_{r=1}^{\infty} \frac{S^r e^{-S}}{r!}\ell_r(\Omega-\nu-r\omega_m) \qquad (1)$$

where ν is the zero-phonon transition frequency and ω_B is the mean frequency for phonons which couple to the electronic transition. The Huang-Rhys factor is S and the Franck-Condon factors for the r = 0, 1,... phonon transitions are governed by the Poisson distribution $(S^r e^{-S}/r!)_r$. Thus, the Franck-Condon factor for the zero-phonon transition is exp(-S); its profile is a Lorentzian (l_0) with a FWHM = γ, which is the homogeneous linewidth of the zero-phonon line. The lineshape for the one-phonon profile is l_1 and is centered at $\nu + \omega_m$ with a FWHM of Γ. It is well known that the one-phonon profiles for electronic transitions of molecules imbedded in amorphous solids carry a width of about 30 cm-1 and the profiles for antenna Chl *a* and *b* are no exception [18]. When the one-phonon profile is taken to be a Gaussian the width of the r-phonon profile (centered at $\nu + r\omega_m$) is given by $\Gamma_r = r^{1/2}\Gamma$. In order to derive an analytic expression for the hole profile

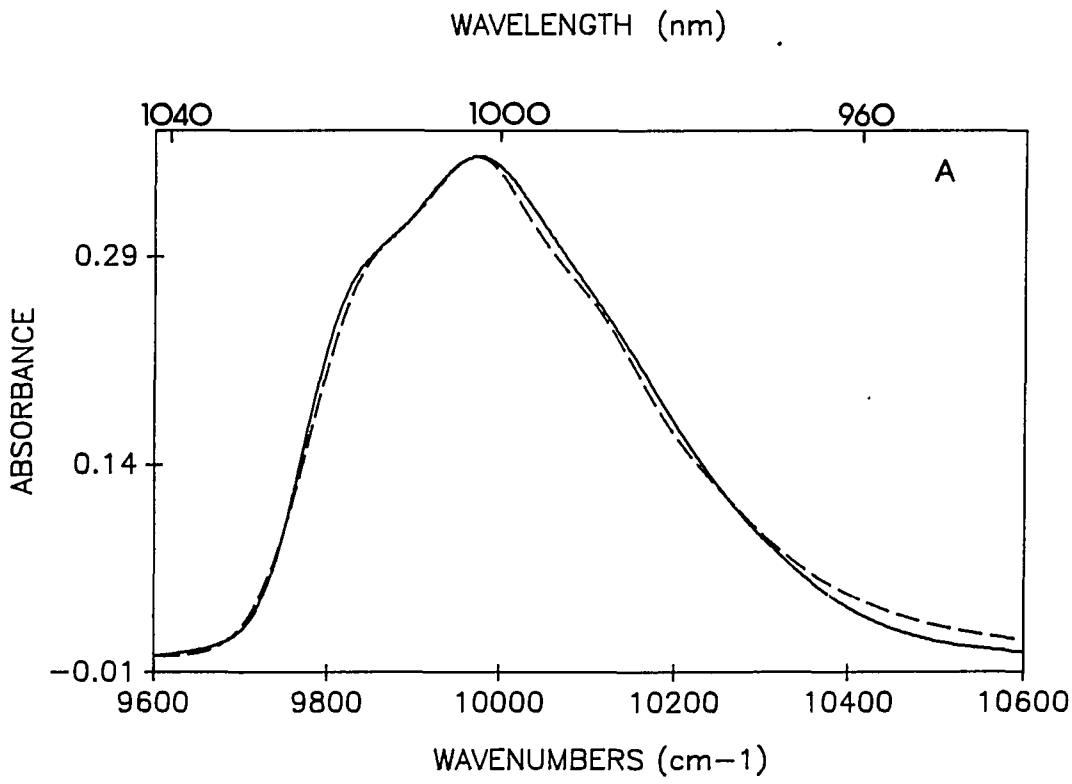

Figure 1. Calculated and experimental absorption spectra for P870 and P960. T = 4.2 K, resolution = 4 cm-1. A) P960 in glycerol glass (LDAO detergent). B) P870 in glycerol glass (NGP detergent)

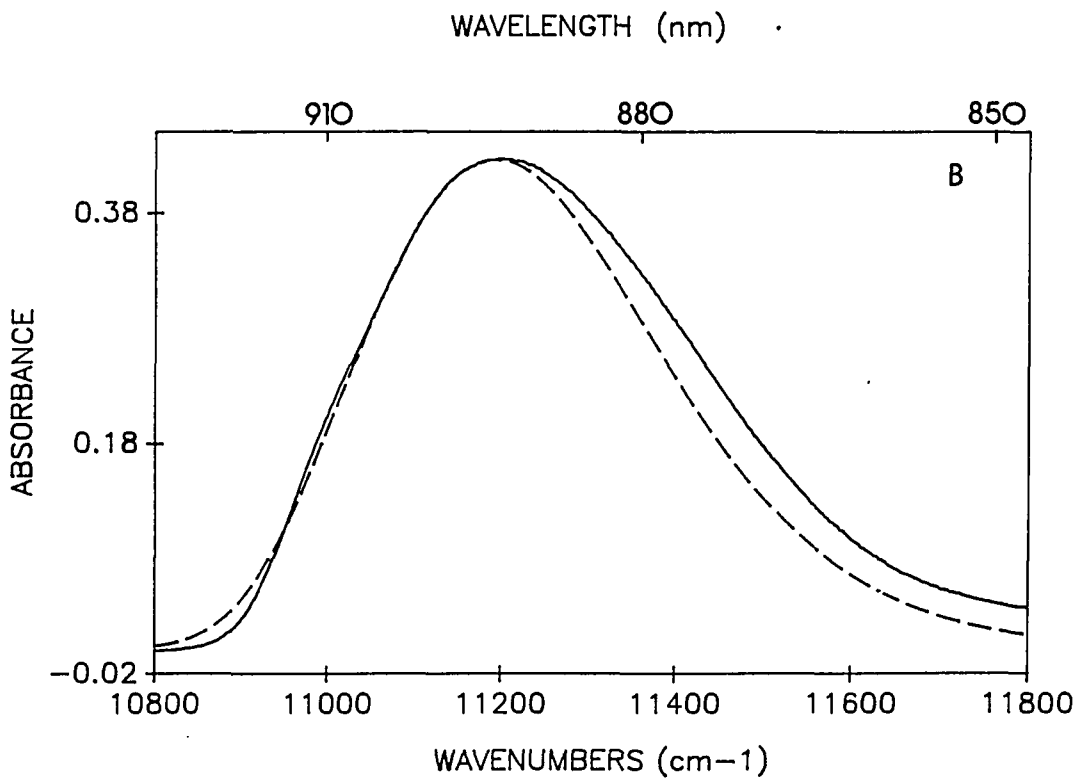

Figure 1. Continued

Table I. Parameters for theoretical fit

	ω_{sp}[a]	S_{sp}	ω_m	S	Γ	Γ_I	S_{tot}	$\Sigma S_i\omega_i$	FWHM(P)
P960	134	1.1	25	2.1	40	120	3.2	200	390
P870	115	1.5	30	2.2	30	170	3.7	240	410
P960	150	1.1	40	1.5	50	120	2.6	225	460
P870	125	1.5	35	2.0	50	130	3.5	260	495
P960	---	---	80	4.5	40	150	4.5	360	530
P870	---	---	80	4.5	50	350	4.5	360	680

[a]All frequencies and widths are in cm^{-1}.

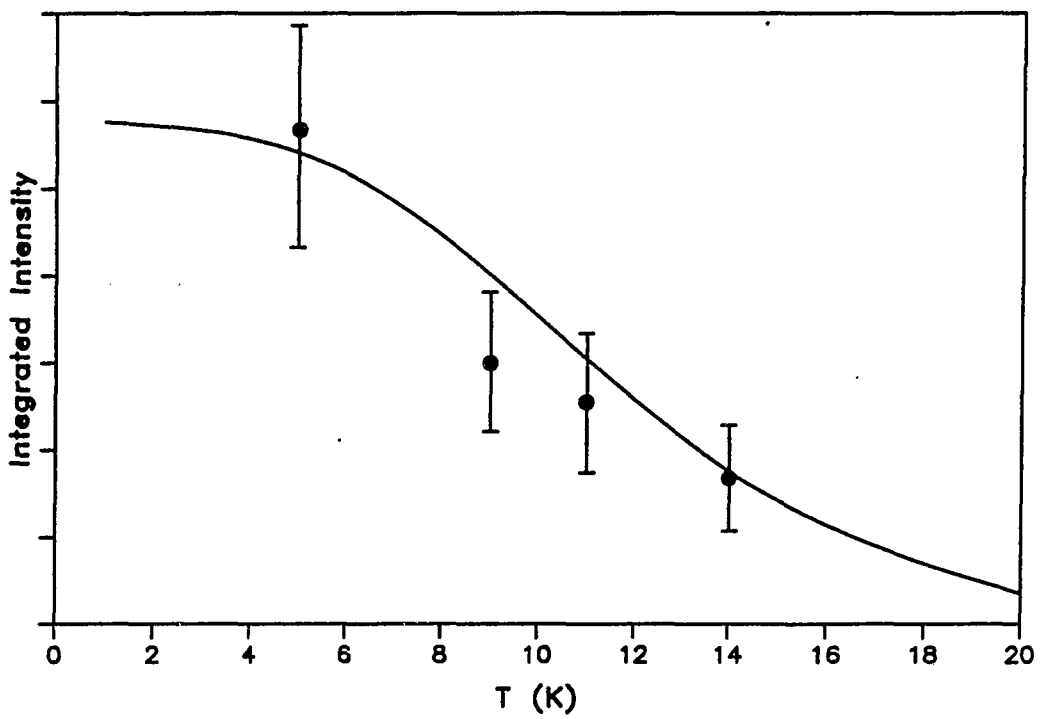

Figure 2. Temperature dependence of the integrated intensity of the zero phonon hole of P870: experimental data (dots with experimental error bars) and theoretical fit (smooth curve). $\lambda_B = 909.5$ nm. (See text for details)

Lorentzians for $l_r(r \geq 1)$ were used [7] with widths governed by the Gaussian values, i.e., $r^{1/2}\Gamma$.

Equation 1 is readily modified to include coupling to the ω_{sp} -mode:

$$L(\Omega-\nu) \doteq \sum_{j=0}^{\infty} \frac{S_{sp}^{j} e^{-S_{sp}}}{j!} \left[e^{-S} \ell_0^j(\Omega-\nu - j\omega_{sp}) + \sum_{r=1}^{\infty} \frac{S^r e^{-S}}{r!} \ell_r^j(\Omega-\nu - r\omega_m - j\omega_{sp}) \right] \quad (2)$$

where S_{sp} is the Huang-Rhys factor for ω_{sp}. In writing Eq. 2 the reasonable assumption that the electron-phonon coupling (S) is independent of the ω_{sp}-mode occupation number j is made. Similarly, the mean phonon frequency ω_m and Γ, the width of the one-phonon profile, are considered independent of j. However, the homogeneous linewidths γ_j of the zero-phonon l_0^j functions may differ due, for example, to rapid vibrational relaxation of the ω_{sp}^j $(j \geq 1)$ levels.

We define $N_0(\nu-\nu_m)/N$ where N is the total number of absorbers and ν_m is the mean zero-phonon frequency. The absorption spectrum is calculated as the convolution of this distribution function with the single site absorption profile $L(\Omega-\nu)$. The integrated absorption cross-section, laser intensity and photochemical quantum yield are denoted by σ, I and ϕ. Following a burn for time τ

$$N_\tau(\nu - \nu_m) = N_0(\nu - \nu_m) e^{-\sigma I \phi \tau L(\omega_B - \nu)} \quad (3)$$

where ω_B is the laser burn frequency and $L(\omega_B-\nu)$ is given by Eq. 2. To obtain the absorption spectrum, A_τ, following the burn we must convolve Eq. 3 with $L(\Omega-\nu)$ and integrate over ν, i.e.,

$$A_\tau(\Omega) = \int d\nu N_0(\nu - \nu_m) e^{-\sigma I \phi \tau L(\omega_B - \nu)} L(\Omega-\nu) \quad (4)$$

With Eq. 4 the hole spectrum following a burn for time τ is given by $A_0(\Omega) - A_\tau(\Omega)$. In our previous calculations Eq. 4 was simplified by making the short burn time approximation where the exponential is expanded as $1 - \sigma I \phi \tau L(\omega_B - \nu)$ so that an analytic expression for the hole spectrum could be obtained. We do not do so here because a physically reasonable Gaussian is employed for the zero-phonon excitation energy distribution function of width â1 and a more realistic line shape given to the one-phonon profile. In regard to the latter we note that the one-phonon profile for Chl *a* of the antenna complex of PS I exhibits a single maximum at ω_m ~25 cm-1 and is asymmetric, with the higher energy half broader (and more tailing) than the lower energy half [18]. For Chl *a* the width (Γ) of the one-phonon profile is ~30 cm-1 and its shape is determined by the product of the protein phonon density of states and a frequency dependent electron-phonon coupling function [19]. The profile can be approximated by a Gaussian for the low energy half and a broader Lorentzian for the high energy half and, thus, we have employed such a profile for the present P870 and P960 calculations.

Unfortunately the phonon sidebands cannot be resolved in the P870 and P960 hole spectra. Thus, in refs. 1 and 2 the Stokes shifts were used to estimate ω_m. This is less than satisfying and so we report here, for P870, a direct determination of ω_m. Our approach involves measuring the intensity of the ZPH, cf. Section I, as a function of burn temperature. As discussed in ref. 7 and as can be seen by making the short burn time approximation in Eq. 4, the effective Franck-Condon factor for the ZPH is, to a good approximation, given by exp (-2S) at O K (when $\omega_B \approx \nu_m$, as is the case for our experiments). Using long established theory [20], it follows that $\exp[-2S(2\langle n_x \rangle_T + 1)]$ is the effective Franck-Condon factor for the ZPH at temperature where $\langle n_x \rangle_T = [\exp(h\omega_m/kT) - 1]^{-1}$ is the phonon occupation number(x is defined here to be ω_m). The results of our experiment are shown in Fig. 2. The fit to the data points (ZPH with acceptable signal/noise ratio could not be measured for $T_B > 14$ K) with the T-dependent Franck-Condon factor leads to $\omega_m = 23 \pm 4$ cm-1. We note that this value is in the range

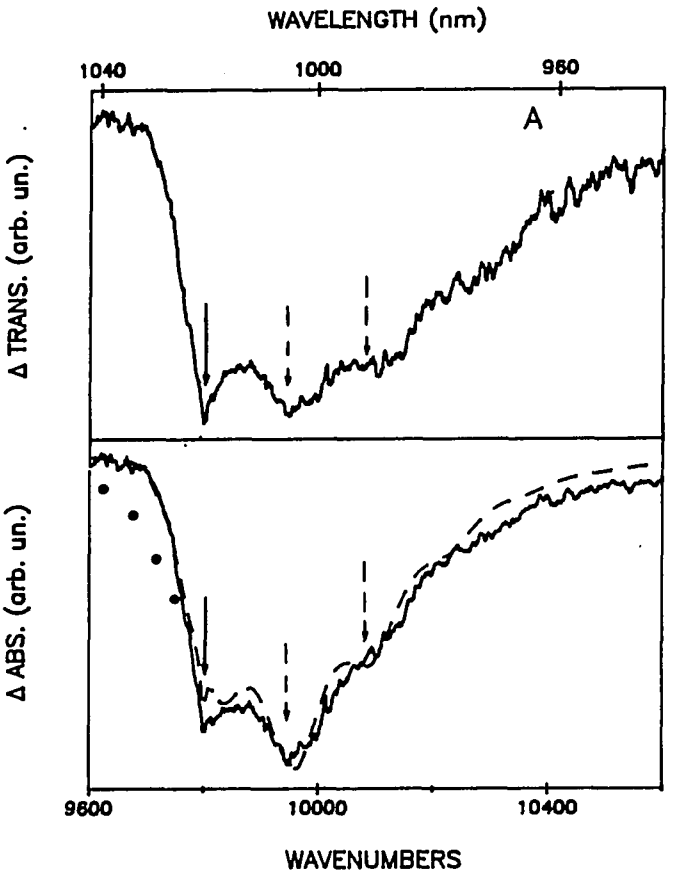

Figure 3. Transient photochemical hole burned spectra (solid line) and theoretical fits (dashed line). A) Rps. viridis (glycerol glass/LDAO), λ_B = 1020 nm; ΔT spectrum (upper frame), ΔA spectrum and fit (lower frame). B) Rb. sphaeroides (glycerol glass/NGP), λ_B = 910 nm; ΔT spectrum (upperframe), ΔA spectrum and fit (lower frame). See Table I and text for details of fits. First five overtones of ω_{sp} were included in the calculations. T = 4.2 K, Resol. = 8 cm-1 for all spectra. Solid arrows indicate burn frequency. Dashed arrows indicate first and second quantum ω_{sp}-satellite holes. The low energy portion of the earlier theoretical fits from ref. 1 and 2 are present as dots (P960) and stars (P870) in the lower two frames

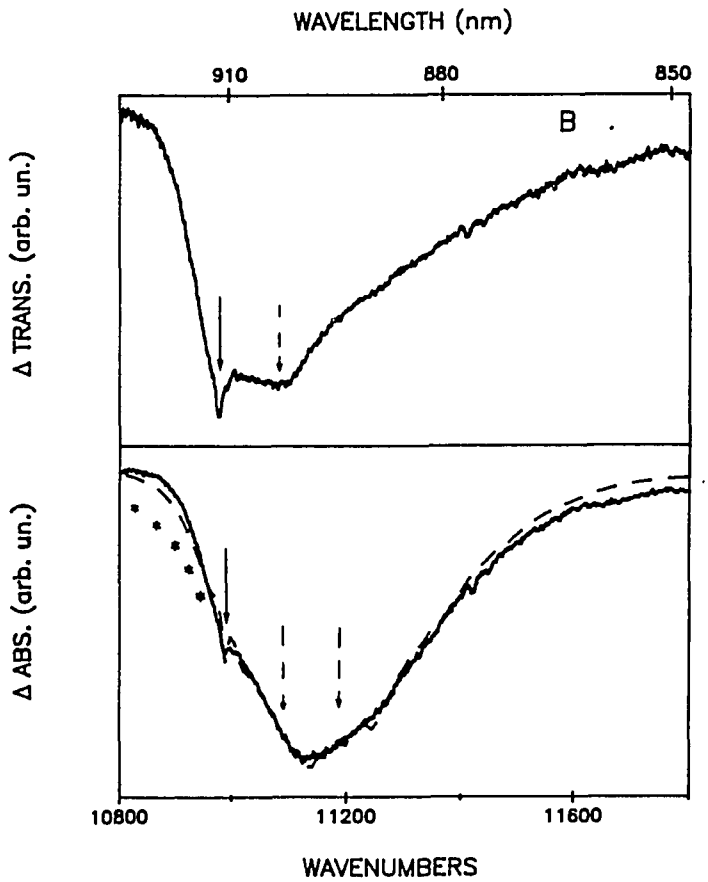

Figure 3. Continued

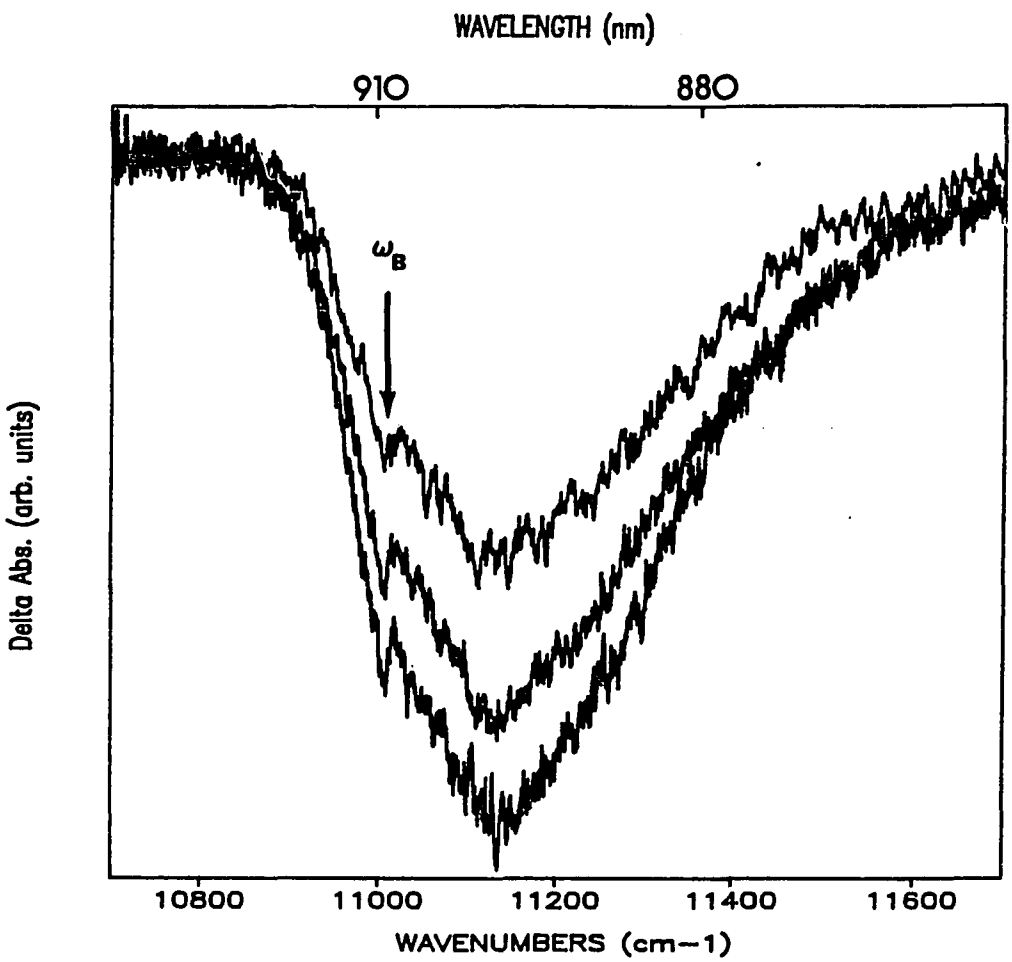

Figure 4. Transient hole burned spectra for P870 using variable gate delay. 2 ms, 5 ms, and 10 ms delay holes are shown with 2 ms being the largest and 10 ms being the smallest change in absorbance. T = 4.2 K, Resol. = 3 cm-1. λ_B = 908 nm. A ~15% change in transmission was obtained with a delay of 2 ms

observed for pigments in antenna complexes [18, 21, 22] and, thus, it appears that protein phonons of this mean frequency are ubiquitous in coupling to electronic transitions.

Examples of our improved simulations to the ω_B-dependent P870 and P960 ΔA (absorbance) hole spectra are shown in Fig. 3. The upper spectra are the corresponding ΔT (transmission) spectra. The values of the parameters used for the simulation are given in Table I. For the spectra shown, ω_B is located near the center of the marker mode origin band (low E shoulders of Fig. 1) and provides optimum line narrowing [1,2]. By comparing the results in Fig. 3 to those of refs. 1 and 2 it can be seen that employment of a Gaussian for the inhomogeneous line broadening contribution in the present work has led to significantly improved fits. For convenience, the significant deviations of our earlier fits on the low energy tail of the spectra are also shown in Fig. 3. The magnitude of the deviations between the low energy sides of the experimental and simulated absorption spectra reported in ref. 2 are comparable. The present calculations also provide a more accurate description of the ω_B-dependence of the hole spectra than that given in ref. 2 [23,24]. This is also true for the absorption spectra, Fig. 1.

To conclude this sub-section we show in Fig. 4 results of an experiment designed to determine whether the ZPH coincident with ω_B for P870 exhibits the same decay kinetics as those for the broad hole upon which it is superimposed. The amplitude of the broad hole decreases by 37% as the delay time is increased from 2 to 10 ms (the decay time of $P870^+Q^-$ is 21 ± 2 ms). The corresponding percentage for the ZPH is estimated to be ~40%. The agreement is reasonable and provides further evidence that the ZPH is an intrinsic feature of the primary donor state.

Transient Spectra for Excitation into Accessory Pigment Bands, Absence of Line Narrowing

With reference to the last two paragraphs of the Introduction, Fig. 5 shows some of a series of transient spectra for the accessory pigment Q_y- region of *Rb. sphaeroides*

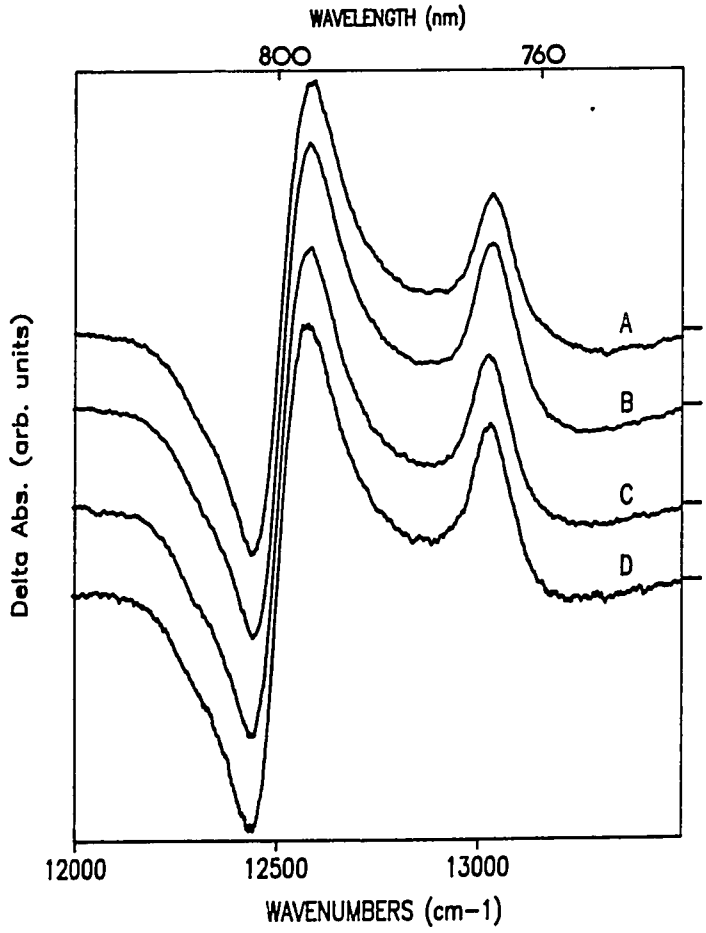

Figure 5. ΔA (absorbance) spectra for hole burning in the pheophytin Qy bands. Burn wavelength: A) 750 nm. B) 760 nm. C) 765 nm. D) 770 nm. T = 4.2 K. Resol. = 3 cm-1. Dashes on right vertical axis indicate ΔA = O for each spectrum

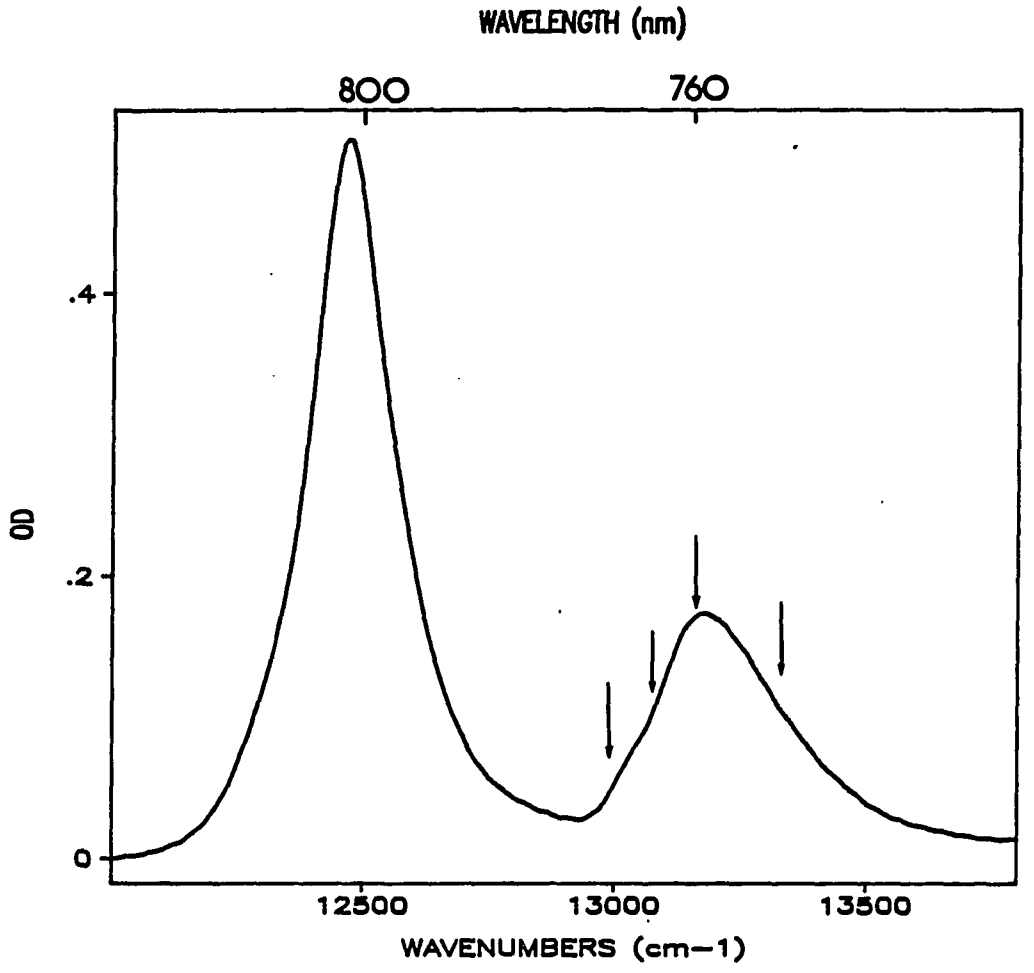

Figure 6. Absorption spectra for Rb. sphaeroides (glycerol glass/NGP) in accessory pigment Qy region. T = 4.2 K. Resol. = 4 cm-1. Burn frequencies indicated by solid arrows. The peak at ~12500 cm-1 (802 nm) is the Bchl a monomer (B_L, B_M) band and the peak at ~ 13200 cm-1 (760 nm) is the BPheo a monomer (H_L, H_M) band

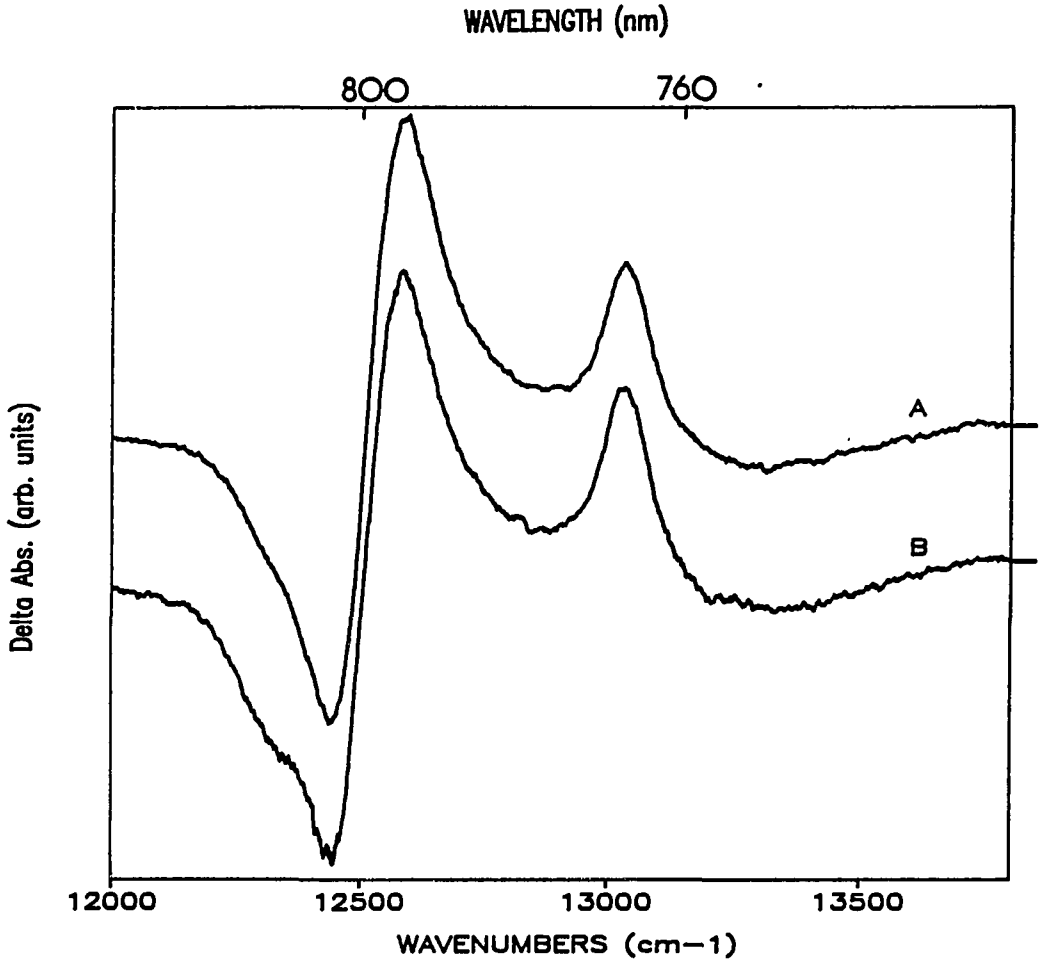

Figure 7. Hole burned spectra in accessory Q_y region for A) λ_B = 750 nm. B) λ_B = 907 nm. T = 4.2 K. Resol. = 3 cm-1. Dashes on right vertical axis indicate $\Delta A = O$ for each spectrum

obtained for a series of ω_B-values ranging from the high to low energy sides of the BPheo absorption band at 760 nm, see absorption spectrum given in Fig. 6. The contributions to this band from the BPheo of the M and L branches [2] are not resolved but are responsible, in part, for its asymmetry. Figure 5 demonstrates that the electrochromically shifted (red) BPheo feature near 13,000 cm-1 due to P^+Q^- is invariant to ω_B. Furthermore, this feature is essentially identical to that obtained by exciting directly into P870, Fig. 7. Thus, the BPheo band does not exhibit the line narrowing expected for a band whose width is dominated by inhomogeneous broadening. A similar result has been observed for the BChl accessory band of *Rps. viridis* [23]. The absence of line narrowing for the bacterial RC accessory bands provides a striking contrast to the RC of PS II [21], for which intense and persistent nonphotochemical ZPH and resolved phonon-sideband holes are observed for the Chl and Pheo accessory pigments. The width of the asymmetric BPheo band in Fig. 6 is 290 cm-1 which sets a lower limit of ~20 fs for the decay time of BPheo* (on either the M- or L-side). We note that the intramolecular modes in the 700-1100 cm-1 region which build on the accessory Bchl band at 802 nm can be expected to contribute to the tailing on the high energy side of the BPheo band. Using the recently determined Franck-Condon factors for Chl *a* [18] in the above region we estimate a FWHM of ~250 cm-1 from the two quasi-degenerate BPheo. Accepting that there is a large homogeneous lifetime broadening contribution to the BPheo band, we draw upon our calculations on the ω_B-dependence of the P870 and P960 hole spectra to estimate the contribution from inhomogeneous broadening to the above 250 cm-1 BPheo bandwidth. In order that a change of the electrochromically shifted BPheo spectrum not be observed as ω_B is tuned across the absorption band it is necessary that the inhomogeneous width be about one-half or less of the homogeneous width. Taking one-half as the upper limit, we obtain from 250 cm-1 inhomogeneous and homogeneous contributions of ~80 and 170 cm-1, respectively. The latter yields a BPheo* lifetime of 30 fs [25]. An immediate question is whether a value of 80 cm-1 for the inhomogeneous broadening is reasonable since we have determined an inhomogeneous linewidth of 170 cm-1 for P870, Table I. We believe it is since the lowest exciton state of the special pair should be far more sensitive to structural variations from

RC to RC. It is germane to note that the width of the $BChl_{M,L}$ band in Fig. 6 at 802 nm is 200 cm-1 and that from the sharpest low temperature absorption spectrum for the RC of *Rps. viridis* we are aware of [26], the widths of the $BChl_{M,L}$, $BPheo_M$ and $BPheo_L$ bands are 205, 240, and 260 cm-1, respectively. From Table I the inhomogeneous linewidth of P960 is 120 cm-1. If it is assumed that this inhomogeneous width is also reduced by about one-half for the *Rps. viridis* accessory bands, one obtains ~30 fs lifetimes for $BChl_{M,L}$, $BPheo_M$, and $BPheo_L$. Although the above arguments are approximate, we believe that ~30 fs lifetimes are very reasonable estimates for the accessory pigment states of both RC. If the lifetimes of $BPheo^*$ of *Rb. sphaeroides* and $BChl^*$ of *Rps. viridis* were as long as 100 fs, a change of their electrochromically shifted profiles with ω_B or line narrowing should have been observed.

DISCUSSION

Having studied the hole spectra of P870 and P960 in several different glass-detergent systems we think it is unlikely that their resolution can be improved significantly with glassy hosts beyond that shown here and in refs. (1,2). The linear electron-phonon and -marker mode coupling are fundamental properties of the RC, only Γ_I (inhomogeneous width) is subject to experimental manipulation. It is unlikely that Γ_I can be appreciably reduced from our values for glass hosts given in Table I. It is appropriate, therefore, to consider the evolution of our simulations which have been stimulated by improvements in resolution of the hole spectra. The P870/P960 parameter set values given in Table I are given in chronological order, from the bottom up. From the outset [15] our model was based on the premise that the large homogeneous broadening of P870 and P960, indicated by the earliest hole burning experiments [16,17], was due to linear electron-phonon coupling, and not ultra-fast electronic relaxation of P^* [10,11,16,17]. The structured hole spectra discussed here and in refs. 1 and 2 prove that the former is the correct picture (the marker mode is, strictly speaking, a localized or resonant phonon [27] since it is intermolecular and of low frequency relative to the intramolecular modes). The lowest entries in Table I do not contain values for ω_{sp} and S_{sp} because the hole spectra available at that time were unstructured, i.e., a single mean phonon frequency approximation was utilized with ω_m = 80 cm-1 and S = 4.5 for both P870 and P960. These values and those for Γ_I led to calculated spectra (for different ω_B-values) in reasonable agreement with the spectra of Boxer and his group [16,17]. The value of Γ_I = 150 cm-1 for P960 is similar to those determined later while the value of 350 cm-1 is considerably higher. The latter is a consequence of the fact that the P870 absorption width reported in ref. (16) for a polyvinyl alcohol film was unusually large (~630 cm-1). It is instructive to compare the value of ω_m = 80 cm-1 with the values of ω_m and ω_{sp} determined later. From Table I one observes that the mean of ($\omega_m + \omega_{sp}$) is roughly equal to 80 cm-1. Furthermore $S_{total} = S_{sp} + S$ from the two upper pairs of entries is not so different from 4.5. These rough agreements

are not surprising since, in the theory (irrespective of the number of modes employed), the sensitivity of the centroid frequency of the total hole profile on B depends on the ratio of Γ_I to $\Sigma S_i\omega_i$. The spectra of Boxer and his group [16,17] give a good indication of the sensitivity. In the limit as $\Gamma_I \Rightarrow 0$ the hole spectrum becomes independent of ω_B.

In comparing the two upper P870/P960 entries of Table I it should be noted that the parameter values were determined by fitting to the same experimental spectra. The middle set was determined with the short burn time limit of the theory and Lorentzians for the inhomogeneous distribution and multi-phonon profiles, see Section III.A., were employed. The present calculations (upper set in Table I) avoid the short burn time approximation, employ more physically realistic inhomogeneous and phonon lineshape functions and utilize mean phonon frequency (ω_m) values in the range determined by experiment. The latter are similar to those observed for pigments of antenna complexes [18,21,22]. According to our analysis, it is the utilization of the improved spectral functions that is primarily responsible for the better agreement with experiment. Nevertheless, the important aspects of the physics remain the same. We note that the ultra-fast relaxation times for the ω^j_{sp} ($j \geq 1$) ZPH levels given in the caption to Table I are discussed in ref. (1). It was the failure to observe, in the experimental spectra, the ω^0_{sp} ($j \geq 1$) ZPH satellite holes associated with the ZPH (at ω_B) of ω^0_{sp} that indicated the ultra-fast relaxation. Without such relaxation, the simulations clearly show the satellite ZPH structure. Furthermore, experiments in which ω_B was located in the vicinity of the ω^1_{sp} component of the absorption profile failed to produce a ZPH at ω_B [23,24]. The implication that marker mode relaxation occurs faster than primary charge separation is consistent with the agreement between the time domain and hole burning decay times for P^*.

In condensed phase spectroscopy the demarcation between weak and strong linear electron-phonon coupling is traditionally set at $S_{total} = 1$. For $S_{total} = 1$, the Franck-Condon factors for the zero-phonon and one-phonon transitions are equal. From Table I one observes that the coupling for P870 and P960 is strong, e.g., for $S_{total} = 3$ the Franck-Condon factor for the zero- phonon line of the origin band is only 0.05.

Earlier it had been stated that reasonable estimates for several of the theoretical parameters were afforded by the experimental data. Obviously ω_{sp} and S_{sp} are two. But S is also since, according to the theory [7,15], the ratio of the integrated intensity of the ZPH to that of the broader ω^{o}_{sp} hole it is superimposed on is $\approx\exp(-2S)$. Furthermore, an experimental determination for ω_m of 23 ± 4 cm-1 is available (Fig. 2). With these estimates and the observed width of the primary donor absorption profile, one can estimate Γ_I. From our simulations we have found that the optimal parameter values are within about 20% of the original estimates. Thus the simulations are best viewed as a refinement procedure for the experimental estimates. Turning now to the energy transfer properties of the higher energy Q_y-states of the bacterial RC we note that Jean et al. [28] have shown that Forster theory falls far short of accounting for the remarkably short (<100 fs) lifetimes of the "accessory" pigment states or the upper special pair state (P_+). Inadequate spectral overlap and large energy spacings between the relevant states make it very unlikely that Forster theory, even if modified, will work. In fact, it is incorrect to apply this "weak coupling" theory to relaxation from P_+ to P_- (primary donor state) since the excitonic splitting far exceeds the energy fluctuations of these states due to pure dephasing from bath fluctuations. An alternative mechanism is afforded by the theory of Davydov [27]. Here one would start with zero-order pigment aggregate states which are diagonal with respect to the excitonic Hamiltonian, $H_{Ex}(o)$, for a suitable static aggregate geometry. Relaxation between eigenstates of $H_{Ex}(o)$ would be induced by variations of H_{Ex} produced by intermolecular displacements associated with modes Q, i.e. $(\delta H_{Ex}/\delta Q)_o Q$ and higher order terms. The modes expected to be most effective are those involving rotational displacements of the pigments [29]. Such a mechanism is known to lead to decay of the upper triplet dimer (Davydov) state to the lower (by 25 cm-1) Davydov state of the anthracene crystal (by one-phonon emission) in 5 ps [30]. Recently, hole burning studies on the antenna complex of *Prosthecochloris aestuarii* have been performed [22,31]. Pair-wise excitonic interactions in the basic subunit of this complex, which contains 7 BChl molecules, are as large as ~200 cm-1 [32]. The experimentally observed exciton structure in absorption occurs over a ~500 cm-1 wide spectral region. The shortest exciton level

decay times for this system are ~250 fs [22,31]. This value can be viewed as consistent with that for anthracene under the expectation that decay is proportional to the exciton bandwidth squared and that in P. aestuarii the relaxation occurs by two-phonon emission. The excitonic interactions between pigments in the RC (other than that between the two Bchl of the special pair) are no larger than those in the P. aestuarii subunit [33]. With this in mind and a consideration of the RC accessory state level spacings, it is not apparent that one can reconcile the fact that decay of the accessory states of the RC is an order of magnitude faster than in P. aestuarii. The problem is more evident when one attempts to understand a <100 fs direct decay from the upper (P_+) to lower (P_-) dimer states of the special pair. In *Rps. viridis* the dimer or exciton splitting is ~2000 cm-1, which is larger than the marker mode or intramolecular vibrational frequencies. Thus, one is in the strong coupling limit [34-36] of the Davydov theory. If, for example, one were to invoke only the marker mode for $P_+ \Rightarrow P_-$ relaxation, creation of ~20 quanta of this mode would be necessary for the process. This is a very high order and improbable event (as in Herzberg-Teller vibronic coupling theory [37], a 2-quantum process is one to two orders of magnitude less probable than a 1-quantum process, etc.) Invoking a high frequency (~1500 cm-1) intramolecular mode plus several quanta of a low frequency intermolecular dimer mode would not appear to be a solution either since the former would not be expected to provide significant modulation of the resonance energy transfer matrix element. Although approximate, the above scaling argument indicates that the Davydov mechanism cannot account for the ultra-fast energy transfer processes of the RC.

A third possibility is that the "dark" charge-transfer (CT) states, which have been invoked to explain the primary charge separation process [38], provide a broad distribution of level structure through the Q_y-region which serves as a conduit for energy transfer from the higher energy optically allowed states to P_-. The fact that such CT states would be characterized by very high S-values for intermolecular modes is consistent with a broad distribution. Within this model decay would be viewed in terms of a breakdown of the Born-Oppenheimer approximation. Hopefully, electronic structure calculations may eventually be able to speak to the viability of this model.

CONCLUSION

An experimental determination of the mean frequency for protein phonons which couple to the primary donor state together with the avoidance of approximations to the theory of Hayes and Small made earlier have led to a significant improvement of the theoretical fits to the absorption and hole spectra of P870 and P960. The optical reorganization energies for P870 and P960 due to low-frequency modes (phonons, marker mode) are about one-third the value determined for the 100% CT state of the anthracene-pyromellitic acid dianhydride crystal [39] but an order of magnitude greater than for Chl in antenna complexes [18,22,31]. This result provides strong support for the suggestion from Stark data that [4,5,6] the primary donor state possesses significant CT character. The reported marker mode frequencies of 115 and 134 cm-1 are for $P870^*$ and $P960^*$; determination of the corresponding ground state frequencies would be important for elucidation of the dynamical nature of the special pair mode.

New experimental results are used to determine decay times of ~30 fs to the accessory Q_y-states of the bacterial RC due to downward energy transfer. An approximate scaling argument is presented which indicates that the Davydov energy transfer mechanism, like the Forster mechanism [28], cannot account for the ultra-fast decays. An alternative mechanism, which invokes intermediacy of a broad distribution of level structure due to charge- transfer states, is suggested for future consideration.

ACKNOWLEDGMENTS

Research at the Ames Laboratory was supported by the Division of Chemical Sciences, Office of Basic Energy Sciences, U.S. Department of Energy. Ames Laboratory is operated for the U.S. Department of Energy by Iowa State University under Contract No. W-7405-Eng-82. Research at Argonne National Laboratory was supported by the Division of Chemical Sciences, Office of Basic Energy Sciences, under Contract No. W-31-109-Eng-38.

REFERENCES

1. Johnson, S.G.: Tang, D.; Jankowiak, R.; Hayes, J.M.; Small, G.J.; Tiede, D.M. J. Phys. Chem. 1989, 93, 5953.
2. Tang, D.; Johnson, S.G.; Jankowiak, R.; Hayes, J.M.; Small, G.J.; Tiede, D.M. In Perspectives in Photosynthesis, Jortner, J., Pullman, B., Eds.; Kluwer Academic: Dordrecht, 1990, p 99.
3. Warshel, A.; Parson, W.W. J.A.C.S. 1987, 109, 6143.
4. L sche, M.; Feher, G.; Okamura, M.Y. Proc. Natl. Acad. Sci. USA 1987, 84, 7537.
5. Boxer, S.G.; Lockhart, D.J.; Middendorf, T.R. In Proceedings in Physics, Primary Processes in Photobiology, Kobayashi, T., Ed.; Springer-Verlag: New York, 1987, Vol. 20, p 80.
6. Lockhart, D.J.; Boxer, S.G. Proc. Natl. Acad. Sci. USA 1988, 85, 107.
7. Hayes, J.M.; Gillie, J.K.; Tang, D.; Small, G.J. Biochim. Biophys. Acta 1988, 932, 287.
8. Fleming, G.R.; Martin, J.L.; Breton, J. Nature (London) 1988, 85, 190.
9. Breton, J.; Martin, J.L; Fleming, G.R.; Lambry, J.-C. Biochemistry 1988, 27, 8276.
10. Won, Y. and Friesner, R.A. J. Phys. Chem. 1988, 92, 2214.
11. Meech, S.R.; Hoff, A.J.; Wiersma, D.A. Chem. Phys. Lett. 1985, 121, 287.
12. Vermeglio, A.; Paillotin, G. Biochim. Biophys. Acta 1982, 681, 32.
13. Chang, C.H.; Tiede, D.; Tang, J.; Smith, U.; Norris, J. FEBS Lett. 1986, 205 82.
14. This was inadvertently misstated in ref. 1 as 34 ± 3 ms and corrected here to 21 ± 2 ms.
15. Hayes, J.M.; Small, G.J. J. Phys. Chem. (1986), 90, 4928.
16. Boxer, S.G.; Lockhart, D.J.; Middendorf, T.R. Chem. Phys. Lett. 1986, 123, 476.
17. Boxer, S.G.; Middendorf, T.R.; Lockhart, D.J. FEBS Lett. 1986, 200, 237.
18. Gillie, J.K.; Small, G.J.; Golbeck, J.H. J. Phys. Chem. 1989, 93, 1620.

19. Rebane, K.K. Impurity Spectra of Solids, Plenum Press, New York, 1970.

20. Richards, J.L.; Rice, S.A. J. Chem. Phys. 1971, 54, 2014.

21. Jankowiak, R.; Tang, D.; Small, G.J.; Seibert, M. J. Phys. Chem. 1989, 93, 1649.

22. Johnson, S.G.; Small, G.J. Chem. Phys. Lett. 1989, 155, 371.

23. Tang, D. Ph.D. dissertation, Iowa State University, 1990.

24. Johnson, S.G. Ph.D. dissertation, Iowa State University, 1990.

25. The origin of the homogeneous contribution to the linewidth is assigned to an ultrafast excited state lifetime and not to strong linear electron-phonon coupling (S ~ 6, $S\omega_m \approx 190\ cm^{-1}$). For strong coupling to account for the large homogeneous width the zero phonon hole (ZPH) would have to be relatively narrow, at most a few cm^{-1} in width, in order to fulfill the conditions of strong coupling (i.e., integrated area of ZPH ≈.002 relative to total integrated area and a totally suppressed ZPH). A ZPH of a few cm^{-1} (FWHM) would indicate an excited state lifetime in the picosecond range which would be inconsistent with energy transfer occurring in ~100 fs [8,9].

26. Fig. 2 of ref. 2. The solvent is glycerol/H_2O (2:1) with LDAO.

27. Davydov, A.S. Theory of Molecular Excitons; Plenum Press: New York, 1971.

28. Jean, J.M.; Chan, C.-K.; Fleming, G.R. Israel J. Chem. 1988, 28, 169.

29. Dissado, L.A. Chem. Phys. 1975, 8, 289.

30. Port, H.; Rund, D.; Small, G.J., Yakhot, V. Chem. Phys. 1979, 39, 175.

31. Johnson, S.G. and Small, G.J. J. Phys. Chem. 1990, to be published.

32. Pearlstein, R.M. In Photosynthetic Light-Harvesting Systems, Scheer, H., Schneider, S., Eds.; De Gruyter: Berlin, 1988, p 555.

33. Knapp, E.W.; Fischer, S.F.; Zinth, W.; Sander, M.; Kaiser, W.; Deisenhofer, J.; Michel, H. Proc. Natl. Acad. Sci. USA 1985, 82, 8463.

34. Witkowski, A. and Moffit, W. J. Chem. Phys. 1960, 33, 873.

35. McClure, D.S. Can. J. Chem. 1958, 36, 59.

36. Gregory, A.R.; Henneker, W.H.; Siebrand, W.; Zgierski, M.Z. J. Phys. Chem. 1975, 63, 5475.

37. Fischer, G., Vibronic Coupling, The Interaction between the Electronic and Nuclear Motions, Academic Press: New York, 1984.

38. Friesner, R.A.; Won, Y. Biochim. Biophys. Acta 1989, 977, 99.

39. Haarer, D. J. Chem. Phys. 1977, 67, 4076.

ADDITIONAL CONCLUSIONS

The nature of the special pair mode, ω_{sp}, can be identified as intermolecular. The hole burning results of Gillie et al. [56] on Chl *a* and *b* in photosystem I antenna showed that the Franck-Condon factors for the intramolecular vibrational modes of these molecules were ≤.04 [56]. This, coupled with the recent narrow line fluorescence spectra for Bchl *a* [73] lead to an estimate of the F.-C. factors for the Bchl *a* of ≤.02 [56]. This is obviously much less than the S_{sp}=1.55 observed here. In addition, no intramolecular modes with a sufficiently low frequency (115 cm^{-1}) were determined in the studies of Renge et al. [73]. Thus, ω_{sp} is identified as an intermolecular vibrational mode, a dimer mode. The dynamical nature of this special pair marker mode is, as yet, undetermined.

The conclusion of Hayes et al. [44] based on fitting the unstructured hole spectra of P870 and P960 [20,21] that the holes could be understood in terms of inhomogeneous broadening (RC to RC heterogeneity) and linear electron-phonon coupling to low frequency protein phonons is essentially correct, and no evidence can be found to support the theory of Won and Friesner [41,42]. Won and Friesner [41,42] invoked coupling to a C-T state, ultrafast decay before charge separation, which would result in no observation of a zero-phonon hole as was clearly observed here and also for P960 of *Rps. viridis* [26,52]. It is pertinent to state that the unstructured hole spectra for P870 and P960 obtained by Boxer et al. [20,21] and fit by Hayes et al. [44] were generated using PVOH hosts. Experiments performed on samples prepared in a like manner (results reported here for P870/PVOH and elsewhere for P960/PVOH [26,52]) yielded similar results to Boxer et al. [20,21] with the notable exception that a weak ZPH was observed for selective burn frequencies (on the low energy shoulder) for P960 [18,49]. The width of this ZPH was ~13. cm^{-1} [26,52]. No ZPH was observed for *Rb. sphaeroides* in PVOH.

The interpretation of Tang et al. [24,25] for their hole burning results on the RC of *Rps. viridis* involved two states, one being an excited state with a strong progression of a 130 cm^{-1} vibrational mode (ω^0_{sp}) and the second being a C-T state. The C-T state was ~300 cm^{-1} higher in energy than their ω^0_{sp} hole. This assignment has to be questioned in

view of the results presented here and those presented elsewhere for P960 [18,49]. Tang et al. [24,25] made use of ΔT spectra obtained with relatively high OD samples (.6) which tend to give unfaithful representations of the ΔA spectra (see Fig. 6). The excited state of P870 is thought to contain some C-T character as evidenced by its moderately strong electron-phonon coupling (monomer chlorophylls typically exhibit weak electron-phonon coupling [56]), however, this differs from the proposal of Won and Friesner in that they coupled a neutral excitonic state to a C-T manifold (with ultra-fast decay). The charge transfer character in this case would be due to an intra-dimer charge transfer state such as $P_M^+P_L^-$ or $P_M^-P_L^+$ (or more likely a linear combination of the two since they are indistinguishable, if C_2 symmetry holds) and not to a state such as P^+B^-H. The presence of an additional C-T state(s) cannot be excluded based on the results presented here, but the oscillator strength of that state would have to be small compared to ω_{sp} (and, of course, these state(s) could not affect the charge separation kinetics).

The spectral hole burning studies performed on RC from *Rb. sphaeroides*, *Rps. viridis* and *Chl. aurantiacus* [26,27,52,74] have demonstrated that the hole burning characteristics of the primary electron donor states are similar for these three bacterial RC and defined by moderately strong linear electron-phonon coupling to the protein and site inhomogeneous broadening. Similar characteristics have also been noted for RC from green plants, PSI [75] and PSII [58], however, no special pair mode was identified for these RC. The identification of a strong Franck-Condon progression of a low frequency (100-150 cm^{-1}) intermolecular mode in the first excited state of the PED has been accomplished for *Rb. sphaeroides*, *Rps. viridis* and *Chl. aurantiacus*(this work and ref. (26,27,52,74)). The energy transfer times for the accessory pigments of the RC from *Rb. sphaeroides* have been determined. The extent to which interaction with a charge transfer state affects energy transfer, charge separation and electron transfer within the RC of *Rb. sphaeroides* is still unresolved. The results presented here do however place a limit on the absorption oscillator strength of a C-T state in the RC of *Rb. sphaeroides* in the 850-930 nm spectral range.

REFERENCES

1. Deisenhofer, J.; Michel, H. Angew. Chem. Int. Engl. Ed. 1989, 28, 829.
2. Deisenhofer, J.; Epp, O.; Miki, K.; Huber, R.; Michel, H. J. Mol. Biol. 1984, 180, 385.
3. Deisenhofer, J.; Epp, O.; Miki, K.; Huber, R.; Michel, H. J. Nature(London) 1985, 318, 618.
4. Michel, H. J. Mol. Biol. 1982, 158, 567.
5. Allen, J. P.; Feher, G.; Yeates, T. O.; Rees, D. C.; Deisenhofer, J.; Michel, H.; Huber, R. Proc. Natl. Acad. Sci. USA 1986, 83, 8589.
6. Chang, C.-H.; Tiede, D. M.; Tang, J.; Smith, U.; Norris, J. R.; Schiffer, M. FEBS Lett. 1986, 205, 82.
7. Allen, J. P.; Feher, G.; Yeates, T. O.; Koyima, H.; Rees, D. C. Proc. Natl. Acad. Sci. USA 1987, 84, 6162.
8. Feher, G.; Allen, J. P.; Okamura, M. Y.; Rees, D. C. Nature (London) 1989, 339, 111.
9. Budil, D. E.; Gast, P.; Chang, C-H.; Schiffer, M.; Norris, J. R. Ann. Rev. Phys. Chem. 1987, 38, 561.
10. Kellogg, E. C.; Kolaczkowski, S.; Wasielewski, M. R.; Tiede, D. M. Photosynth. Res. 1987, 22, 47.
11. Yeates, T. O.; Koyima, H.; Chirino, A.; Rees, D. C.; Allen, J. P.; Feher, G. Proc. Natl. Acad. Sci. USA 1988, 85, 7993.
12. Michel, H.; Epp, O.; Deisenhofer, J. EMBO J. 1986, 3, 2445.
13. Youvan, D. C.; Marrs, B. L. Scient. Am. 1987, 256, 42.
14. Breton, J.; Bylina, E. J.; Youvan, D. C. Biochemistry 1989, 28, 6423.
15. Kirmaier, C.; Holten, D.; Bylina, E. J.; Youvan, D. C. Proc. Natl. Acad. Sci. USA 1988, 85, 7562.
16. Kirmaier, C.; Holten, D. Isr. J. Chem. 1988, 28, 79.

17. Johnson, S. G.; Lee, I.-J.; Small, G. J. In Chlorophylls, Scheer, H., Ed.; CRC Press: Boca Raton, 1990, in press.

18. Lutz, M.; Robert, B. In Biological Applications of Raman Spectroscopy, Spiro, T. G., Ed.; Wiley&Sons: New York, 1987, Vol. 3, 347.

19. Breton, J.; Martin, J.-L.; Fleming, G. R.; Lambry, J.-C. Biochem. 1988, 27, 8276.

20. Boxer, S. G.; Lockhart, D. J.; Middendorf, T. R. Chem. Phys. Lett. 1986, 123, 476.

21. Boxer, S. G.; Middendorf, T. R.; Lockhart, D. J. FEBS Lett. 1986, 200, 237.

22. Meech, S. R.; Hoff, A. J.; Wiersma, D. A. Chem. Phys. Lett. 1985, 121,287.

23. Meech, S. R.; Hoff, A. J.; Wiersma, D. A. Proc. Natl. Acad. Sci. USA 1986, 83, 9464.

24. Tang, D.; Jankowiak, R.; Gillie, J. K.; Small, G. J.; Tiede, D. M. J. Phys. Chem. 1988, 92, 4012.

25. Tang, D.; Jankowiak, R.; Small, G. J.; Tiede, D. M. Chem. Phys. 1989, 131, 99.

26. Johnson, S. G.; Tang, D.; Jankowiak, R.; Hayes, J. M.; Small, G. J.; Tiede, D. M. J. Phys. Chem. 1989, 93, 5953.

27. Johnson, S. G.; Tang, D.; Jankowiak, R.; Hayes, J. M.; Small, G. J.; Tiede, D. M. J. Phys. Chem. 1990, accepted.

28. Marcus, R. A. Chem. Phys. Lett. 1987, 133, 471.

29. Won, Y.; Friesner, R. A. Biochim. Biophys. Acta 1988, 935,9.

30. Bixon, M.; Jortner, J.; Michel-Beyerle, M. E.; Ogrodnik, A.; Lersch, W. Chem. Phys. Lett. 1987, 140, 626.

31. Friesner, R. A.; Won, Y. Biochim. Biophys. Acta 1989, 977, 99.

32. Jortner, J. Biochim. Biophys. Acta 1980, 594, 193.

33. Breton, J.; Martin, J.-L.; Petrich, J.; Migus, A.; Antonetti, A. FEBS Lett. 1986, 209, 37.

34. Holzapfel, W.; Finkele, U.; Kaiser, W.; Oesterhelt, D.; Scheer, H.; Stilz, H. U.; Zinth, W. Chem. Phys. Lett. 1989, 160,1.

35. Creighton, S.; Hwang, J.-K.; Warshel, A.; Parson, W. W.; Norris, J. R. Biochemistry 1988, 27, 774.

36. Braun, H. P.; Michel-Beyerle, M. E.; Breton, J.; Buchanan, S.; Michel, H. FEBS Lett. 1987.

37. Lockhart, D. J.; Boxer, S. G. Biochemistry 1987, 26, 664.

38. Boxer, S. G.; Lockhart, D. J.; Middendorf, T. R. In Proceedings in Physics, Primary Processes in Photobiology, Kobayashi, T., Ed.; Springer-Verlag: New York, 1987, Vol. 20, p 80.

39. Losche, M; Feher, G.; Okamura, M. Y. Proc. Batl. Acad. Sci. USA 1987, 84, 7537.

40. Won, Y.; Fiesner, R. A. Proc. Natl. Acad. Sci. USA 1987, 84, 5511.

41. Won, Y.; Friesner, R. A. J. Phys. Chem. 1988, 92, 2214.

42. Won, Y.; Friesner, R. A. J. Phys. Chem. 1988, 92, 2208.

43. Hayes, J. M.; Small, G. J. J. Phys. Chem. 1986, 90, 4928.

44. Hayes, J. M.; Gillie, J. K.; Tang, D.; Small, G. J. Biochim. Biophys. Acta 1988, 932, 287.

45. Martin, J.-L.; Breton, J.; Hoff, A. J.; Migus, A.; Antonetti, A. Proc. Natl. Acad. Sci. USA 1986, 83, 957.

46. Shuvalov, V. A.; Klevanik, V. A.; Sharkov, A. V.; Matveetz, Y. A.; Kryukov, P. G. FEBS Lett. 1978, 91, 135.

47. Shuvalov, V. A.; Klevanik, A. V. FEBS Lett. 1983, 160, 51.

48. Kirmaier, C.; Holten, D.; Parson, W. W. FEBS Lett. 1985, 185, 76.

49. Breton, J.; Martin, J.-L.; Migus, A.; Antonetti, A.; Orszag, A. Proc. Natl. Acad. Sci. USA 1986, 83, 5121.

50. Wasielewski, M. R.; Tiede, D. M. FEBS Lett. 1986, 204, 368.

51. Wraight, C. A.; Clayton, R. K. Biochim. Biophys. Acta 1973, 333, 246.

52. Tang, D.; Johnson, S. G.; Jankowiak, R.; Hayes, J. M.; Small, G. J.; Tiede, D. M. In Perspectives in Photosynthesis, Jortner, J. and Pullman, B., Ed.; Kluwer: Dordrecht, 1990, p 99.

53. Scherer, P. O. J.; Fischer, S. J. Phys. Chem. 1989, 93, 1633.

54. Vermeglio, A.; Paillotin, G. Biochim. Biophys. Acta 1982, 681, 32.

55. Taremi, S. S.; Violette, C. A.; Frank, H. A. Biochim. Biophys. Acta 1989, 975, 86.

56. Gillie, J. K.; Small, G. J.; Golbeck, J. H. J. Phys. Chem. 1989, 93, 1620.

57. Angerhofer, A. thesis(Ph. D.) 1987, Universitat Stuttgart, West Germany.

58. Jankowiak, R.; Tang, D.; Small, G. J.; Seibert, M. J. Phys. Chem. 1989, 93, 1649.

59. Wasielewski, M. R.; Johnson, D. G.; Govindjee; Preston, C.; Seibert, M. Photosynth. Res. 1989, 22, 89.

60. Johnson, S. G.; Small, G. J. J. Phys. Chem. 1989, 155, 371.

61. Johnson, S. G.; Small, G. J. J. Phys. Chem. 1990, submitted for publication.

62. Parot, P.; Delmas, N.; Garcia, D.; Vermeglio, A. Biochim. Biophys. Acta 1985, 809, 137.

63. Rafferty, C. N.; Clayton, R. K. Biochim. Biophys. Acta 1979, 546, 189.

64. Vermeglio, A.; Clayton, R. K. Biochim. Biophys. Acta 1976, 449, 500.

65. Mar, T.; Gingras, G. Biochim. Biophys. Acta 1976, 440, 609.

66. Breton, J.; Vermeglio, A. In Photosynthesis: Energy conversion by Plants and Bacteria, Govindjee, Ed.; Academic Press: New York, 1982, vol. 1, p 153.

67. Shuvalov, V. A.; Asadov, A. A. Biochim. Biophys. Acta 1979, 545, 296.

68. Clayton, R. K.; Rafferty, C. N.; Vermeglio, A. Biochim. Biophys. Acta 1979, 545, 58.

69. Gagliano, A. G.; Breton, J. Geacintov, N. E. Photobiochem. Photobiophys. 1986, 10, 213.

70. Vermeglio, A.; Breton, J.; Paillotin, G.; Cogdell, R. Biochim. Biophys. Acta 1978, 501, 514.

71. Kohler, W.; Breinl, W.; Friedrich, J. J. Phys. Chem. 1985, 89, 2473.

72. Breton, J. Biochim. Biophys. Acta 1985, 810, 235.

73. Renge, I.; Mauring, K.; Avarmaa, R. J. Lumin. 1987, 37, 207.

74. Johnson, S.G.; Tang, D.; Jankowiak, R.; Hayes, J. M.; Small, G. J. In Proceedings of 6th International Conference on Energy and Electron Transfer, Prague, Czechslovakia (Aug. 14-18, 1989), in press.

75. Gillie, J. K.; Lyle, P. A.; Small, G. J.; Golbeck, J. H. Photosynth. Res. 1989, 22, 233.

GENERAL CONCLUSIONS

Temperature-dependent absorption and fluorescence spectra and line-narrowed fluorescence and excitation spectra are reported for a synthetically prepared chlorophyll dimer. This molecule is a model for the special pair in bacterial reaction centers. Data obtained for four solvents of widely differing polarity show that the dimer exists in two conformations (A and B) and that excited state relaxation from A to B onsets near the glass transition temperature (T_g). Molecular modelling suggests that the conformations are related by "bicycling" of the two single bonds joined to the vinyl group linkage. For a solvent of sufficiently high polarity (DMF), the excited state of B is shown to access a new radiationless decay channel for $T \geq T_g$. A charge-transfer state is suggested to be important for this decay. The model presented is shown to provide a qualitative explanation for the frequency domain and recently obtained picosecond and fluorescence quantum yield room temperature data.

Persistent spectral hole burning is reported for the antenna complex of the green sulfur bacterium *Prosthecochloris aestuarii*. This complex contains three subunits which contain seven Bchl *a* molecules. The hole burning data are shown to be consistent with a excitonically coupled system. The data also provide the magnitude of linear exciton-phonon coupling of the optical transitions associated with the two lowest energy absorbing components, the number of exciton components in the Q_y spectral region and their Q_y transition energies. In addition, the excited state (S_1) decay times of the exciton components are presented. A recent proposal concerning the existence of a third crystal structure is discussed and support for it is found in the data presented.

Structured photochemical hole burned spectra are presented for P870 of the reaction center (RC) of *Rhodobacter sphaeroides*. A special pair marker mode Franck-Condon progression is identified. The zero-phonon hole yields $P870^*$ decay times in good agreement with the time domain values. Site excitation energy selection is used to establish correlation between a higher energy RC state of *Rb. sphaeroides* and P870. Temperature dependent hole burning data for P870 are reported which lead to the

determination for the mean frequency of the protein phonons which couple to the optical transition. Utilization of this frequency, ω_m~25-30 cm^{-1}, together with a special pair mode, ω_{sp}~115 cm^{-1}, with the theory of Hayes and Small lead to theoretical fits of the P870 absorption and hole spectra. Time dependent P870 hole spectra are reported which provide additional evidence that the previously observed zero-phonon hole is an intrinsic feature of P870 for active RC. Transient spectra obtained by laser excitation into the accessory Q_y-absorption bands of the RC presented which show both an absence of line narrowing and an absence of any dependence on the location of the excitation frequency. These results, which are consistent with ultra-fast energy transfer processes from the accessory states, are discussed in terms of earlier time domain data.

LITERATURE CITED

1. Kamen, M. D. Primary Processes in Photosynthesis; Academic Press: New York, 1963.
2. Govindjee; Govindjee, R. In Bioenergetics of Photosynthesis, Govindjee, Ed.; Academic Press: New York, 1975, p 1.
3. Lawlor, D. W. Photosynthesis: Metabolism, Controll, and Physiology; Longman Scientific & Technical: New York, 1987.
4. Sauer, K. In Encycleopedia of Plant Physiology, Staehlin, L. A., Artzen, C. J., Eds.; Springer-Verlag: Berlin, 1986, Vol. 19, p 85.
5. Hipkins, M. F.; Baker, N. R. Photosynthesis Energy Transduction, a Practical Approach; IRL Press: Oxford, 1986.
6. Foyer, C. H. Photosynthesis; Wiley & Sons: New York, 1984.
7. Clayton, R. Molecular Physics in Photosynthesis; Blaisdell: New York, 1965.
8. Clayton, R. K.; Sistrom, W. R. The Photosynthetic Bacteria; Plenum Press: New York, 1978.
9. Mauzerall, D.; Greenbaum, N. L. Biochim. Biophys. Acta 1989, 974, 119.
10. Deisenhofer, J.; Epp, O.; Miki, K.; Huber, R.; Michel, H. J. Mol. Biol. 1984, 180, 385.
11. Deisenhofer, J.; Epp, O.; Miki, K.; Huber, R.; Michel, H. Nature (London) 1985, 318, 618.
12. Allen, J. P.; Feher, G.; Yeates, T. O.; Rees, D. C.; Deisenhofer, J.; Michel, H.; Huber, R. Proc. Natl. Acad. Sci. USA 1986, 83, 8589.
13. Chang, C. H.; Tiede, D.; Tang, J.; Smith, U.; Norris, J.; Schiffer, M. FEBS Lett. 1986, 205, 82.
14. Johnson, S. G.; Tang, D.; Jankowiak, R.; Hayes, J. M.; Small, G. J.; Tiede, D. M. J. Phys. Chem. 1989, 93, 5953.
15. Szabo, A. Phys. Rev. Lett. 1970, 25, 924.
16. Personov, R. I.; Al'Shits, E. I.; Byskovskaya, L. A. Opt. Commun. 1972, 6, 169.

17. Personov, R. I. In Spectroscopy and Excitation Dynamics of Condensed Molecular Systems, Agranovich, V. M., Hochstrasser, R. M., Eds.; North-Holland: Amsterdam, 1983, Vol. 4, p 555.
18. Jankowiak, R.; Small, G. J. Anal. Chem. 1989, 61, 1023A.
19. Jankowiak, R.; Cooper, R. S.; Zamzow; Small, G. J.; Doskocil, G.; Jeffrey, A. M. Chem. Res. Toxicol. 1988, 1, 60.
20. Zamzow, D.; Jankowiak, R.; Cooper, R. S.; Small, G. J.; Tibbels, S. R.; Cremonosi, P.; Devaneson, P.; Rogan, E. G.; Cavalieri, E. L. Chem. Res. Toxicol. 1989, 2, 29.
21. Avarmaa, R. A.; Rebane, K. K. Spectrochim. Acta 1985, 41A, 1365.
22. Hala, J.; Pelant, I.; Parma, L.; Vacek, K. J. Lumin. 1981, 24/25, 803.
23. Funfschilling, J.; Williams, D. F. Photochem. Photobiol. 1977, 26, 109.
24. Johnson, S. G.; Small, G. J.; Johnson, D. G.; Svec, W. A.; Wasielewski, M. R. J. Phys. Chem. 1989, 93, 5437.
25. Funfschilling, J.; Walz, D. Photochem. Photobiol. 1983, 38, 389.
26. Johnson, S. G.; Small, G. J. J. Phys. Chem. 1990, to be published.
27. Avarmaa, R.; Renge, I.; Mauring, K. FEBS Lett. 1984, 167, 186.
28. Renge, I.; Mauring, K.; Avarmaa, R. Biochim. Biophys. Acta 1984, 766, 501.
29. Johnson, S. G.; Lee, I.-J.; Small, G. J. In Chlorophylls, Scheer, H.; CRC Press: Boca Raton, in press.
30. Macfarlane, R. M.; Shelby, R. M. Phys. Rev. Lett. 1979, 42, 788.
31. Voelker, S.; Macfarlane, R. M. Chem. Phys. Lett. 1979, 61, 421.
32. Boxer, S. G.; Middendorf, T. R.; Lockhart, D. J. FEBS Lett. 1986, 200, 237.
33. Meech, S. R.; Hoff, A. J.; Wiersma, D. A. Proc. Natl. Acad. Sci. USA 1986, 83, 9464.
34. Gorokhovski, A. A.; Kikas, J. Opt. Comm. 1977, 21, 272.
35. Gorokhovski, A. A.; Kaarli, R. K.; Rebane, L. A. JETP Lett. 1974, 20, 216.
36. Friedrich, J.; Haarer, D. Angew. Chem. Int. Ed. Engl. 1984, 23, 113.
37. Jankowiak, R.; Small, G. J. Science 1987, 237, 618.

38. Gillie, J. K.; Small, G. J.; Golbeck, J. H. J. Phys. Chem. 1989, 93, 1620.

39. Jankowiak, R.; Tang, D.; Small, G. J.; Seibert, M. J. Phys. Chem. 1989, 93, 1649.

40. Johnson, S. G.; Small, G. J. Chem. Phys. Lett. 1989, 155, 371.

41. Johnson, S. G.; Tang, D.; Jankowiak, R.; Hayes, J. M.; Small, G. J.; Tiede, D. M. J. Phys. Chem. 1990, to be published.

42. Hayes, J. M.; Fearey, B. L.; Carter, T. P.; Small, G. J. Int. Rev. Phys. Chem. 1986, 5, 175.

43. Moerner, W. E., Ed., Persistent Spectral Hole Burning: Science and Applications; Springer-Verlag: Berlin, 1988, Vol. 44.

44. Berg, M.; Walsh, C. A.; Narasimhan, L. R.; Littau, K. A.; Fayer, M. D. J. Phys. Chem. 1988, 88, 1564.

45. Voelker, S. In Relaxation Processes in Molecular Excited States, Funfschilling, J., Ed.; Kluwer Academic: Dordrecht, 1989, 113.

46. Fearey, B. L.; Carter, T. P.; Small, G. J. Chem. Phys. 1986, 101, 279.

47. Fearey, B. L.; Small, G. J. Chem. Phys. 1986, 101, 269.

48. Hayes, J. M.; Small, G. J. Chem. Phys. 1978, 27, 151.

49. Anderson, P. W.; Halperin, B. I.; Varma, C. M. Philos. Mag. 1972, 25, 1.

50. Phillips, W. A. J. Low Temp. Phys. 1972, 7, 351.

ACKNOWLEDGEMENTS

I wish to acknowledge several people for their help, guidance and support during my Ph. D. studies. Firstly, I wish to thank my advisor, Dr. Gerald J. Small, for his guidance, support and patience on my path towards a Ph. D. He always showed willingness and enthusiasm in our discussions of my research.

Dr. John M. Hayes and Dr. Ryszard Jankowiak are two scientists to whom I owe a great deal for their advice on experimental and theoretical aspects of my research, as well as, their friendship and patience. Mr. Deming Tang played a significant role in my research as he was my main collaborator on the reaction center project. Although, we will both probably acknowledge that we did not always agree on the same approach to research-related problems or analysis of data we did form, I believe, an extremely productive team for the 6 months we worked together.

Ames Laboratory and the Dept. of Chemistry of Iowa State University have financially supported me throughout my graduate school stay, Thank you.

This research would not have been possible without the generous donations of samples by the following people: Dr. M. R. Wasielewski, Argonne National Laboratory (synthetic dimer), Dr. R. E. Fenna, Univ. Miami, Fl. (*Prosthecochloris aestuarii*), and Dr. D. M. Tiede, Argonne Laboratory (*Rhodobacter sphaeroides*). Dr. Doug Johnson of Argonne National Laboratory, I wish to thank for his many discussions of the headache that we shared, the synthetic dimer project.

The members of Small's group have lightened my days of research with conversation, friendship and an occasional practical joke or two (I still am wondering where my first name plate is guys). The following members I wish to thank especially: Dr. Scott Cooper, Dr. Maureen Connolly, Dr. Bryan Fearey, Dr. Kyuseok Song, Dr. Kevin Gillie, and Mr. Michael Kinney. A special thanks to Dan Zamzow and Dave Sanders who both helped me work off the frustration that comes with research either by attacking a squash ball or by "attempting" to attack pheasants, squirrels or other wild beasts.

I would like to thank my parents, Helen and Glenn Johnson, for their support throughout the last decade, which I have spent in one college or another. A very special thanks to Cynthia Hasegawa for her moral support when things were not going well and for her friendship and love.